Review of LNAPL Monitoring Techniques in Groundwater

Project Record P2/080/1/M

A D Erskine, H R Green and J A Heathcote

Research Contractor:
Entec UK Ltd

Further copies of this report are available from:
Environment Agency R&D Dissemination Centre, c/o
WRc, Frankland Road, Swindon, Wilts SN5 8YF

tel: 01793-865000 fax: 01793-514562 e-mail: publications@wrcplc.co.uk

Publishing Organisation:
Environment Agency
Rio House
Waterside Drive
Aztec West
Almondsbury
Bristol BS32 4UD

Tel: 01454 624400 Fax: 01454 624409

ISBN:

Dissemination status
Internal: Released to Regions
External: Released to the Public Domain

Statement of use
This document provides guidance and information for those responsible for assessing volumes of Light Non-Aqueous Phase Liquids (LNAPLs) in the ground.

Research contractor

Entec UK Ltd
160-162 Abbey Foregate
Shrewsbury
Shropshire
SY2 6BZ

Tel: 01743 236464 Fax: 01743 236303

Environment Agency Project Leader
The Environment Agency's Project Leader was:
Jonathan Smith

Amendments
Any corrections or proposed amendments to this manual should be made through the regional Agency representative on the Water Resources National Abstraction Licensing Group.

CONTENTS

TABLES

FIGURES *After Page*

APPENDICES

GLOSSARY

Symbol	Definition
α_{LW}	Van Genuchten LNAPL-water displacement pressure (N/m^2)
α_{AL}	Van Genuchten air-LNAPL displacement pressure (N/m^2)
β_{LW}	Scaling factor for LNAPL-water ($= p_{AW}/p_{LW}$)[]
β_{AL}	Scaling factor for air-LNAPL($= p_{AW}/p_{AL}$)[]
C	Concentration
ε	Dielectric permittivity(F/m)
ε^*	Complex dielectric permittivity
ε_0	Dielectric permittivity of free space ($= 8.854\times10^{-12}$ F/m)
ε_r	Dielectric constant []
f	Frequency ($Hz = s^{-1}$)
g	Acceleration due to gravity (m/s^2)
H_C	Height of the top of the capillary zone above piezometric level (m)
H_L	Capillary thickness of LNAPL (m)
H_p	Intensity of the primary magnetic field (H)
H_s	Intensity of the secondary magnetic field (H)
k	Intrinsic permeability (m^2)
λ	Brooks-Corey pore size distribution index
μ	Magnetic permeability (H/m)
μ_0	Magnetic permeability of free space (4.1×10^{-7} H/m)
n	Van Genuchten pore size distribution index []
p	Pore pressure (N/m^2)
p_{AL}	Air-LNAPL displacement pressure (N/m^2)
p_{AW}	Air-water displacement pressure (N/m^2)
p_{LW}	LNAPL-water displacement pressure (N/m^2)
ρ	Resistivity (ohm m)
ρ^*	Complex resistivity
ρ_W	Density of water (kg/m^3)
ρ_L	Density of LNAPL (kg/m^3)
ρ_A	Density of air (kg/m^3)
σ	Surface tension (N/m)
σ_{AW}	Surface tension between air and water (N/m)
σ_{AL}	Surface tension between air and LNAPL (N/m)
T	Observed LNAPL thickness in the borehole (m)
Tc	Buoyancy surface elevation (m)
T_G	Actual LNAPL thickness in the ground (m)
θ	Contact angle
φ	Porosity []
V	Volume of LNAPL per unit area (m)
v	Velocity (m/s)
ω	Angular frequency (s^{-1})

1. INTRODUCTION

This document is the Project Record of the research project entitled "Review of LNAPL Monitoring Techniques in Groundwater" (Environment Agency reference P2D(97)09). This research was carried out by Entec UK Ltd under contract to the Environment Agency, starting in September 1997.

The Project Record output of a research project is a full account of all the work carried out during the course of the project. The most important output of the project is the Technical Report which will be issued as a separate document. The Technical Report presents the findings of the study clearly and concisely. The Project Record however includes all the material presented in the Technical Report and additional material describing the sources of data, the details of how the work was carried out and an account of the technical material that was not thought worthy of inclusion in the Technical Report.

1.1 Project Description

The main objective of this research project was to produce a methodology for the interpretation of borehole monitoring data to determine the thickness of free-phase LNAPL (Light Non-Aqueous Phase Liquids) in a shallow aquifer. The most common LNAPLs are hydrocarbon pollutants such as oil, petrol and diesel. In addition, methods of determining the entire volume of LNAPL in an aquifer were to be evaluated.

In an unconfined shallow aquifer, LNAPLs tend to occur as a layer floating on the surface of the water table. Borehole monitoring data are frequently used to determine the thickness of free-phase LNAPL in a shallow aquifer since if a borehole is screened across the floating LNAPL layer, a layer is also formed in the borehole. Unfortunately, the thickness of this layer is not the same as the thickness in the aquifer due to a phenomenon called the "exaggeration effect".

The practical applicability of a methodology to calculate total LNAPL volume is considerable. In the event of a hydrocarbon pollution incident, it will enable the volumes of hydrocarbon in the aquifer to be quantified. This is vital information for deciding the method and scale of remediation. It will also be used to monitor the effectiveness of remediation systems and ultimately to approve completion.

The potential methods of estimating the true LNAPL thickness can be sub-divided into the following categories:

- direct correction for the exaggeration effect using soil and LNAPL properties
- baildown tests

- direct measurement by sampling the soil
- down-hole geophysics (on boreholes or probes).
- non-invasive geophysical techniques.

In addition, the project was to propose methods to quantify the entire volume of LNAPL in the aquifer. This involved consideration of interpolation of spot readings and integration techniques. Sampling strategies were also reviewed.

In deciding which method of LNAPL plume delineation and monitoring is appropriate for a site, the final use of the data must be considered. Measurements can be made of total or mobile LNAPL thickness, lateral extent of the plume (both dissolved and free-phase) and with varying degrees of accuracy and cost.

The ultimate objective of this project is to present the key findings of the study, condensed down to a concise and clear methodology, in a Pollution Prevention Guidance Note which will be published by the Environment Agency.

1.2 Report Structure

The methods of obtaining published research, commercial information and expert opinions for this project are described in Section 2. The theory behind LNAPL behaviour in porous media and the exaggeration effect is discussed in Section 3. The theory of the exaggeration effect has been presented by several authors since it was first observed, with sometimes conflicting opinions. Available data from sand tank studies have been reviewed and used to test the theoretical studies.

Section 4 describes methods of obtaining spot measurements by invasive techniques, including sampling (soil, water and gas), borehole logging and cone penetrometer technology. Non-invasive geophysical survey methods are discussed in Section 5.

Sampling strategies and methods of interpolating spot-readings to quantify the total LNAPL volume in the aquifer are described and tested in Section 6, and the conclusions and recommendations are given in Section 7. A table containing the entire list of references collated for this research project is given in Section 8.

2. LITERATURE REVIEW SOURCES

2.1 Literature Search Methods

The literature search has so far compiled a library of about 100 academic papers. A number of texts have also been consulted and advice has been sought from various organisations.

The main methods of finding references have been as follows:

- Review of main periodicals
- Searches on reference databases using keywords.
- Contacting Universities and Geological Surveys for information on current research
- Visiting World Wide Web sites for relevant literature and contact names
- Secondary references referred to by authors of papers already obtained
- Commercial material provided by contractors providing services with some of the techniques reviewed.

2.2 Review of Main Periodicals

The more recent editions of the main periodicals have been searched for relevant papers. These were Water Resources Research, Journal of Hydrology, Ground Water, Ground Water Monitoring Review and Water Research. The editions from January 1995 to present have been searched since these titles may not have been input to the reference databases yet.

2.3 Searches on Reference Databases using Keywords

The databases used are given in Table 2.1. Some of the searches have been conducted using the World Wide Web. Search words generally included the following words in various combinations: LNAPL, non-aqueous phase liquid, hydrocarbon, baildown, resistivity, electromagnetic, ground penetrating radar, fluorescence, thickness, TEM, plus searches for various authors who are known to have published literature on the subject.

Table 2.1 Literature Searches

Database	Comments
USEPA publications	USEPA documents only
Geological Society database	Periodicals
Science Citation Index	Periodicals
'Uncover'	Periodicals
NGWA Groundwater On-line abstracts database	Periodicals, NGWA Conference Proceedings
Entec Library	General textbooks and papers

2.4 Universities, Geological Surveys and other Agencies

Universities and Geological Surveys were contacted for information on current research. The people contacted are given in Table 2.2. There were few responses from the Universities indicating that there is little current research in this area in the UK. Contacts with overseas agencies, such as the United States Environmental Protection Agency (USEPA) were attempted although little response has been met so far.

Table 2.2 Contacts with Universities, Geological Surveys

Contact	Reply?
Universities	
Mr M Price, University of Reading	Y
Ms J Dottridge, University of Central London	
Dr P Younger, Newcastle University	
Dr J Tellam, Birmingham University	
Dr R Barker, Birmingham University	Y
Dr M Rivett, Birmingham University	Y
Dr K Hiscock, University of East Anglia	Y
Professor D Lerner, Bradford University	Y
Professor Keuper, University of Waterloo, Canada	
Geological Surveys	
Mr D Banks, Norwegian Geological Survey	Y
Dr R Ogilvy, British Geological Survey	Y

2.5 Visiting World Wide Web sites

Several useful sites were encountered on the World Wide Web. These are summarised in Table 2.3. Most of the sites had information on contacts but little on recently published literature. Literature searches were available from the National Groundwater Association Abstracts Database, Science Magazine, Journal of Hydrology and the US EPA sites.

Table 2.3 World Wide Web Sites Visited

Site	Comments
USEPA	National Centre for Environmental Publications Information (NCEPI) - search available for USEPA publications.
NGWA	Groundwater On-line abstracts database, produced very good reference lists including abstracts from papers.
USGS	USGS library - literature search only for members.
Hydrology Web	A few contacts to other sites, no useful literature.
Science Magazine	Oct 95-Nov 97 issues searched.
Journal of Hydrology	Vols 74-186 (1984-1996) searched.
International Association of Hydrogeologists	Hydrogeological contacts page led to various Norwegian, Dutch, Danish University sites. None of the recent publications lists showed anything relevant.
EEGS	Engineering and Environmental Geophysics page, nothing useful.
Waterloo University	Publications list for LNAPL related and geophysics research.
Technical University of Denmark, Groundwater Research Centre	Nothing useful.
Amsterdam University Hydrology Dept.	Nothing useful.
Wagenenger	Nothing useful.

2.6 Commercial Material

Commercial material has been obtained from contractors providing services for some of the geophysical and monitoring techniques reviewed. These included Fugro Ltd, Zeneca, Geocone Ltd, Geo-Services International and Ground Remediation Systems Ltd. Several papers published by these companies were also provided.

3. THEORY REVIEW

3.1 LNAPL Movement in Porous Media

The review of the theory presented below is intended to be brief. Rather than reproduce text from textbooks we have listed the sources where possible with an indication of the quality. In general terms a lot of the straightforward material in this chapter is well presented in Domenico and Schwartz (1990) and in Fetter (1993).

3.1.1 General

When two liquids are both present in a porous medium they may either be miscible or immiscible. This project is concerned with the interaction of water and liquids immiscible with water. In physical terms, a fluid is immiscible with water if it is not able to fully dissolve in water (which may depend on the quantities involved). In practice most hydrocarbon contaminants fall into this category including petrol and diesel.

The other restriction on a liquid for it to be called an LNAPL (Light Non-Aqueous Phase Liquid) is that its density must be less than the density of water. It will therefore float on water, and in an aquifer will be found close to the phreatic surface of an unconfined aquifer, or at the top if the aquifer is confined. The other possibility (if the density contrast is small or the liquids are being agitated) is that an emulsion may form. This is the name given to the mixture where one liquid is suspended as colloidal particles in the other liquid.

Although LNAPLs are basically immiscible with water by definition, they will undergo some dissolution on contact with groundwater. The amount of partial dissolution depends on the properties of the LNAPL. For example lighter compounds such as the BTEX compounds (benzene, toluene, ethylbenzene and xylene) dissolve more readily than heavier long-chain hydrocarbons. The amount entering the groundwater depends on the solubility limits of the compounds in the LNAPL. Solubility limits are dependent on the mixture of compounds present in the LNAPL as well as the nature of each compound.

The actual concentration in the groundwater away from the LNAPL source is dependent on the amount of dilution by fresh water - solubility is only likely to be a limiting factor close to the source. The LNAPL thickness will probably not affect the dissolved concentration, as LNAPL availability is unlikely to be a limiting factor.

Once dissolved, hydrocarbons will migrate faster than the free-phase LNAPL on the water table, due to the process of dispersion caused by groundwater advection. In addition the

LNAPL may be slowed down compared to water because it has a lower mobility (the mobility of a liquid is equal to density÷viscosity).

In a multi-phase system the ability of each fluid component to flow is described by its *relative permeability*, which is a function of its saturation (Fetter, 1992). A fluid has an *irreducible saturation*, below which the relative permeability is zero and the fluid will not flow.

Towards the edge of the free-phase plume, the LNAPL will become immobile as its relative permeability reduces to zero as the saturation reduces to the irreducible saturation. These factors mean that the dissolved plume is likely to be larger than the free-phase plume, although it is at much lower concentrations.

3.1.2 LNAPL Phases

LNAPLs may exist in a porous medium in several different forms:

- Free phase. The LNAPL is occupying the entire effective void space of the soil.
- Mixed with air (for example around the air-LNAPL interface)
- Mixed with water (for example around the water-LNAPL interface)
- Mixed with air and water
- Adsorbed. This indicates LNAPL that is chemically attached to a material present in the soil. Such reactions are often reversible and this does not necessarily imply that the LNAPL will not detach from the soil at a later stage
- Dissolved. Although this appears to contradict the definition given above, small quantities of LNAPL (or chemical components of an LNAPL) can dissolve in the groundwater.

The behaviour of LNAPLs in the ground is ultimately a three-phase problem. At any point the effective porosity of the soil matrix is shared by air, LNAPL and water with the proportion of each measurable as a percentage saturation. The relative permeability of each component is dependent on its the percentage saturation.

3.1.3 Wettability

Any two fluids may be ordered in terms of their wetting ability with respect to a given solid. This can be decided according to the contact angle where the fluids interface against the solid: the fluid forming a contact angle less than 90° is the more wetting. In general, water is a wetting fluid compared to an oil-based LNAPL unless the solid is organic in character. Oils are wetting in comparison to air.

Imbibition is the displacement of the non-wetting fluid by the wetting fluid and drainage is the reverse process.

3.1.4 Retention in the Unsaturated Zone

When an LNAPL is released in the unsaturated zone of an aquifer, it will move in the same way as water - downwards. However a certain quantity of the LNAPL is usually left behind on the way. The retention can involve adsorption but more usually is a consequence of the reduction in the relative permeability of the LNAPL to zero below a certain percentage saturation. This is illustrated in Figure 3.1. Clearly once the LNAPL has entered a zone, the last 10% or so cannot drain.

Some authors have attempted to quantify the losses of LNAPL due to retention in this way. For example de Pastrovich *et al* (1979) gave the empirically-based figures in Table 3.1. These are consistent with the figure of 10% given above, remembering that it is around 10% of the effective porosity, which for a porosity of 20% is equivalent to 2% of the volume or 20 l/m^3.

Table 3.1 Retention Capacity

Soil	Oil Retention Capacity (l/m^3)		
	Low Viscosity e.g. gasoline	**Medium Viscosity e.g. kerosine, gasoil**	**High Viscosity e.g. light fuel oil**
Stones, Coarse gravel	2.5	5	10
Gravel, Coarse sand	4	8	16
Coarse sand, Medium sand	7.5	15	30
Medium sand, Fine sand	12.5	25	50
Fine sand, Silt	20	40	80

When the LNAPL then comes in contact with the groundwater, the interaction of the two fluids commences. This process involves a number of concepts which will be explained in the subsequent sections. However at this point it is enough to observe that the LNAPL can arrive in sufficient quantities that a layer of free product can 'float' on the surface of the groundwater. This is frequently the case after major oil spills or pipeline ruptures. The floating layer is sometimes referred to as a 'pancake.'

3.1.5 Capillarity

Capillarity is the ability of a liquid to rise above its piezometric elevation when in contact with a solid because of surface tension. Surface tension allows the maintenance of a difference in pressure across an interfacial surface. In the case of a water-air interface the phenomenon allows water to climb up the narrow tubes formed by the pore spaces to above the level that water in equilibrium with atmospheric pressure would rest (the piezometric elevation). The water above this level has pressure less than atmospheric because at the interface between water and air the pressure discontinuously 'jumps' back up to atmospheric pressure. This pressure below atmospheric is often conceptualised as 'negative pressure.'

It is this phenomenon whereby the 'capillary fringe' forms on unconfined aquifers. For a metre or more above the piezometric surface the soil remains fully saturated, only falling away to the retention capacity above this point. The actual size of the capillary zone depends on the sizes of the pore spaces: narrow tubes cause greater tension forces which cause a larger capillary zone. The equation for the height of a capillary column in a tube is:

$$h = 2\sigma \cos \theta / \rho g r \qquad (3.1)$$

where h is the height of the column (m)
σ is the surface tension (N/m)
θ is the contact angle with the wall of the tube
ρ is the density of the fluid (kg/m^3)
g is the acceleration due to gravity (m/s^2)
r is the radius of the tube (m).

From equation (3.1), the height of the capillary column of clean water in a glass tube can be calculated. For a water-glass system, θ is taken to be zero and the surface tension of water/air is approximately 73×10^{-3} N/m so that:

$$h = 1.5\times10^{-5}/r \qquad (3.2)$$

where h is the height of the column (m)
r is the radius of the tube (m)

In a well-sorted material the tubes may all be similar in size so the capillary zone has a sharp upper surface. In graded materials there may be a lot of variation in the height of the zone. At the macroscopic scale this can result in a much slower transition from full saturation to retention capacity.

Although the mathematical expression exists for the capillary pressure a fluid can generate in a tube of a given radius this is not transferable to the complex soil system. More empirical

approaches have to be taken. In equilibrium, a soil exhibits a natural relationship between the height of the fluid above the piezometric elevation (equivalent to capillary pressure, p_{AW}) and the soil saturation. Rose and Bruce (1949), Brooks and Corey (1964) and Van Genuchten (1980) have all proposed mathematical expressions for the shape of these curves. Mishra *et al* (1989) provide an account of the various experimental methods for derivation of saturation and permeability curves from Particle Size Distribution Data.

The situation is further complicated by hysteresis. As shown in Figure 3.2, the saturation curves are different according to whether imbibition or drainage is taking place. This is because of the variability of pore diameter: on wetting, the imbibing liquid will progress until it reaches a pore which is too large for the liquid to enter under capillary pressure. During drainage, liquid movement is controlled by the narrower diameter pores and liquid may remain at a higher constriction, so that there is a higher saturation for a given pressure during drainage than during imbibition. Hysteresis also applies to the relative permeability curves which were illustrated in Figure 3.1.

However, it is often assumed that this curve may be condensed to a single number representing the average height of the 100% saturation level (or slightly less because of the irreducible air component above the water table). This concept is illustrated in Figure 3.3. The pressure associated with these rises is called the *displacement pressure* (or the 'bubbling pressure' in some texts) which is the change in pressure across the interface. From equation (3.1), the displacement pressure and capillary rise are related by:

$$p_{AW} = (\rho_W - \rho_A)\, g\, h \quad \approx \rho_W\, g\, H_C \qquad (3.3)$$

where H_C is the height of the top of the capillary zone above piezometric level (m)
p_{AW} is the air-water displacement pressure (N/m^2)
ρ_W is the density of water (kg/m^3)
ρ_A is the density of air (kg/m^3)
g is the acceleration due to gravity (m/s^2)

Table 3.2 gives typical values of the capillary rises in unconsolidated soils from two sources in the literature.

Table 3.2 Water Capillary Zone Thicknesses

Material	Capillary Rise (cm) Bear (1979)	Capillary Rise (cm) Lohman (1972)
Very Coarse Sand		6.5
Coarse Sand	2-5	13.5
Medium Sand	12-35	24.6
Fine Sand	35-70	42.8
Silt	70-150	105.5
Clay	>200-400	

Equations for these rises in terms of particle size parameters and porosity have also been developed (e.g. Mavis and Tsui, 1939, Polubarinova-Kochina, 1962 and Leverett, 1940). For example, Leverett's experiments suggested the empirical equation:

$$H_C = \frac{C\sigma\sqrt{\varphi}}{(\rho_W - \rho_A)g\sqrt{k}} \qquad (3.4)$$

where C is a constant equal to 0.29 for drainage (and 0.17 for imbibition)
k is the intrinsic permeability (m^2)
φ is the porosity.

3.1.6 Sharp Interface Theory

The description of the capillary zone using a single displacement pressure as a well-defined zone with an upper surface across which the pore pressure changes by the displacement pressure is known as the sharp interface model. This conceptual model of a sharp interface between the two fluids is not totally accurate but it assists a great deal in explaining the processes that occur when an LNAPL arrives at the water table.

The interface between LNAPL and water behaves in a similar way as that between air and water. The surface tension forces between LNAPL and water allow a discontinuity in the pore pressure curve. The pressure curve increases by the water-LNAPL displacement pressure from below the interface to above the interface. This is illustrated in Figure 3.4.

Figure 3.4 also demonstrates the concept of 'mobile LNAPL.' When the pore pressure is positive the LNAPL becomes mobile (or in some texts the word 'free' is used). This implies that the LNAPL can move laterally into a well.

Figure 3.4 shows some residual air saturation at the top of the mobile water. This is due to air being entrapped during imbibition. Below the zone of water table fluctuation, the air saturation is zero because, given enough time, entrapped air will dissolve in the groundwater.

3.1.7 Arrival of LNAPL

When the LNAPL arrives at the top of the water capillary zone some authors contend that it 'piles up' at this point until adequate pressure is generated to displace the water from the pore spaces (e.g. Blake and Hall, 1984). This implies that the water capillary zone remains the same thickness until the oil becomes mobile. This is not what happens according to the conceptual model described above. Evidence from laboratory experiments also suggests that this is not the case and that the water capillary zone starts immediately thinning (e.g. Eckberg and Sunada, 1984). In practice this may be a consequence of the piezometric head rising rather than the LNAPL displacing water, depending on the transmissivity of the aquifer.

Scheigg (1984) suggests that as the LNAPL arrives, the capillary zone can reduce in height. This is a consequence of a single water-air interface changing into two interfaces close together: a water-LNAPL and a LNAPL-air interface. If the sum of the water-LNAPL and LNAPL-air displacement pressures is less than the water-air displacement pressure then the top of the capillary zone will adjust to a new level (before it is pushed downwards by the weight of the LNAPL). This is illustrated by a figure in Scheigg's paper which appears to show the top of the capillary surface falling by about 4 cm as the LNAPL arrives. However this phenomenon (the "virgin effect") has not been noted by any other authors.

In the longer term it can be assumed that the piezometric surface is at a constant elevation since water at depth will move in order to equalise the pressures. In this case, as more LNAPL arrives, it will push the LNAPL-water interface downwards and the LNAPL-air interface upwards. A mound will be formed and the LNAPL may then migrate laterally. The direction of migration will depend on the rate at which the LNAPL is arriving - the LNAPL will spread out in all directions away from the source until the plume is wide enough for all the LNAPL arriving to be taken away in the direction of the piezometric gradient. This is illustrated schematically in Figure 3.5.

It is instructive to consider the pressure curves against elevation as the LNAPL piles up on the water table. These have been experimentally verified by Abdul (1988) as shown in Figure 3.6. As the oil arrives the capillary fringe thins (b), then the oil reaches positive pressure (c) which means it forms an oil table and is mobile. Only after that does the water capillary zone finally disappear (d). In this example it is assumed that the process happens fairly quickly so that the water at depth does not flow away and the pressure increases as oil arrives. The constant factor in this case is the level of the oil-water interface.

3.1.8 Comments on Shape of LNAPL Plume

According to pressure theory, an LNAPL plume should spread out indefinitely until its relative permeability reduces to zero as its saturation reduces. In practice this process may be very slow such that a quasi-steady-state thickness is often reached which does not appear to thin any further.

The LNAPL can continue to be replaced at the arrival point (either because the leak still exists or because a thick saturated zone has smoothed out the original plug flow to a nearly constant rate of addition). This process will also cause a steady-state thickness to be sustained.

It can also be the case that the LNAPL may migrate with the regional water table gradient. This can cause a plume to be spread out thinly over a large area.

A number of authors have investigated the effects of rising and falling water tables on LNAPL plumes (e.g. Hunt *et al*, 1993, Kemblowski and Chiang, 1990, and Yaniga, 1985). There seems no doubt that a rising water table tends to compress the LNAPL thickness and a falling water table tends to increase the LNAPL thickness. This is a result of hysteresis, although the process may also be partly a result of transient effects.

3.2 Exaggeration Effect

3.2.1 Sharp Interface Theory

The 'exaggeration effect' is the phenomenon whereby a borehole drilled and screened through an LNAPL pancake and in good hydraulic contact with the aquifer does not reflect the true depths of the top and bottom of the LNAPL layer in the ground. As has been commonly observed, the thickness measured in the well will be much larger than the actual thickness in the ground. This observation is explained by the 'sharp interface theory,' as illustrated in Figure 3.7.

The upper surface of the LNAPL in the borehole will generally be lower than that in the ground because LNAPL can only flow into the well if the pore pressure is positive. The fully saturated LNAPL capillary zone will not directly affect the level in the well. The bottom of the LNAPL layer in the well usually will have to be much lower than that in the ground in order to reduce the pressure head in the well because of the displacement pressure between water and LNAPL.

By careful consideration of the pressures involved in Figure 3.7, it can be shown that

$$T_G = T + p_{AL}/\rho_L g \; - \; p_{LW}/g(\rho_W - \rho_L) \qquad (3.5)$$

where T_G is the actual thickness of LNAPL in the ground (m)
T is the observed thickness of LNAPL in the borehole (m)
p_{AL} is the air-LNAPL displacement pressure (N/m^2)
p_{LW} is the LNAPL-water displacement pressure (N/m^2)
ρ_L is the density of the LNAPL (kg/m^3)

Note on units: Frequently the displacement pressures are quoted in m H_2O (displacement equivalent height) rather than the SI units given above - if this is the case replace p in the above equations by $hg\rho_W$ where h is the displacement equivalent height (in m H_2O).

The first term in the above equation ($p_{AL}/\rho_L g$) represents the capillary zone of the LNAPL. The second term represents the difference between the base of LNAPL in the well and the base in the aquifer.

It is unfortunate that, the only easily measurable parameters in the field (top of LNAPL in well, bottom of LNAPL in well, density of LNAPL) will allow the calculation of the piezometric elevation but not the true thickness of LNAPL in the aquifer. Since the displacement pressures are unknown, T_G cannot be calculated from equation (3.5).

The exaggeration effect was probably first noted by Van Dam (1967) although Zilliox and Muntzer (1975) were the first to derive the above equation. Most authors have been able to accept the above equation and have directed their efforts in to trying to find ways of quantifying or simplifying the above equation. De Pastrovich's suggestion in CONCAWE (1979) that the effect could be approximated as a multiplicative factor (T_G = T/4) was a little over-simplistic and led the effect being widely referred to as the exaggeration factor. In fact it is purely additive in the equation above.

The logic of de Pastrovich's deduction is reproduced for completeness: if the mobile phase is assumed to be very thin then $T_G = p_{AL}/\rho_L g$ and $T = p_{LW}/g(\rho_W-\rho_L)$. If we then also assume $p_{AL} = p_{LW}$ and $\rho_L = 0.8\ \rho_W$ then we have $T_G = T/4$.

One of the consequences of this sharp interface version of the theory is that as LNAPL builds up, it does not move into the well until a certain threshold is reached. At this point, when $T_G = p_{AL}/\rho_L g$, the LNAPL becomes mobile as its pressure becomes larger than zero and suddenly the well fills up to a thickness of $p_{LW}/g(\rho_W-\rho_L)$. In effect the thickness in the well is defined by:

$$\begin{array}{ll} T = 0 & T_G < p_{AL}/\rho_L g \\ T_G - p_{AL}/\rho_L g + p_{LW}/g(\rho_W-\rho_L) & T_G > p_{AL}/\rho_L g \end{array} \qquad (3.6)$$

The threshold thickness of LNAPL which appears in the well is usually referred to as critical thickness $p_{LW}/g(\rho_W-\rho_L)$.

Observations in the field frequently suggest that this does not happen and this discrepancy will be discussed in detail in Section 3.3.

Figures 3.8 and 3.9 show in section the way an LNAPL layer will build up. The difference between these two illustrations is that the first assumes the piezometric surface remains constant across the graph and the second assumes the LNAPL-water interface remains constant. In other words the first represents a 'constant head' boundary - for example an older plume where the pressures at depth have equalised, plotted with the x-axis representing distance. The other figure is more like a plot against time during a rapid arrival of LNAPL. The head builds up and the deep boundary is effectively no-flow. This second diagram is more relevant in the consideration of sand tank experiments.

3.2.2 Displacement Pressures

Apart from de Pastrovich mentioned above, several other authors have tried to simplify equation (3.5) and make it more applicable. The measurement of p_{AL} and p_{LW} in particular are not very easy although occasionally p_{AW} is available, for example from measurement of capillary rise.

Lenhard and Parker (1987) note that these parameters can be estimated according to the ratios of the surface tension. The Zilliox Equation is modified to:

$$T_G = T + p_{AW}\sigma_{AL}/(\sigma_{AW}\rho_L g) - p_{AW}\sigma_{LW}/\sigma_{AW}g(\rho_W-\rho_L) \qquad (3.7)$$

where σ_{AL} is the surface tension between air and LNAPL (N/m)
σ_{AW} is the surface tension between air and water (72.5×10^{-3} N/m)

Equation (3.7) can also be expressed in terms of the air-water capillary thickness, H_C, as:

$$T_G = T + H_C\rho_W\sigma_{AL}/(\sigma_{AW}\rho_L) - H_C\rho_W\sigma_{LW}/\sigma_{AW}(\rho_W-\rho_L)$$

$$= T + H_C\rho_W/\sigma_{AW}\,[\sigma_{AL}/\rho_L - \sigma_{LW}/(\rho_W-\rho_L)] \qquad (3.8)$$

Using data derived from Weiss (1980) for 'gasolines,' Lenhard and Parker (1987) establish scaling factors of 3.2 (air-LNAPL) and 1.45 (LNAPL-water). This implies that

$$\beta_{AL} = 3.2 = p_{AW}/p_{AL} \text{ and } \beta_{LW} = 1.45 = p_{AW}/p_{LW} \quad (3.9)$$

where β_{AL} is the scaling factor for air-LNAPL
β_{LW} is the scaling factor for LNAPL-water.

Farr *et al* (1990) gives the surface tensions for aged gasoline as 22.5×10^{-3} N/m (air-gasoline) and 9.8×10^{-3} N/m (gasoline-water). This last figure is surprisingly low given the Lenhard and Parker (1987) ratios. The air-water surface tension is 72.5×10^{-3} N/m which implies that

$$\beta_{AL} = 3.2 \text{ and } \beta_{LW} = 7.40$$

These figures can be used to express the exaggeration equation in terms of the capillary rise for water. Since the capillary rise for water in air is $H_C = p_{AW}/\rho_W g$ we have:

$$T_G = T + H_C \rho_W/\beta_{AL} \rho_L - H_C \rho_W/\beta_{LW} (\rho_W-\rho_L) \quad (3.10)$$

$$\text{or} \quad T_G = T + \frac{H_C \rho_W}{\sigma_{AW}} \left[\frac{\sigma_{AL}}{\rho_L} - \frac{\sigma_{LW}}{\rho_W - \rho_L} \right] \quad (3.11)$$

and therefore using a relative density of 0.8 for gasoline

$$T_G = T + 0.39\, H_C - 3.45\, H_C \approx T - 3.1\, H_C \text{ (Lenhard and Parker, 1987)} \quad (3.12)$$

$$T_G = T + 0.39\, H_C - 0.68\, H_C \approx T - 0.3\, H_C \text{ (Farr } et\ al\text{, 1990)} \quad (3.13)$$

Scheigg (1984) uses a similar method to derive the following relation

$$T_G = T + 0.3\, H_C - 2.2\, H_C = T - 1.9\, H_C \quad (3.14)$$

Although the first term (relating to the LNAPL-air capillary zone) is similar, the second term is markedly different, particularly because of Farr (1990)'s low value for the surface tension of 'aged gasoline.'

In a recent paper, Busby, Lenhard and Rolston (1995), the relations between the various displacement pressures are considered in more detail. By comparing the saturation curves, Busby *et al* (1995) conclude that the shapes are basically the same and therefore only scaling factors are needed to convert from one to the other. These scaling factors are, in effect, the ratios that we require. Unfortunately in their experiments they only used toluene, Soltrol 170® (a branched alkane) and trichloroethylene (or TCE, a DNAPL). The scaling factors produced are given in Table 3.3. The coefficients in the exaggeration equation have been calculated using densities of 0.785 for Soltrol and 0.865 for toluene.

Table 3.3 Scaling Factors for Various LNAPLs and Porous Media

	Scaling factor, β Air-LNAPL	Scaling factor, β LNAPL-water	Implied first coeff	Implied second coeff	Total multi-plier
Soltrol in quartz sand	2.93	1.66	0.43	-2.80	-2.4
Soltrol in Crozier Loam	2.94	1.86	0.43	-2.50	-2.1
Toluene in quartz sand	2.38	2.34	0.49	-3.17	-2.7
Toluene in Crozier Loam	2.81	2.75	0.41	-2.69	-2.3

These results cast some doubt on the theory that the ratios can be estimated from the surface tensions alone (and are independent of the soil) as suggested by Lenhard and Parker (1987) and Farr *et al* (1990).

Hall *et al* (1984) also concluded from sand tank experiments that the effect is additive (at least after a specified point) and derived a similar relationship as shown in Table 3.4.

Table 3.4 Exaggeration Effects in Coarse, Medium and Fine Sand

	T_G-T (cm)	Minimum Applicable T (cm)	H_C [from Table 3.2] (cm)	Implied Multiplier
Coarse sand	5	8	3.5	1.4
Medium Sand	7.5	15	23.5	0.3
Fine sand	12.5	23	52.5	0.2

The conclusion is that the exaggeration effect could be anything from 0.2 (Table 3.4) to 3.1 times (Equation 3.12) the water capillary zone thickness! However most of the results produce a multiplier in the range 2 to 3.

3.2.3 Advanced Theories

These theories have been developed in two important papers: Lenhard and Parker (1987) and Farr *et al* (1990). Their validity has been further endorsed by "Contaminant Hydrogeology," the well-known text book by Fetter (1993).

Essentially these theories consider the LNAPL saturation curves against depth produced by the Brooks and Corey (1966) equation and the Van Genuchten (1980) equations and integrate them vertically to produce a total quantity of LNAPL. These theories do not assume sharp interfaces but a gradual change from water to LNAPL to air as illustrated in Figure 3.10.

The details of the theories and their integrations are as follows:

Brooks-Corey Equations

This theory was developed in an important paper published in 1966 by Brooks and Corey.

Ignoring the residual saturation of water the equations proposed for saturation with reference to Figure 3.7 are given in Table 3.5. In this table, p_W is the solid pressure line in the water zone in Figure 3.7 extended upwards and p_L is the solid pressure line in the capillary zone extended upwards.

Table 3.5 Brooks-Corey Saturation Equations

	Saturation of Air (S_A)	**Saturation of LNAPL (S_L)**	**Saturation of Water (S_W)**
AIR	$1-[-p_{AL}/p_L]^{\lambda}$	$Max(1-S_W-S_A, 0)$	$[p_{LW}/(p_L-p_W)]^{\lambda}$
LNAPL CAP ZONE	0	$1-S_W$	$[p_{LW}/(p_L-p_W)]^{\lambda}$
LNAPL MOBILE	0	$1-S_W$	$[p_{LW}/(p_L-p_W)]^{\lambda}$
WATER CAP ZONE	0	0	1
WATER	0	0	1

The parameter, λ, in the above table is the Brooks-Corey pore size distribution index which increases with uniformity of soil. Typically for real soils it ranges from 1 to 5.

Integration of the above equations leads to the expression below:

$$V = \phi[T - \lambda D/(\lambda-1) + (D/T)^{\lambda}T/(\lambda-1)] \qquad (3.15)$$

where V is the volume of LNAPL per unit area (m)

ϕ is the effective porosity (i.e. excluding the residual saturation)

$D = p_{AL}/\rho_L g - p_{LW}/g(\rho_W-\rho_L)$

If λ is large, this equation simplifies to $V = \phi[T - D]$ which is the same equation as (3.5) above and represents the sharp interface case. Some authors have been confused by the change of units between volume per unit area and thickness which of course requires multiplication by a porosity term.

Van Genuchten Equations

These equations are based on more recent work by Van Genuchten (1980). Three parameters are required for this formulation. The equations are shown in Table 3.6.

Table 3.6 Van Genuchten Saturation Equations

	Saturation of Air (S_A)	**Saturation of LNAPL (S_L)**	**Saturation of Water (S_W)**
AIR	$1-[1+\alpha_{LW}^{n}(-p_L)^n]^{(n-1)/n}$	$Max(1-S_W-S_A,0)$	$[1+\alpha_{AL}^{n}(p_L-p_W)^n]^{(n-1)/n}$
LNAPL CAP ZONE	$1-[1+\alpha_{LW}^{n}(-p_L)^n]^{(n-1)/n}$	$Max(1-S_W-S_A,0)$	$[1+\alpha_{AL}^{n}(p_L-p_W)^n]^{(n-1)/n}$
LNAPL MOBILE	$1-[1+\alpha_{LW}^{n}(-p_L)^n]^{(n-1)/n}$	$Max(1-S_W-S_A,0)$	$[1+\alpha_{AL}^{n}(p_L-p_W)^n]^{(n-1)/n}$
WATER CAP ZONE	0	$1-S_W$	$[1+\alpha_{AL}^{n}(p_L-p_W)^n]^{(n-1)/n}$
WATER	0	$1-S_W$	$[1+\alpha_{AL}^{n}(p_L-p_W)^n]^{(n-1)/n}$
WATER below base of LNAPL in well	0	0	1

In the above expressions it is clear that n is related to λ in the Brooks-Corey formulation and that α is related to the displacement pressures.

The integration of this solution is unfortunately not possible analytically and must be done numerically.

The proportions of air, water and LNAPL derived from these equations are shown in Figure 3.10. It is interesting to note that the main difference between these two is that the Van Genuchten formulation predicts 'tails' of LNAPL and air extending below the top of the capillary zones beneath. This is not in accordance with the basic definition of the capillary zone (Section 3.1.5) which implies 100% saturation is still present at the top (see Figure 3.3). It may, however, be more realistic.

3.3 Case Study Data Analysis

3.3.1 Sand Tank Studies

These sort of experiments are fairly easy to arrange and ought to provide good validation of the theory both in the ground and in the interaction with wells. However although the pressure systems in the soil have usually agreed with the theory there are clearly some other phenomena interfering with the interactions with wells.

The following accounts of sand tank studies have been identified:

i) Abdul, Kia and Gibson (1989)

This paper includes a good demonstration that the classical theory as demonstrated in Figure 3.6 is closely matched by reality in the ground. Abdul *et al*'s sand column showed a water capillary zone of 23 cm and used diesel oil. The oil-water displacement pressure was measured to be 10 cm H_2O. A plot of the thickness of LNAPL in the soil and in the well is shown in Figure 3.11 and a plot of the full dataset in Figure 3.12. The match in both graphs is reasonable although the slope of the points in Figure 3.12 is a little shallower than the expected slope of 1. The lines have been generated using data provided by Abdul *et al* (including an oil-air displacement pressure of 14 cm H_2O which corresponds to a capillary fringe of 16 cm as measured by Abdul *et al*) with the exception of the oil density which is not presented in the paper and has been assumed to be 0.85 g/cm^3.

Incidentally the sum of the air-oil and oil-water displacement pressures is 24 cm, which according to Scheigg (1984)'s "virgin effect" theory (Section 3.1.7) means the capillary zone should rise by 1 cm as the oil arrives - too small to be observable.

ii) Ballestero, Fielder and Kinner (1994)

The data provided in this paper has been analysed in the same way as the Abdul *et al* (1989) data (Figures 3.13 and 3.14). Ballestero *et al* (1994) measured the top of the mobile LNAPL because they used a series of piezometers. The density was provided in this paper (0.78 g/cm^3 for unleaded gasoline) but the displacement pressures were matched (air-gasoline 0.4 cm H_2O and gasoline-water 5.0 cm H_2O). The data fit is good although there is again a suggestion that the gradient of the thickness plot is less than 1.

Ballestero *et al* (1994) attempted a comparison of the various predictive equations although he has not fully understood that all are essentially additive with the exception of his own theory and de Pastrovich's (the factor of four). His own theory apparently follows that of Blake and Hall (1984) although the connection is not obvious to us. The theory claims that the line in the product plot graph (e.g. Figure 3.14) will be at a shallower gradient:

$$T_G - H_L = (1-\rho_L/\rho_W)T - H_C \qquad (3.16)$$

where H_L is the capillary thickness of LNAPL (m)

Equation 3.16 is true but H_C is not a constant as assumed by Ballestero. This theory depends on a layer of mobile product forming on top of the water capillary zone but not compressing it. Nevertheless, the fact that the data points for the base of the water capillary zone are slightly beneath the expected line in Figure 3.13 is consistent with the equation. A possible reason for the flatter lines is that the sand tank has not been left long enough to reach equilibrium after each addition of gasoline.

According to Ballestero *et al* (1994), after the thickness of mobile LNAPL exceeds a certain number the gradient increases to 1. According to his own calculations this happens after the thickness exceeds 23.3 cm but the maximum reached in his experiment is 5.5 cm. These values are determined using maximum and minimum displacement pressures derived from the tube equation. Ultimately the additive exaggeration effect predicted by Ballestero *et al* (1994) is over 80 cm, which, considering the water capillary zone is a mere 3 cm, does not seem likely.

On the whole, the Ballestero *et al* (1994) theory seems unlikely and the data do not seem to bear out the theory - a best-fit line has the gradient 0.374. Nonetheless the reasons for the flatter gradients observed by both Ballestero *et al* (1994) and Abdul *et al* (1989) remains unexplained.

iii)Blake and Hall (1984) and Hall *et al* (1984)

The data presented in these papers have not been tabulated but we reproduce one of their figures as Figure 3.15 to show its similarity to Figures 3.13 and 3.11. These data points do not show the flatter gradients mentioned above but demonstrate a gradient very close to 1. There is some evidence from this figure that oil is entering the well before the theory predicts.

Hall *et al* (1984) conclude that the effect is additive (and define a 'Formation Factor' which represents the difference) but note that this relationship is not very accurate below a certain threshold value (see Section 3.2.1). In the Blake and Hall (1984) paper the equation

$$T_G = T - D\,\rho_W/\rho_L$$

is introduced, where D is the portion of T below the water table. This is not so useful since it is fairly obvious that $D = T\,\rho_L/\rho_W$ which means $T_G = 0$. Later on in the paper it is suggested by worked example that the formation factor is $H_C\,\rho_L/(\rho_W - \rho_L)$ for reasons which are hard to follow.

iv) Hampton and Miller (1988)

This is a good paper reviewing a lot of earlier material and providing a good account of sand tank experiments. The phenomenon of LNAPL entering the wells before the LNAPL thickness has reached the critical thickness and become mobile is clearly demonstrated. Only one measurement is taken and it is at sub-critical thickness (the aquifer has 2.2 cm and the well 18.8 cm). The basic equation should still be valid (assuming LNAPL has been made mobile) and with Scheigg (1984)'s equation, the formation factor is 16.3 cm (very close to the observed 16.6 cm).

3.4 Miscellaneous Observations

3.4.1 Size of Well

Wells of larger diameter can take considerably longer to reach equilibrium because of the volume of LNAPL that has to flow into the wells. This has been observed by Chaffee and Weimer (1983), Cummings and Trenter (1986) and Hampton and Miller (1988). This last paper provides a very good indication that transient effects may frequently be influencing thicknesses. Hampton *et al's* 5 cm and 10 cm diameter wells both absorbed 18.8 cm of LNAPL within about a day (even showing some rebound and oscillation) while the 15 cm diameter well clearly approaches equilibrium exponentially taking about 20 days to reach 18.8 cm.

3.4.2 Sub-Critical Ingress

This theory is derived mainly from Hampton and Miller (1988). It appears that LNAPL can enter wells before it has reached the critical thickness that allows it to become mobile ($T_G > p_{AL}/\rho_{LG}$). It is thought that this is possible because of the existence of occasional larger pore spaces. In these spaces the displacement pressures are reduced, allowing LNAPL to compress the water capillary zone in isolated pores. The LNAPL then finds its way down to an elevation where it becomes mobile and enters the well (see Figure 3.16).

This same effect, it is surmised, could also allow gravel packs to act as conduits for LNAPL entry. Gravel packs will generally have displacement pressures considerably smaller than the aquifers in which they are placed.

This theory does not affect the Zilliox equation, but means that it may be valid for $0 > T_G > p_{AL}/\rho_{LG}$ (see Figure 3.17). However, in practice, transient effects complicate the situation, and there may not be enough time for this thickness to be attained due to short term drainage of the larger pores around the borehole, before the LNAPL thickness in the soil increases.

Sub-critical ingress has been observed both by Blake and Hall (1984) and Hampton and Miller (1988). In figures in these papers, the top of the LNAPL in the well is clearly below the top of the water in the 'aquifer' and the system is known to be in steady-state. In the field it would also explain the existence of large numbers of wells where only one or two centimetres of LNAPL are observed in the well (i.e. less than the critical thickness). According to the sharp interface theory such thicknesses should not occur in steady-state unless the soil has a very low displacement pressure.

This effect has not been mentioned in the literature very much. Evidence suggests that it is a real phenomenon and should be taken into account.

3.4.3 Fissured Aquifers

The concepts mentioned above have been further developed to theorise about LNAPL distribution in fissured aquifers (e.g. the Chalk). This is shown in Figure 3.18. The surmised distribution between matrix and fissures has not yet been validated by field observations.

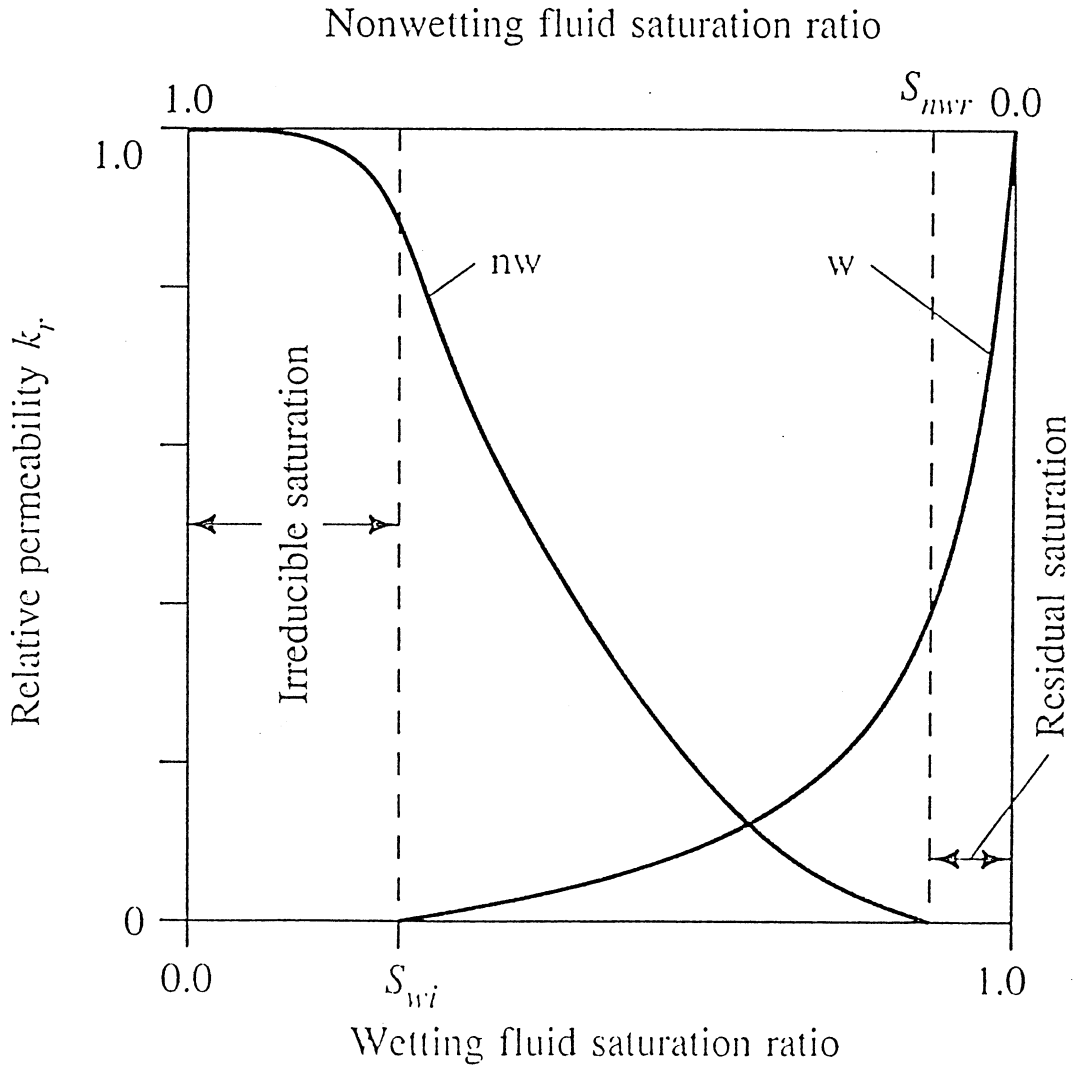

Figure 3.1 Typical relative permeability curves for a two-phase system (after Fetter, 1993)

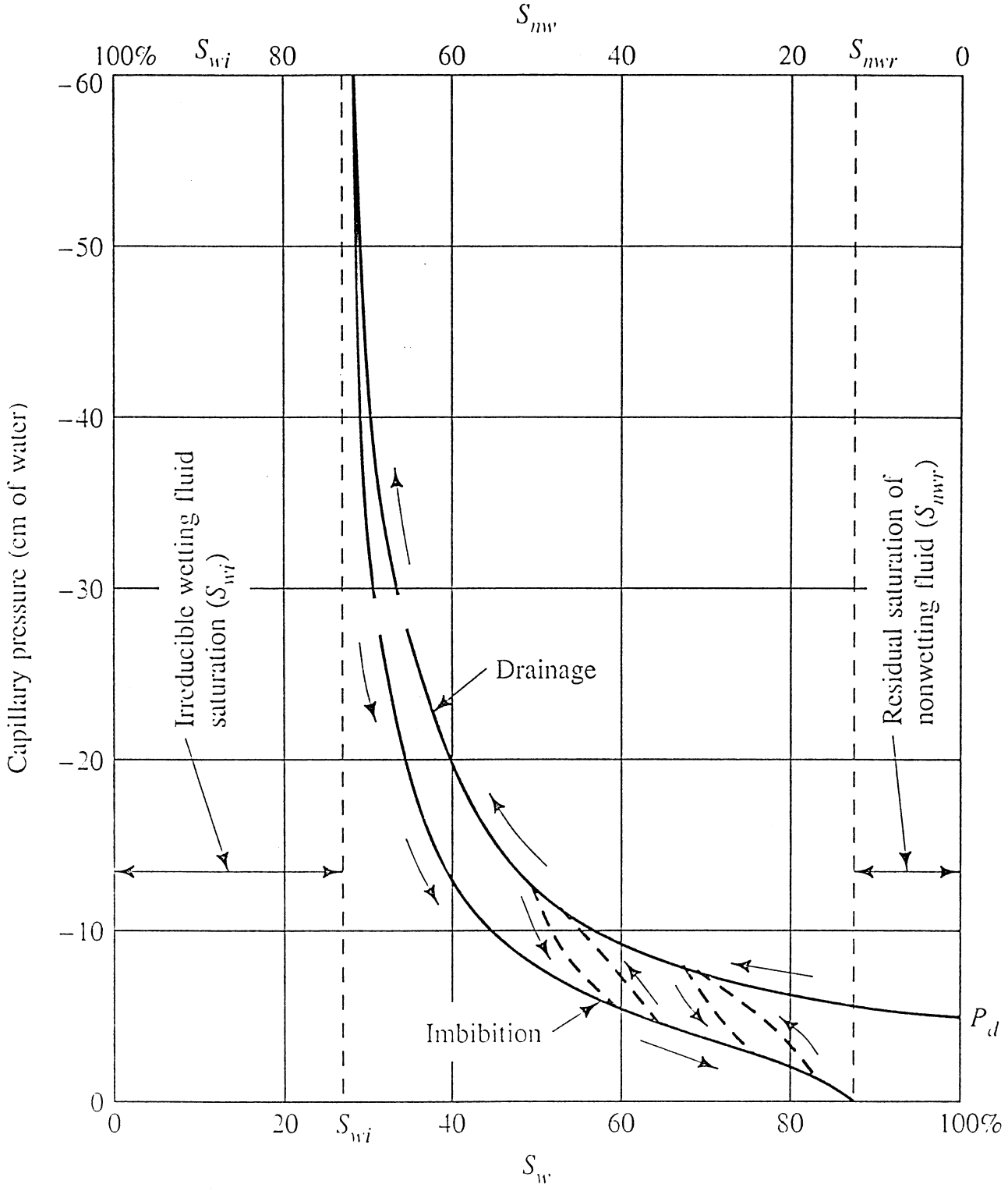

Figure 3.2 Capillary pressure-saturation curves for two-phase flow (after Fetter, 1993)

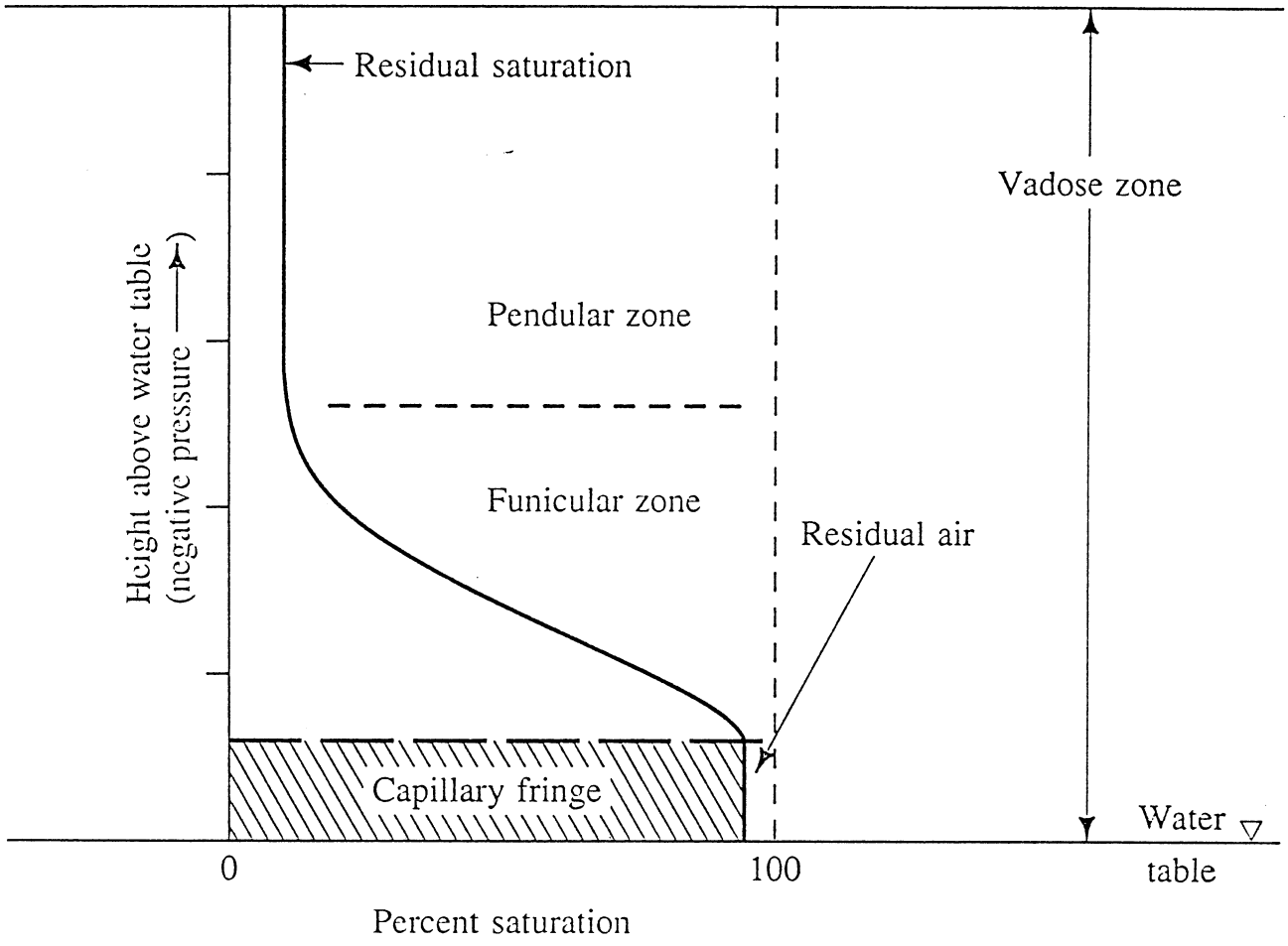

Figure 3.3 Vertical distribution of water in the vadose zone (after Fetter, 1993)

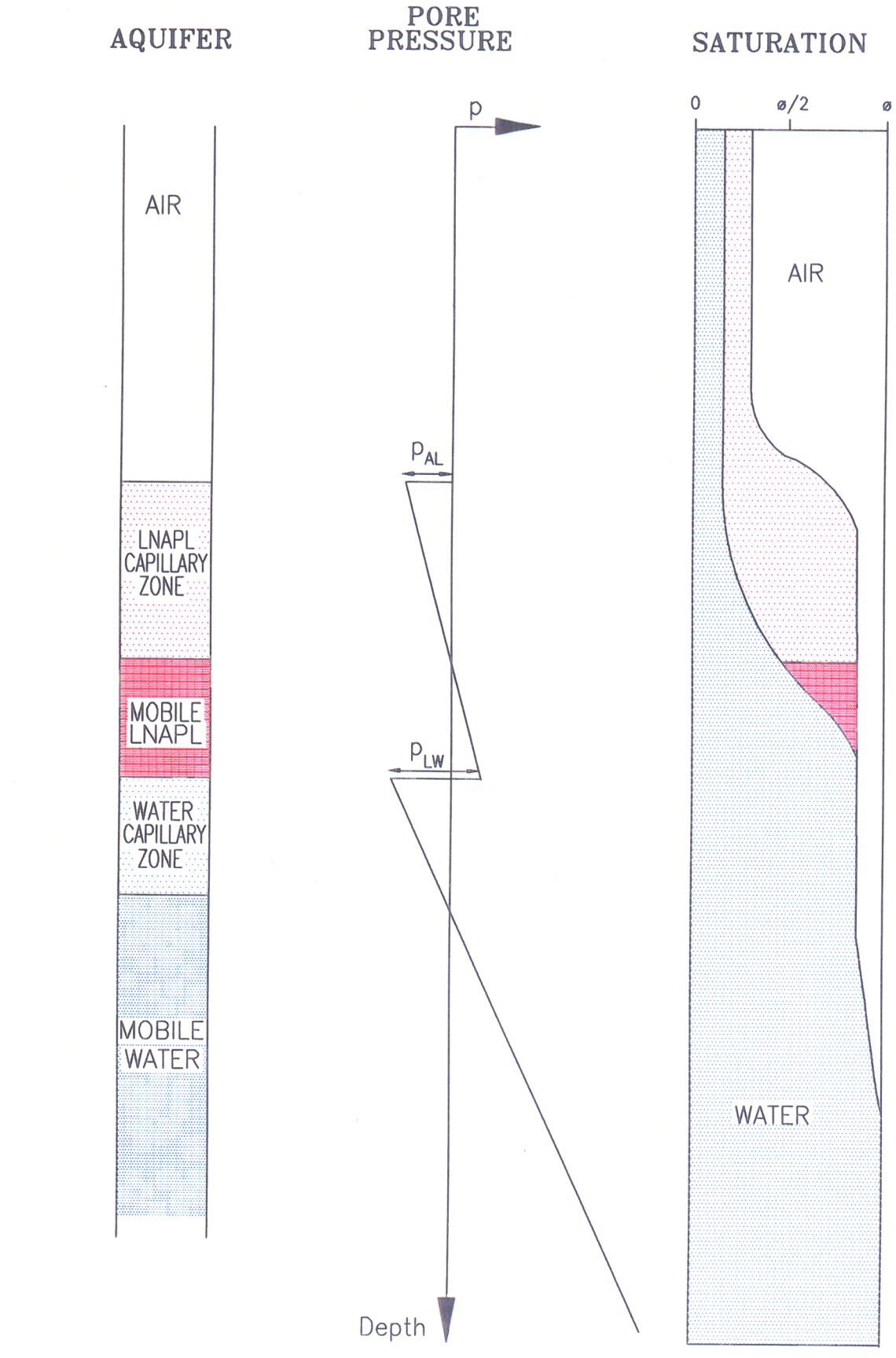

P_{LW} Water–LNAPL displacement pressure
P_{AL} Air–LNAPL displacement pressure
——— Pressure in Aquifer
ø Porosity

Figure 3.4 Interface between water and LNAPL

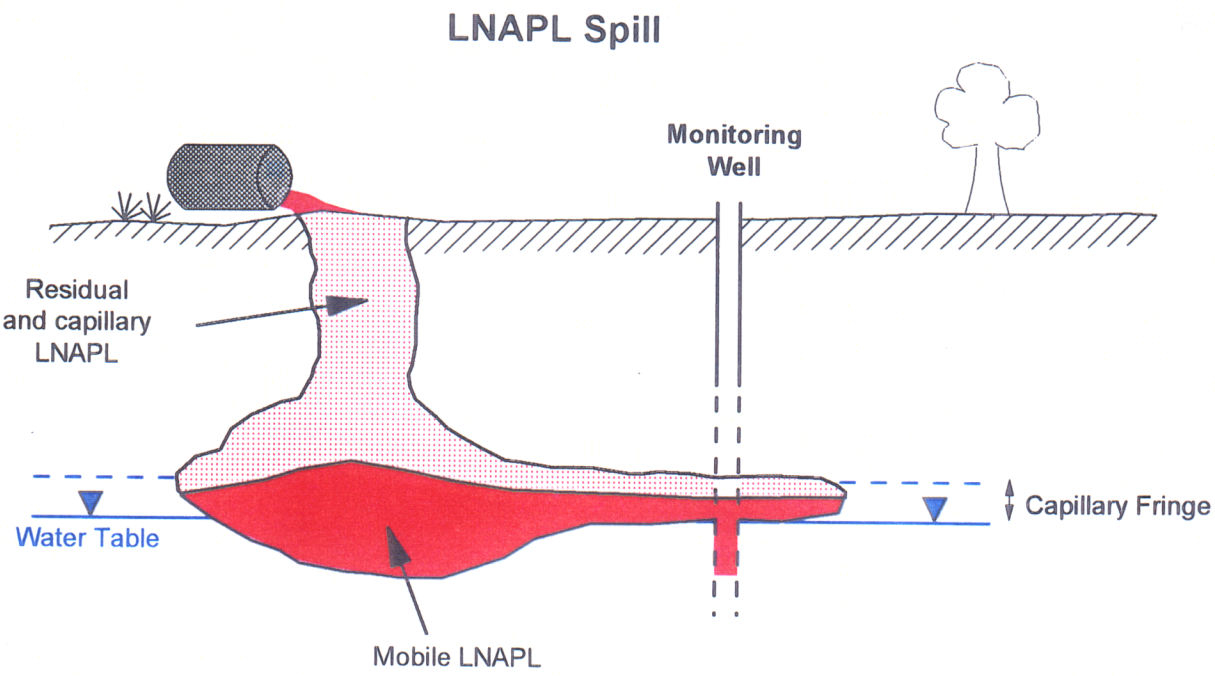

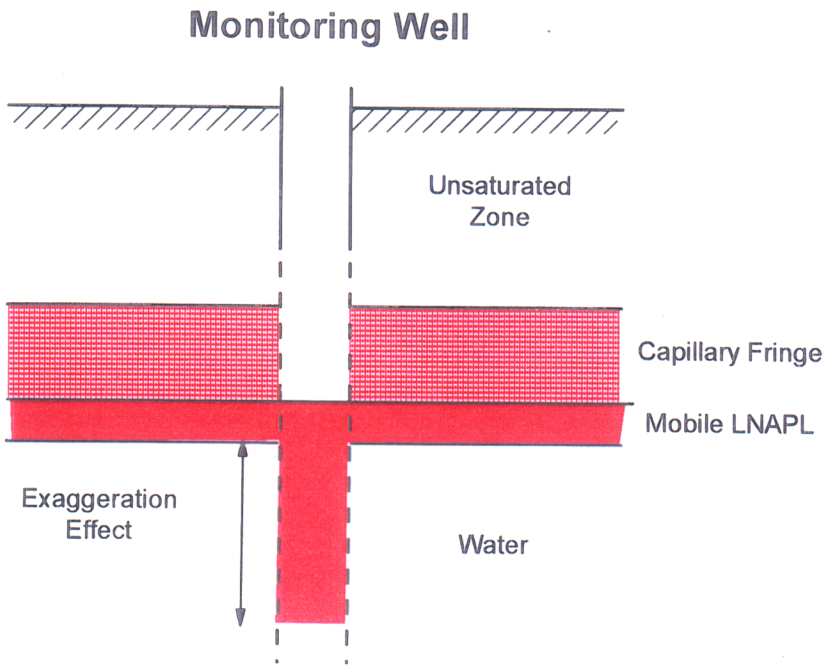

Figure 3.5 Schematic diagram of LNAPL spill in the ground and a monitoring well

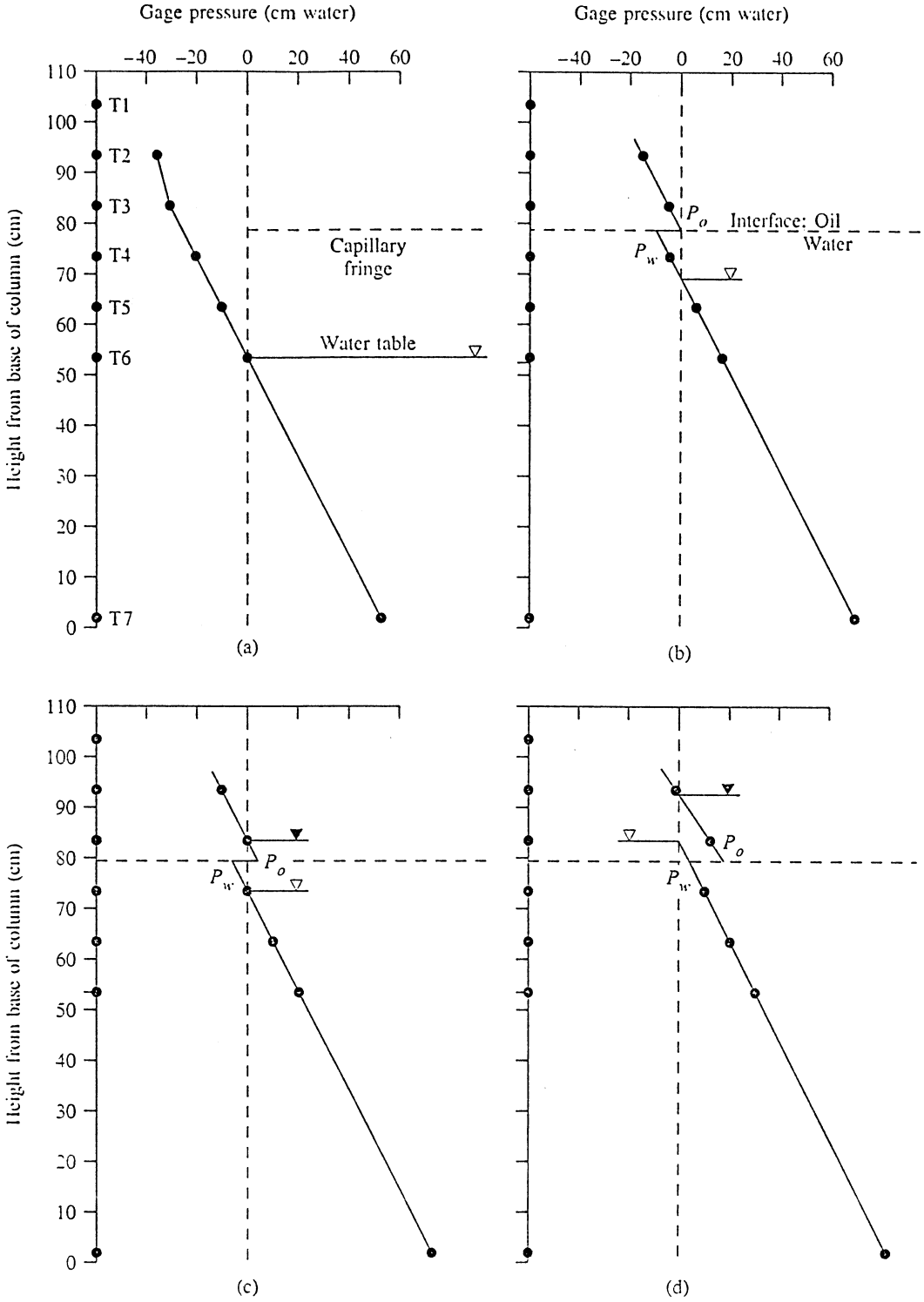

(a) Before the addition of the oil, (b) after addition of the oil showing the development of an oil fringe, (c) after addition of sufficient oil for an oil table to form, and (d) after sufficient mobile oil has accumulated to eliminate the water capillary fringe. *Source:* A. S. Abdul, *Ground Water Monitoring Review* 8, no. 4 (1988):73–81. Copyright © 1988 Water Well Journal Publishing Co.

Figure 3.6 **Pore pressure distribution in a sand column to which oil is being added to the top of the column (after Abdul, 1988)**

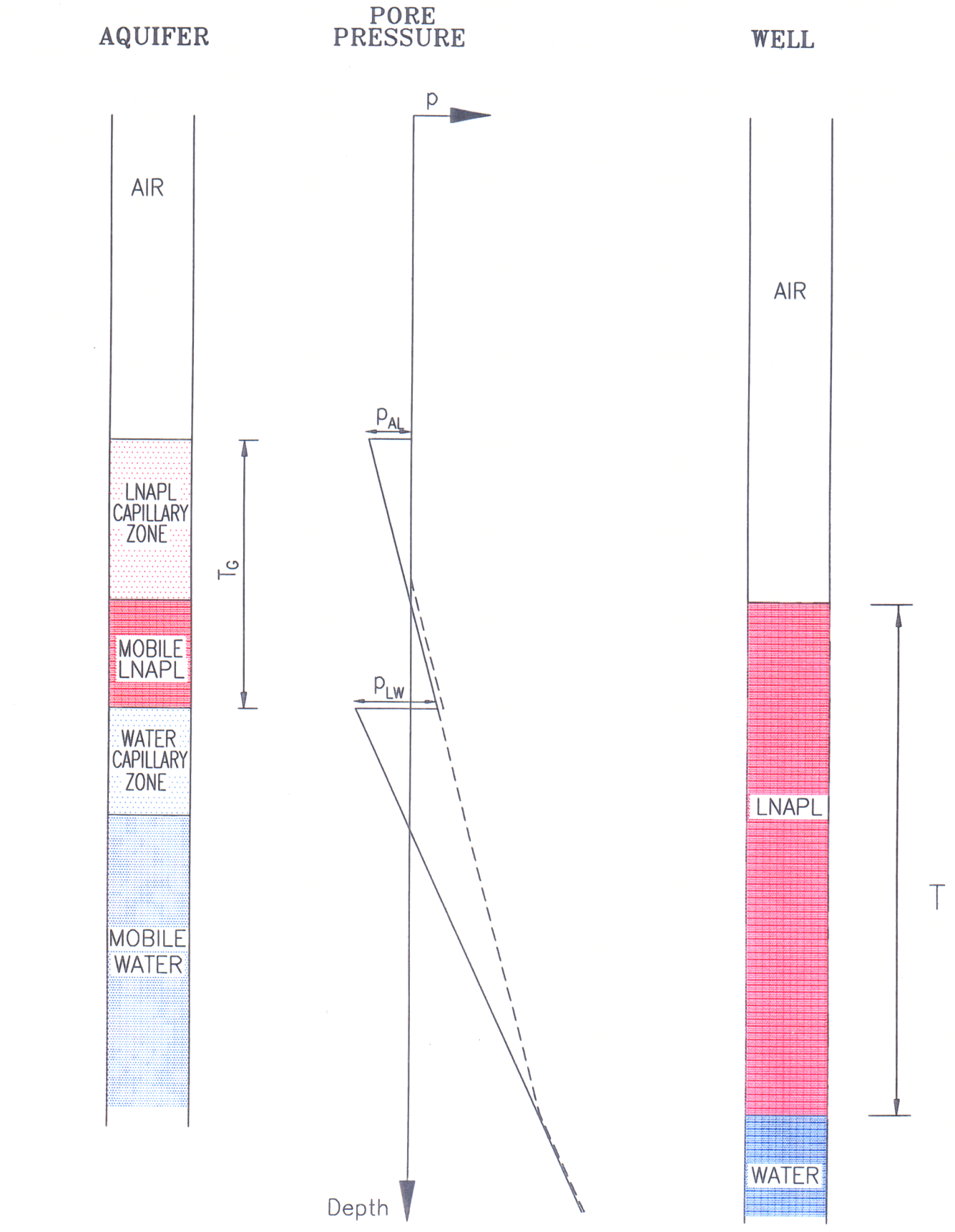

Figure 3.7 The Exaggeration Effect

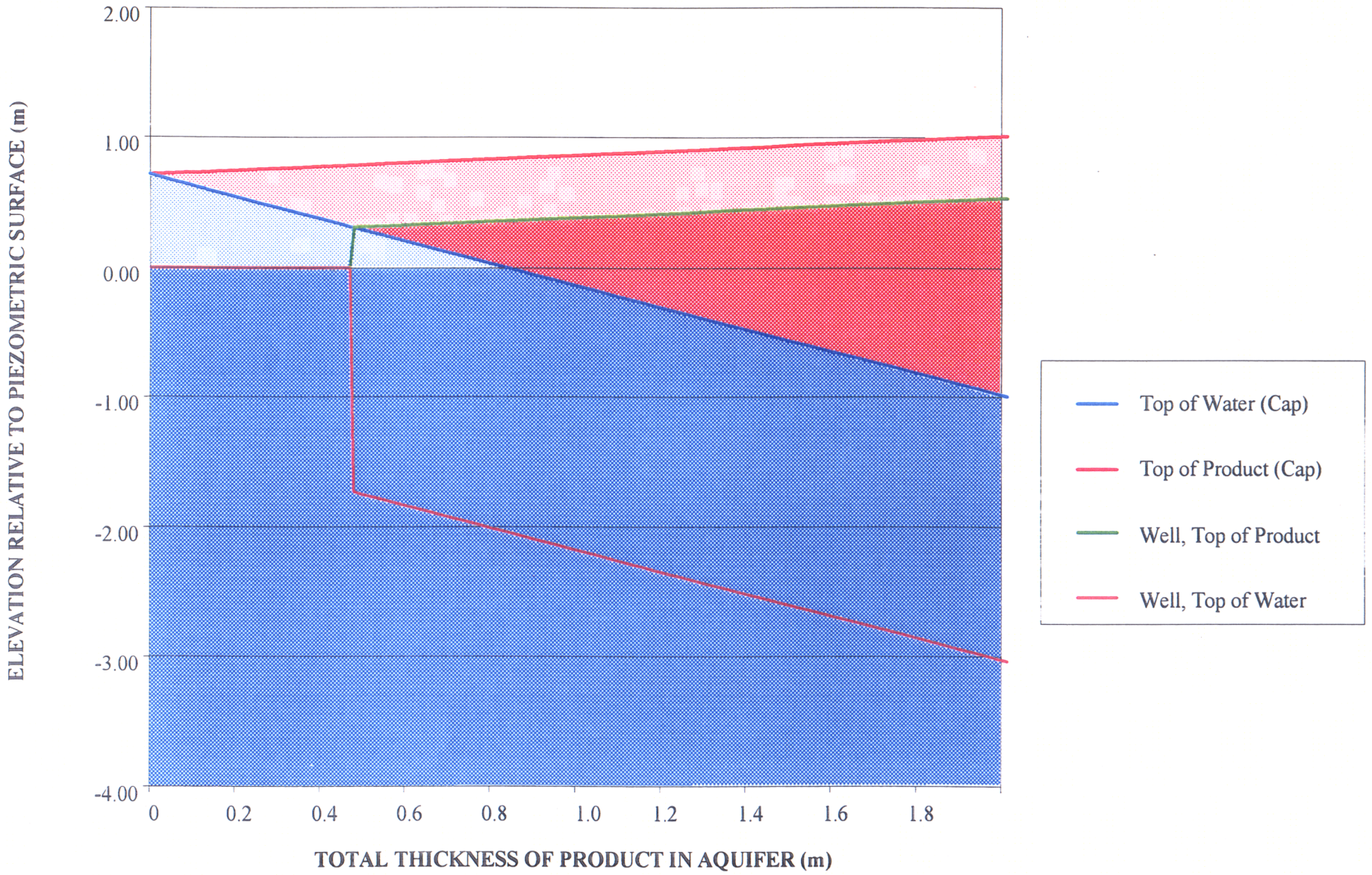

Figure 3.8 **Development of observed product elevations (Constant Pressure at Depth)**

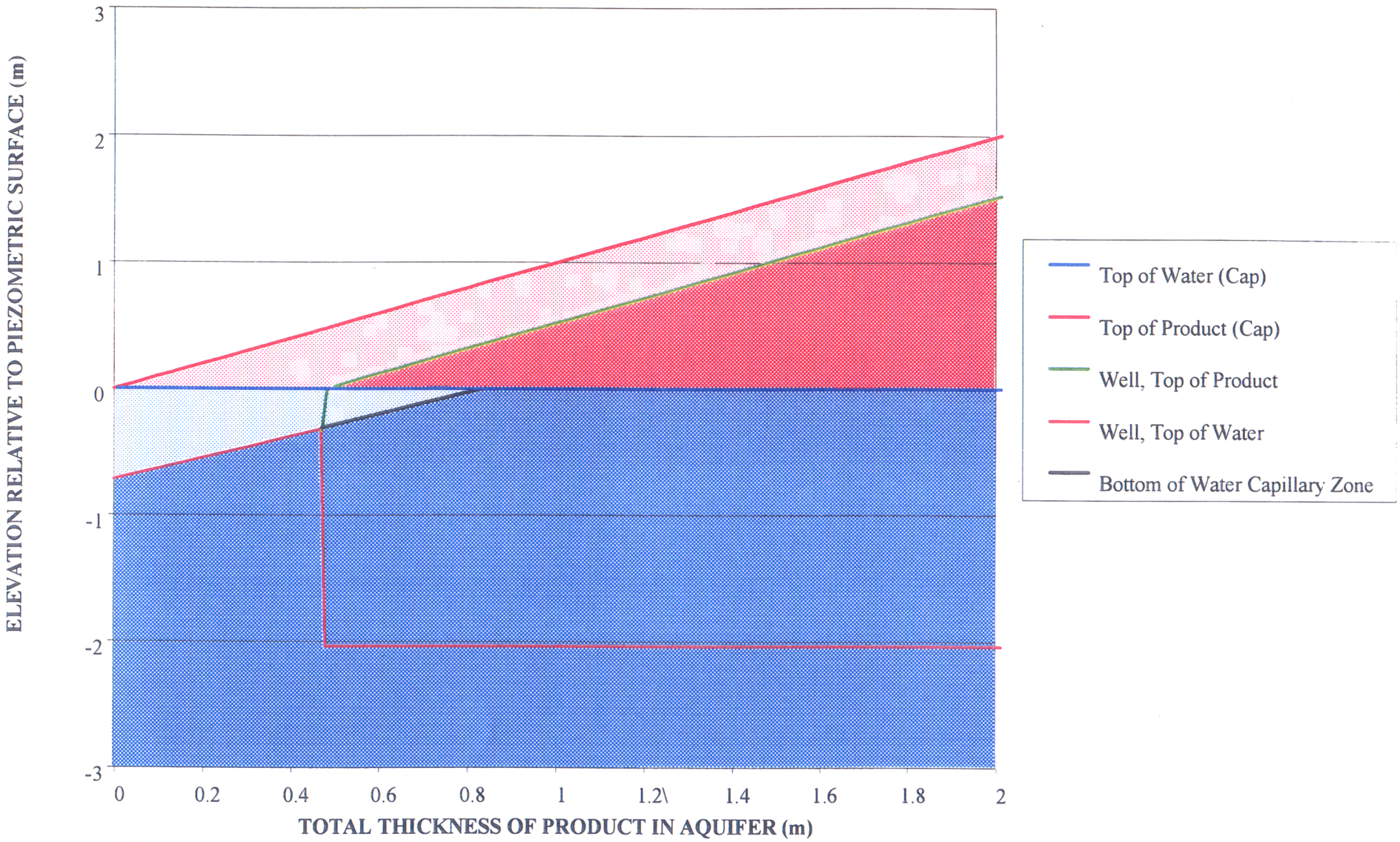

Figure 3.9 Development of observed product elevations (Constant Product-Water Interface)

Brooks-Corey Parameters:

$\lambda = 4$

p_{AL} = 0.35 m H_2O

p_{LW} =0.35 m H_2O

Van Genuchten Parameters:

$n = 7$

α_{AL} = 2.5 /m H_2O

α_{LW} = 2.5 /m H_2O

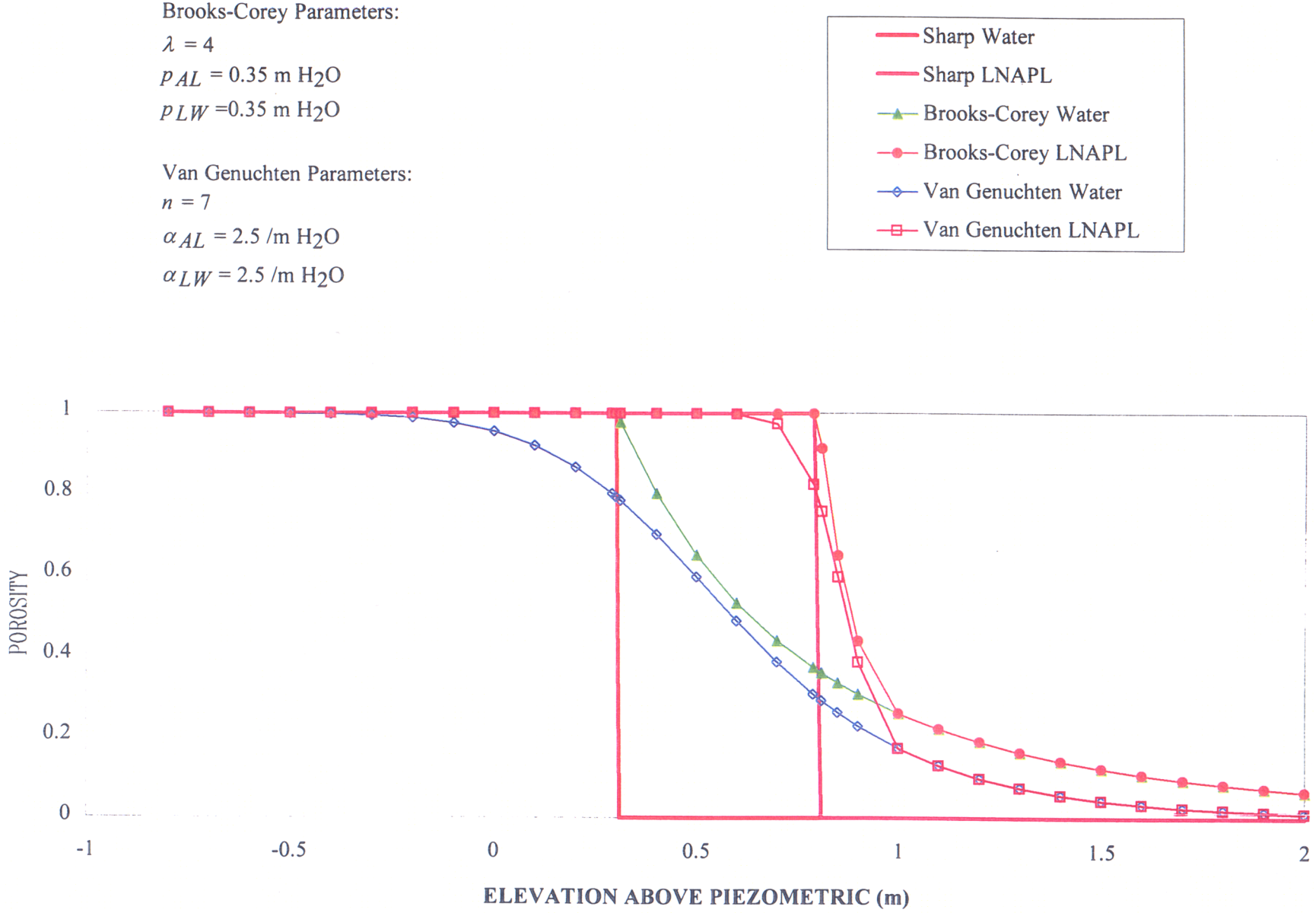

Figure 3.10 Comparison of saturations predicted by Brooks-Corey and Van Genuchten fomulae

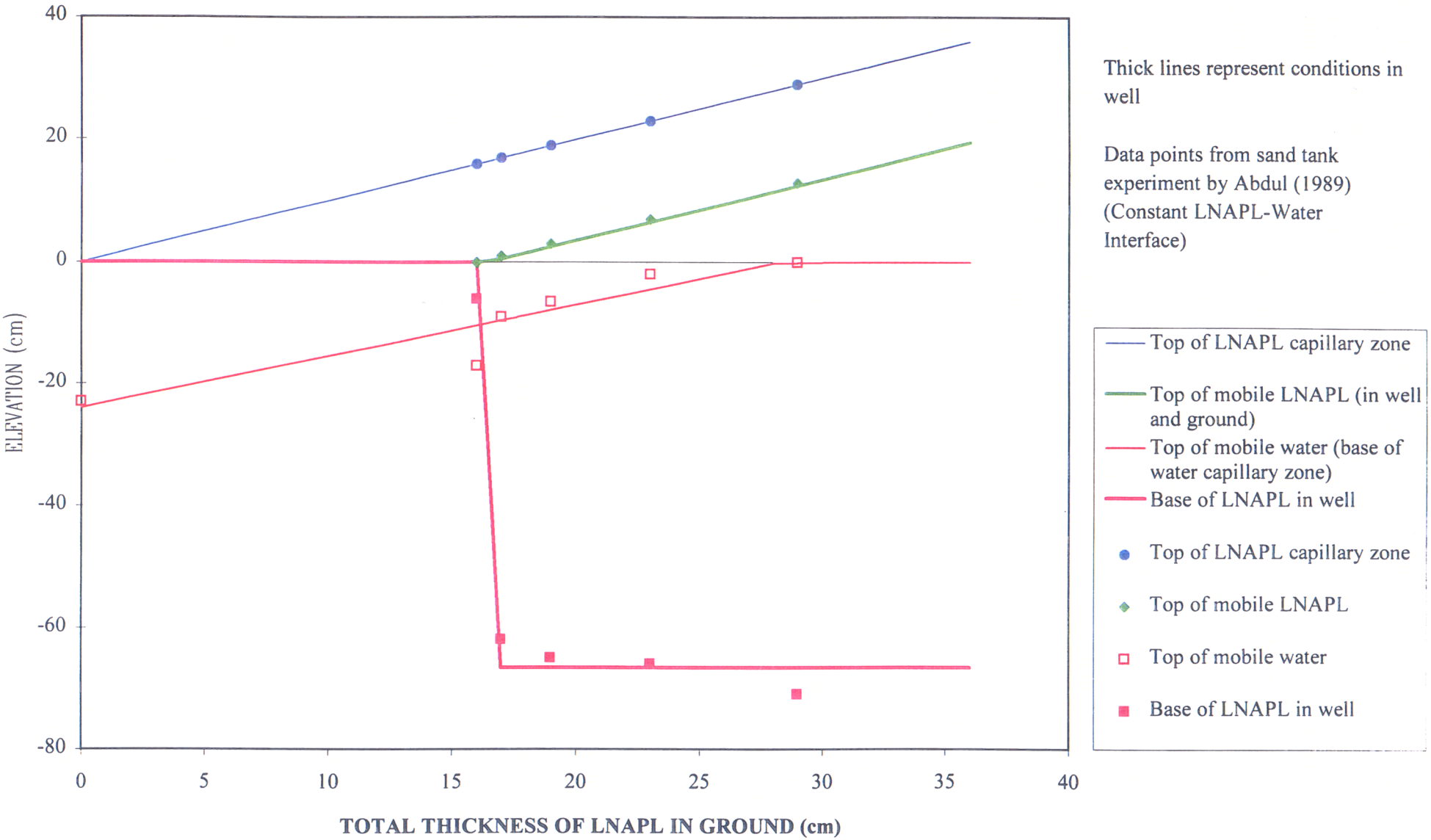

Figure 3.11 Abdul data - fluid elevations against thickness of mobile LNAPL in gound

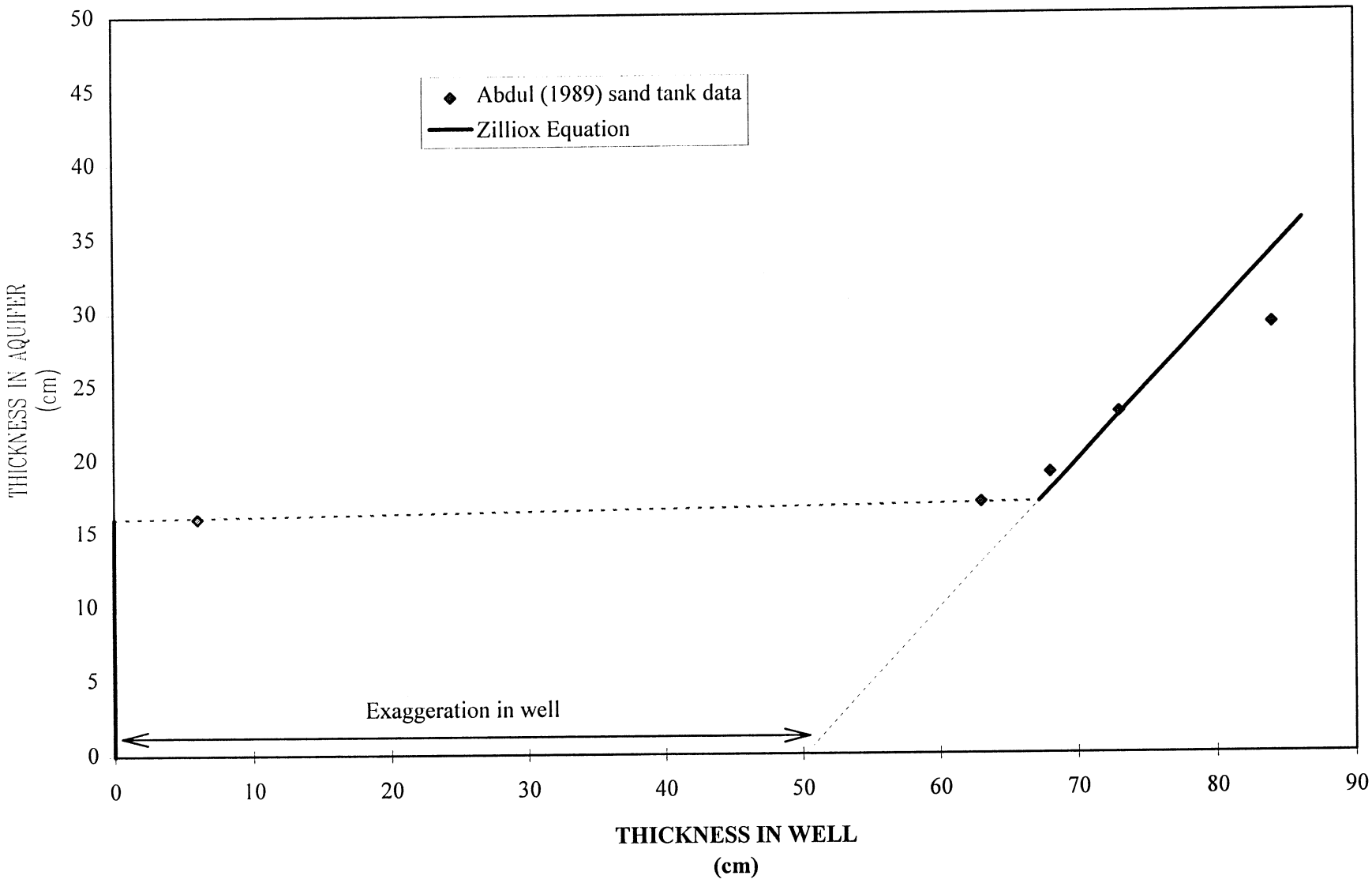

Figure 3.12 Abdul data - thickness of LNAPL in well against thickness in ground

h:\projects\wr\15690\calcs\BALLEST.XLS fig3.13

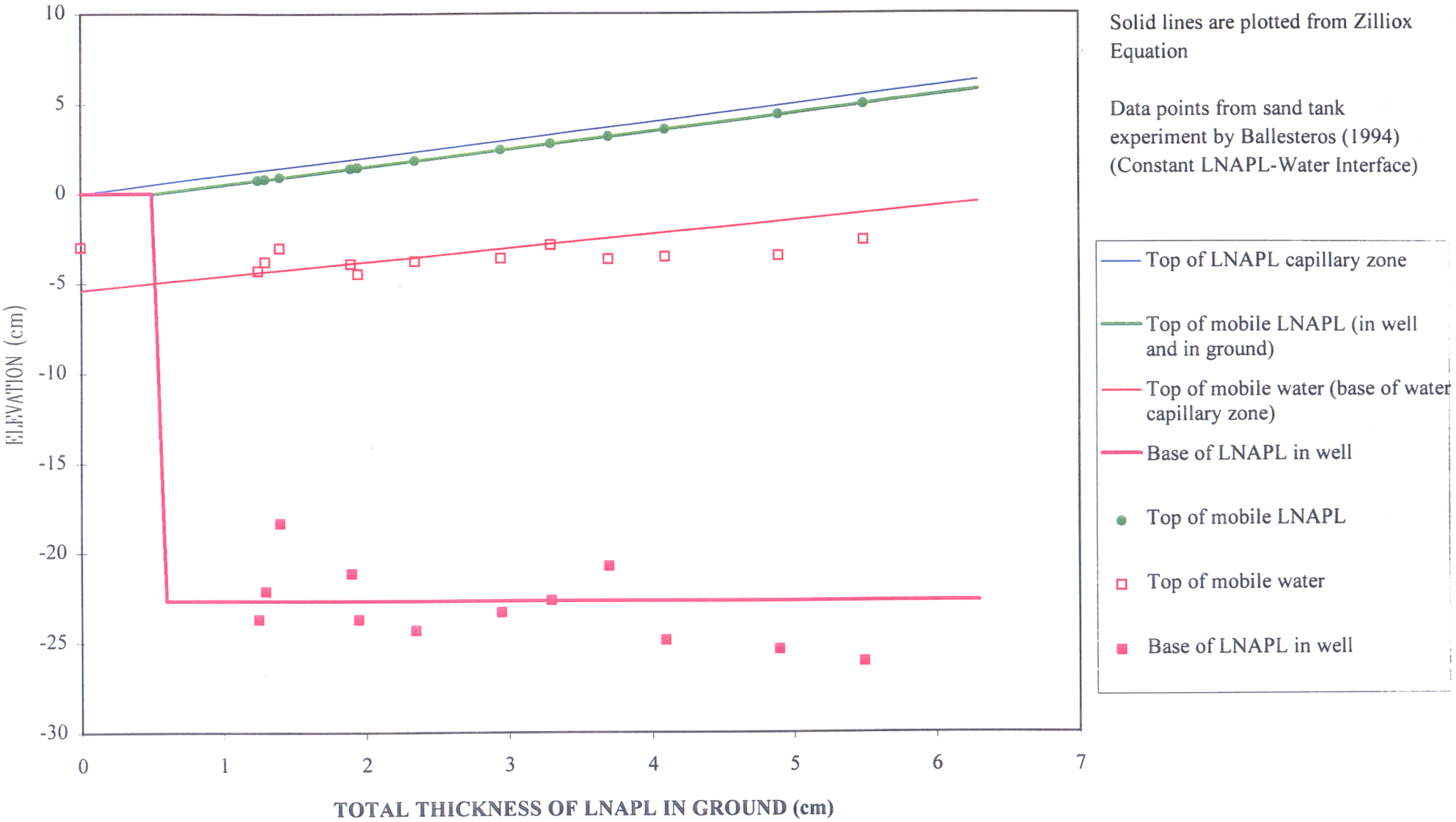

Figure 3.13 **Ballesteros data - fluid elevations against thickness of LNAPL in ground**

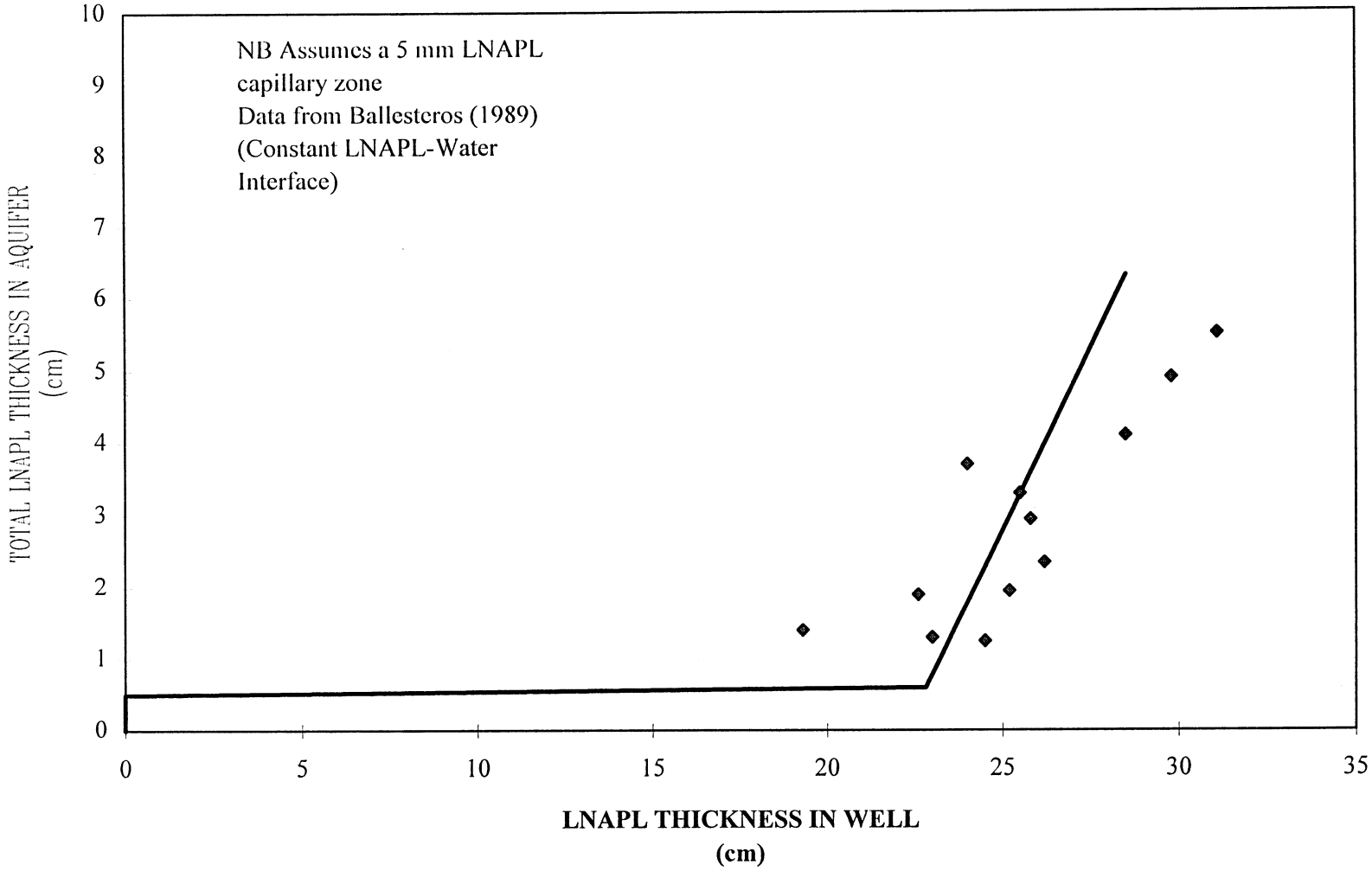

Figure 3.14 **Ballesteros data - fluid elevations against thickness of LNAPL in ground**

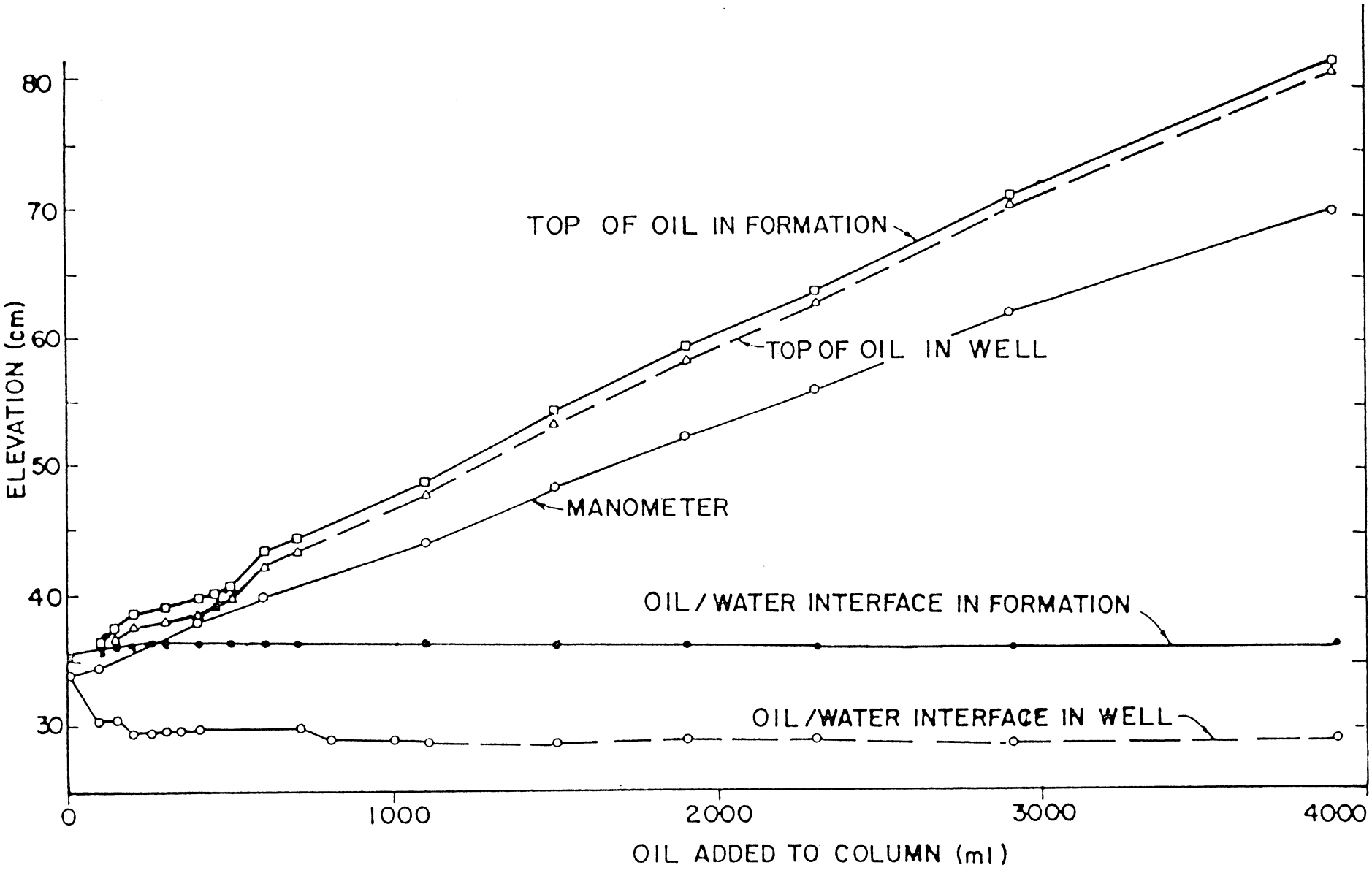

Figure 3.15 Fluid elevations against volume of oil added (after Blake & Hall, 1984)

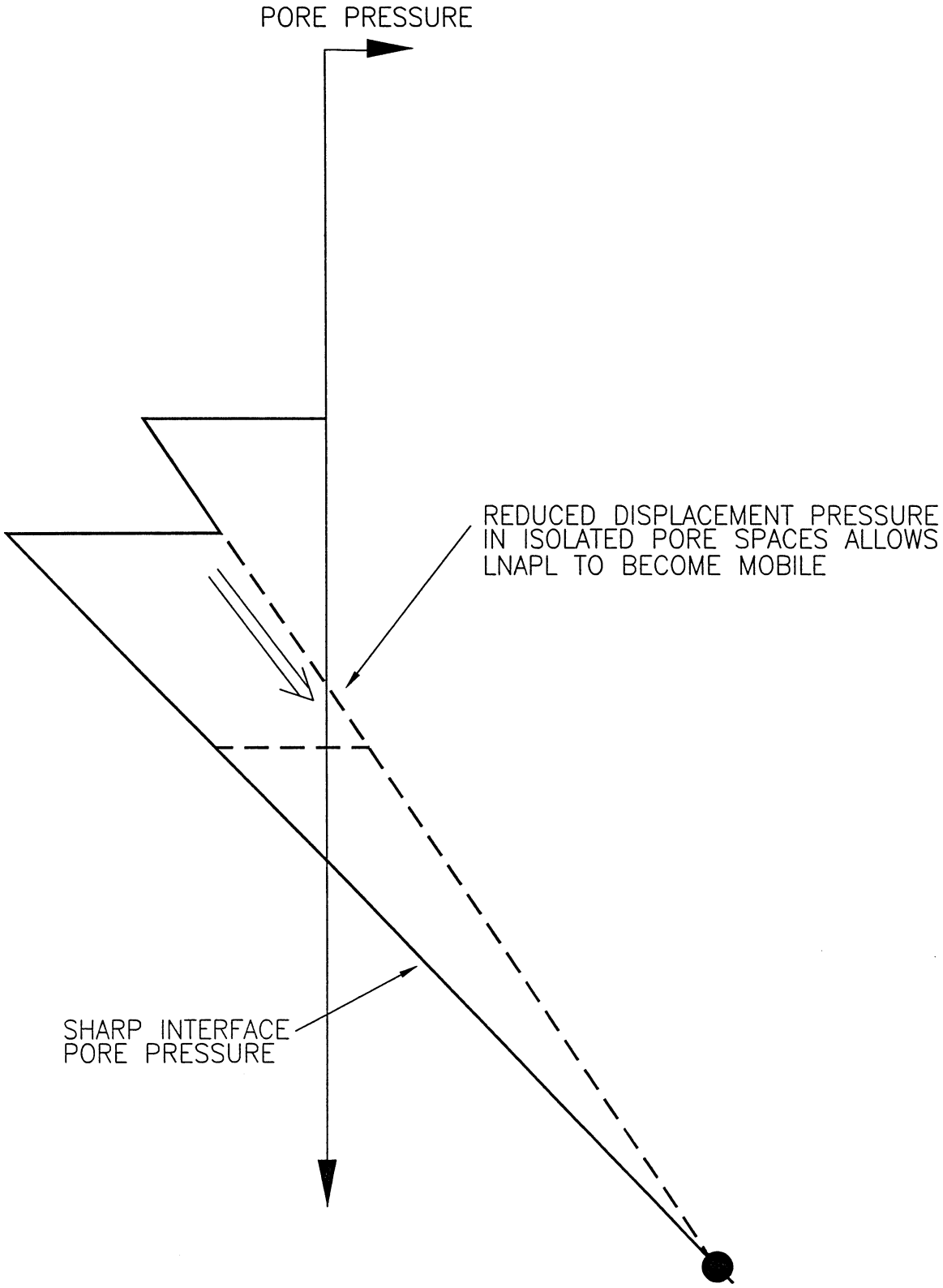

Figure 3.16 Sub-critical ingress

h:\projects\wr\15690\cales\X138.XLS fig3.17

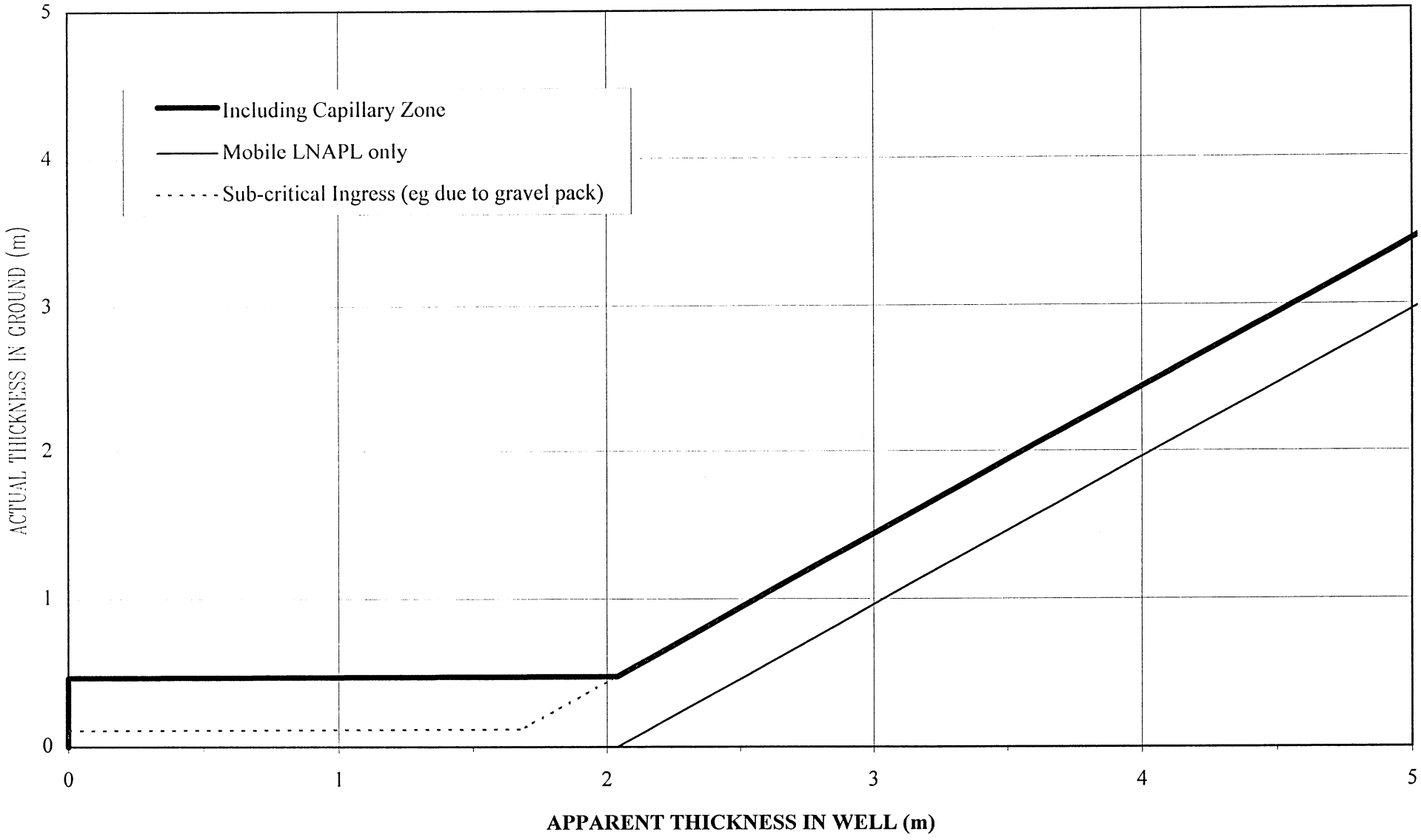

Figure 3.17 The effect of sub-critical ingress on thickness of LNAPL in well

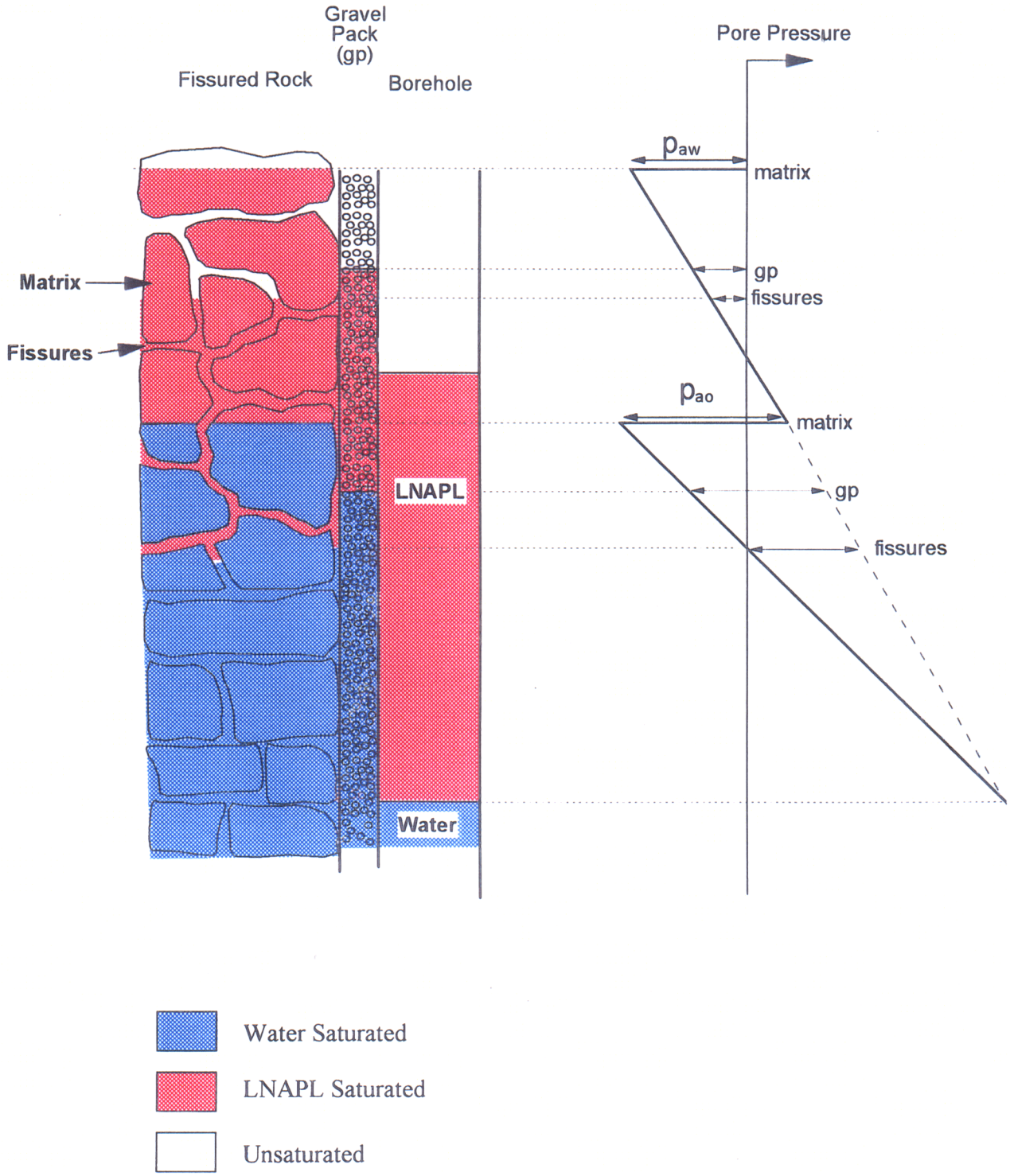

Figure 3.18 **LNAPL distribution in fissured aquifers**

4. METHODS OF OBTAINING SPOT READINGS

4.1 Introduction

This Section describes methods of obtaining measurements of LNAPL at spot locations These may be indirect measurements of thickness (for example cone penetrometers, borehole logging), concentrations (soil sampling) or a qualitative measurements. This section also covers methods of obtaining LNAPL thickness from monitoring wells, either by baildown testing or corrections to the well thickness based on calculations of the exaggeration effect. Non-invasive geophysical methods, which in general sample a larger volume of ground and are therefore not spot readings, are covered in Section 5.

4.2 Sampling

4.2.1 Soil Sampling Methods

Soil sampling may be undertaken during drilling, cone penetrometer testing or trial pitting. For the cheapest method of drilling, shell and auger (percussion), sampling can be by split spoon or U100 sampling. U100 samples are basically undisturbed, whilst split spoon samples are disturbed but quicker to take. The sample volume is fairly large which is an advantage since it is more likely to be representative of the ground conditions. Cone penetrometers can also take samples from unconsolidated ground, although these are limited by the size of the probe (for example, Geostar® Soil Sampler is 22 mm diameter, 15 cm in length).

In consolidated ground, rotary drilling is necessary and undisturbed samples must be taken by coring. Coring is expensive but can provide a continuous record (depending on ground conditions - core may be lost). A disadvantage of coring is that the high pressures generated by the drilling process may disperse the LNAPL plume and exacerbate the problem.

During trial pitting, only disturbed samples can be taken from the excavated material although undisturbed soil may be sampled from the walls of the excavation. The ability to inspect a large volume of ground is an advantage.

4.2.2 Soil Analysis

Laboratory analysis of samples is costly and several methods are available to enable qualitative assessment of soil samples or core in the field. Samples may then be selected to send to a laboratory to allow calibration of the field testing results.

Soukup and Scheuing (1996) made a comparison of five field screening techniques for hydrocarbon contaminated soil samples recovered during drilling. The methods used in this

study were cheap and simple and did not involve laboratory analysis: visual/odour examination, head space analysis, hydrophobic dyes, hydrocarbon test kits and UV fluorescence. A similar study was made earlier by Cohen *et al* (1992).

The simplest technique is visual and odour examination, where the odour, colour, texture, sheen or layering of the sample may indicate LNAPL presence. This technique worked well for LNAPLs in the tests by Soukup and Scheuing (1996) although it is best for dark or coloured LNAPLs or those which have a low odour threshold. If possible, the properties of the LNAPL should be determined prior to investigation to ensure it is not odourless and colourless.

The hydrophobic dye used by both Soukup and Scheuing (1996) and Cohen *et al* (1992) was Sudan IV, a red-brown powder which is insoluble in water but which dyes organic liquids red. The soil sample is mixed with about 1 mg of powder and shaken manually. This technique worked well for LNAPLs and DNAPLs but it could not be used for clayey samples as the dye powder could not be evenly distributed within the sample. In addition, the red-brown colour could not be easily distinguished from natural iron staining in the soil. Cohen *et al* (1992) used the dye in combination with a centrifuge to enhance detection by separating the pore fluids from the sample.

The hydrocarbon test-kit used by Soukup and Scheuing (1996) consisted of test-tubes containing a liquid tracer dye, to which a few grams of soil are added. If hydrocarbons are present above a level of 10 ppm then a blue line occurs at the top of the liquid in the test tube.

Another simple technique is the viewing of the samples or a rock core under a portable UV light. The method works well for petroleum hydrocarbons and crude oils which fluoresce, although this will not work for non-fluorescent compounds (e.g., chlorinated solvents). Cohen *et al* (1992) found the technique worked best for darker soils where there was greater contrast between the soil and the fluorescent LNAPL. The fluorescence of hydrocarbons is discussed in more detail in Section 4.5.1.

Head space analysis, a method of soil gas sampling, was also reviewed by Soukup and Scheuing (1996) and is discussed further in Section 4.2.3.

4.2.3 Gas Sampling

Analysis of gas samples can indicate the presence of LNAPLs and give a general indication of relative concentrations. Although no measurement of actual thickness is possible, gas concentrations are easily and quickly measured and may be useful for field screening and may help delineate the contamination. Gas samples may be taken either from *in situ* spiking, borehole gas or head space analysis of soil samples. Usually to indicate the presence of LNAPL the gas would be analysed for volatile or semi-volatile organic carbons (VOCs or

semi-VOCs). This method is obviously not applicable for non-volatile LNAPLs. However the breakdown of non-volatile hydrocarbons produces carbon dioxide, which may be detected by soil gas measurements.

Gas sampling can only give semi-quantitative measurements of LNAPL concentrations. If VOCs or semi-VOCs are measured, the concentrations depend on the volatility of the LNAPL -a small amount of a highly volatile LNAPL would give the same results as a larger amount of a less volatile LNAPL.

Gases can be measured in the field by photoionization detectors (PIDs), flame ionization detectors or volatile hydrocarbon test kits (e.g. Dräger tubes). All these methods measure a relative concentration of hydrocarbon. Samples can be analysed more accurately using gas chromatography (mostly in the laboratory although some field instruments have been used).

Head space analysis involves sealing the soil sample in an air-tight bag and leaving it to equilibrate at room temperature. The air in the bag is then measured (usually with a PID) which detects any volatile organic compounds which have entered the head space from LNAPL in the soil. Head space analysis works well at detecting the presence of LNAPLs and gives an indication of the relative amounts of LNAPL, although it is sensitive to the sampling method. This is likely to be fairly inconsistent in the field, with variations in volume of soil and air in the bag, equilibration time and measurement temperature all affecting the measurement.

Soil gas sampling using PIDs is very common as a phase 1 site investigation because it is rapid and fairly cheap. It must be stressed that data from these surveys alone is not a reliable method for delineating a free-phase LNAPL plume for the reasons mentioned above, especially for less volatile LNAPLs or where the water table is deep. However, the method can be useful for targetting further investigations.

4.2.4 Groundwater Sampling

Although LNAPLs are basically immiscible with water, they may undergo some dissolution on contact with groundwater. The amount of partial dissolution depends on the properties of the LNAPL, with lighter compounds such as BTEX dissolving more readily than heavier long-chain hydrocarbons. Dissolved LNAPL may help delineate the free-LNAPL plume by indicating the direction of groundwater movement, but often dissolved LNAPL will have migrated further than the free-product plume. For older spills, breakdown products may also be detectable in the groundwater and may cause an increase in electrical conductivity and a reduction in dissolved oxygen concentrations.

Groundwater can be sampled from monitoring wells or cone penetrometers tests and analysed in the laboratory. Field testing kits are also available which can measure the concentration of

total petroleum hydrocarbons or specific hydrocarbon compounds in groundwater. Currently, a new dipping instrument, "Petrosense", is available which can do instantaneous measurements of total petroleum hydrocarbon concentrations down a borehole, although this is quite costly.

4.3 Corrections to Borehole Thicknesses Based on Calculation

4.3.1 Measuring Thickness of LNAPL in Boreholes

Methods for measuring free phase hydrocarbon within the well have been reviewed by Scheinfeld (1986). The most reliable and commonly used method for measuring the thickness of LNAPL in the well is with an interface probe, which is a dipper with optical and conductivity sensors to indicate whether oil or water is present. Both the air/LNAPL and LNAPL/water interfaces can be measured, distinguished by a change in tone of the bleeper.

Various other methods were discussed by Scheinfeld (1986) which could measure the presence of free LNAPL but could not accurately measure the LNAPL thickness. These included:

- Bailing - the LNAPL layer is visible as a floating film, although the thickness of the film is not the same as that in the borehole. The LNAPL may be detected by odour even if a film is not visible.

- Hydrocarbon sensitive pastes which change colour in the presence of hydrocarbon. The pastes are placed on a rod and lowered into the borehole to the water table.

- Thermal conductivity probe - this is a floating device which responds to the differences in thermal conductivity between air, water and LNAPL.

- Electrical Resistivity devices - these sensors are made of a hydrocarbon soluble substance, styrene butadiene copolymer compound, which dissolves on contact with hydrocarbons. This technique is designed to act as a warning system as the sensor breaks down upon breakthrough of hydrocarbon in the borehole.

Scheinfeld *et al* (1986) compares several types of early warning systems which have been developed for monitoring underground storage tanks. These are usually devices installed in boreholes or U-tubes close to the tank and attached to an alarm for long-term monitoring. The devices may be hydrocarbon-sensitive resistivity/thermal conductivity sensors, as described above, or hydrocarbon vapour/combustible gas indicators.

4.3.2 Calculations

In Section 3 the main options for direct calculation have been described in detail. These are reproduced below:

Zilliox and Muntzer (1975)

- $T_G = T - p_{LW}/(\rho_W - \rho_L)g + p_{AL}/\rho_L g$ (4.1)

This equation is thought to be a good representation of the physics of the situation. The concept of a critical thickness, below which ingress does not occur, does not seem to exist in real soils and this is thought to be a result of heterogeneity. However the equation still applies beneath critical thickness if this is the case.

In practical terms, the quantities p_{LW} and p_{AL} are not easy to measure without sampling a large volume of soil. From the literature collated in this study, it appears that this approach has never been attempted outside laboratories.

CONCAWE/de Pastrovich (1979)

- $T_G = T(\rho_W - \rho_L)/\rho_L$ (4.2)

This equation is simple and convenient, but unfortunately a rather poor approximation. It is fundamentally multiplicative whereas the physical situation is fundamentally additive. It is accurate at critical thickness ($T_G = p_{AL}/\rho_L g$) but not otherwise.

Hall *et al* (1984)

- $T_G = T - F$ (4.3)

The formation factor, F, is defined as 5 cm (coarse sands), 7.5 cm (medium sands) and 12.5 cm (fine sands). While this method is essentially correct, the definition of the formation factor is a little crude. It does not take account of the relative density of the LNAPL nor the detailed composition of the soil.

Ballestero *et al* (1994)

- $T_G = T(\rho_W - \rho_L)/\rho_W - H_C$ $\quad T < T_a$
- $T_G = T - \rho_L T_a/\rho_W - H_C$ $\quad T > T_a$ (4.4)

where $T_a = (H_C + 2\sigma\cos\theta/0.3\rho_L g D_1)\,\rho_W/(\rho_W - \rho_L)$
D_1 is the 1-percentile grain size of the soil

This theory, that for small LNAPL thicknesses a different gradient relates the well and ground thicknesses, has not been adequately proved.

Advanced Theories

These theories have the advantage that they include the LNAPL in the partially saturated phase. However they involve measurement of at least as many parameters as the Zilliox-Muntzer simplification. For example with the Brooks-Corey formulation the pore-size distribution parameter, λ, has to be determined.

It should be noted that software exists to perform these calculations. OILVOL®, for example, produced by Draper Aden Environmental Modelling, is a Windows-compatible program which calculates the total volume of LNAPL based on the Van Genuchten formulation. This software has been acquired and reviewed (see below).

Scheigg (1984) etc

These equations express the Zilliox-Muntzer equation in terms of the capillary height of water, H_C. This is more accessible than the displacement pressures required by the full equation. To estimate it, either use Table 3.2 (originally derived from Bear, 1979) or one of the more advanced methods. The Scheigg (1984) version, which does not take account of density, is:

$$T_G = T - 1.9\,H_C \qquad (4.5)$$

Our own calculations (see Section 3.2) from various sources suggest that the number generally falls between 2 and 3. This is probably a reasonable approach if the accuracy required is satisfactory. The version of equation (4.5) including densities and scaling factors is as follows:

$$T_G = T + H_C\,\rho_W/\beta_{AL}\,\rho_L - H_C\,\rho_W/\beta_{LW}\,(\rho_W-\rho_L) \qquad (4.6)$$

If it was assumed that β_{AL} is generally about 3 and β_{LW} about 2 (from the Busby *et al* (1995) results) the following equation is derived:

$$T_G = T + 0.3\,H_C\,\rho_W/\rho_L - 0.5\,H_C\,\rho_W/(\rho_W-\rho_L) \qquad (4.7)$$

This is consistent with Scheigg's version, since if the relative density is 0.8 then the factor is calculated to be 2.8.

OILVOL®

OILVOL® takes monitoring well LNAPL thicknesses and interpolates them by kriging across a rectangular grid. It than calculates the total LNAPL volume at each node using the Van Genuchten equation (Section 3.2.3) and adds these to estimate the total LNAPL volume at the site.

The input data for OILVOL® are the LNAPL thicknesses measured in monitoring wells, plus nine parameters derived from the soil and LNAPL properties, listed below:

- the Van Genuchten parameters α and n (see Section 3.2.3)
- soil porosity
- maximum residual oil in the saturated soil
- maximum residual oil in the unsaturated soil
- minimum water saturation
- LNAPL density
- scaling factors β_{AL} and β_{LW}. (see Table 3.3)

The soil and LNAPL parameters should be site specific but are often hard to measure or even estimate. Although default parameters exist within the software, these are not justified by the authors.

The output of the program is the total LNAPL volume in the soil, the total residual volume in the unsaturated zone and the total residual volume in the saturated zone. The interpolated (kriged) data, in terms of either volume per unit area or 'oil heads', can be exported to surfer for contouring. The 'oil heads' option is simply the LNAPL thickness in monitoring wells (i.e. observation data) rather than the actual LNAPL thickness in the ground. A contour plot of this data is of dubious value and may be misleading.

4.4 Corrections to Borehole Thicknesses based on Baildown Tests

4.4.1 Introduction

This section describes the common practice of baildown or bailer tests. A baildown test is similar to a standard pumping test but it carried out in a well with free-LNAPL present and both the water-LNAPL and LNAPL-water interfaces are monitored during the test. As with pumping tests, there is the potential for many different types of test based on steady state

pumping, rising head tests or more complex pumping regimes. The most commonly used test generally involves bailing the well out as quickly as possible to the interface (i.e. not removing too much water) and then monitoring the thickening of the LNAPL layer in the well as it returns to its steady-state elevations. Both surfaces have to be measured usually with an interface probe.

The theory behind most of these methods is not strong and, as Hampton *et al* (1990) say, "They are derided primarily because there is no established basis for how or why they work." It should be said that although there are doubts over their value for calculating true thickness of LNAPL, this does not mean they are without value. A baildown test will always provide information on the way LNAPL comes back into the well. The speed at which it returns is crucial to the outcome of remediation with skimmer wells - a baildown test can be used to support the decision to use Total Fluids Pumping instead.

Regarding methods for measuring the water level and interface level, this was covered in Section 4.3.1. However since many accurate readings have to taken in a short section of time the interface probe is strongly recommended.

4.4.2 Gruszczenski (1987)

Gruszczenski's method uses data derived from a standard baildown test described in Section 4.4.1, i.e. bailing the well out to the interface (i.e. not removing too much water) and then monitoring the thickening of the LNAPL layer in the well as it returns to its steady-state elevations.

Having plotted a graph of the elevations of the LNAPL surface and the water surface against time, find the 'inflection' point (where the water surface is at its maximum). The thickness of the LNAPL in the well, at this point in time, is the thickness of the LNAPL in the soil. If there is no inflection point (Type 1 Curves') then the well thickness was the same as the soil thickness.

The justification for this method is hard to explain. It is assumed that the thickness of the LNAPL capillary zone is not given by this method.

4.4.3 Hughes Baildown

This method, based on Hughes *et al* (1988), uses the same standard baildown test. However instead of plotting the two elevations, the thickness of LNAPL is plotted against time. The 'inflection point' is the point where the rate of increase in thickness reduces. It has been suggested that plots against log-time can more readily identify this point.

This point should occur when the elevation of the top of the LNAPL in the well becomes higher than the elevation of the bottom of the LNAPL in the ground. The driving force

pushing LNAPL from soil to well is now reducing so that the rate of movement will reduce. The thickness of the LNAPL capillary zone is not given by this method.

The reasoning behind this method seems sensible. However the question of whether the slope of the elevation curve will actually change can be investigated further. The method can be analysed by considering the driving force in detail. The rate of inflow is likely to be proportional to the difference between the head in the column and the head in the well, integrated from bottom of the LNAPL in the soil to the top. This expression can be easily calculated and simplifies to:

$$Q = \begin{cases} A(T_G^2 - x^2)/2 & x>0 \\ AT_G^2/2 & x<0 \end{cases} \qquad (4.8)$$

where A is a constant
Q is the rate of LNAPL inflow (proportional to dT/dt)
x is the elevation of the top of the LNAPL in the well, relative to the bottom of the LNAPL in the soil
T_G is the thickness of LNAPL in the soil

It is immediately clear that the rate of change of thickness, Q, is continuous across the "inflection point". That implies that a graph of thickness against time will not show a sharp change in slope. Not only that but the next derivative (dQ/dt) also seems to be continuous and it is only the third derivative that is discontinuous. This effectively makes the 'inflection point' described unspottable - unless the data is exceptionally good and the second derivative of thickness is plotted against time.

Plots against log-time may also help but there is also a danger of ultimately picking up the wrong point. The curve of thickness against time is related to the hyperbolic tangent (from the form of the equation above) and there is an intrinsic inflection point in the gradient of this curve (at time unit 0.707) which may overshadow the point we are looking for (which is at time 0).

4.4.4 Hughes Recovery

This is not a baildown test but a pumping test using a skimmer pump. The LNAPL is pumped from the well until the steady state conditions are reached. The pump is then switched off and the recovery of the top of the LNAPL in the well and the top of the water in the well monitored. The elevation of the top of the LNAPL layer is plotted against time and a sharp reduction in gradient ('inflection point') is identified.

According to Hughes *et al* (1988), the mobile LNAPL layer is condensed down to a single point (which is called the 'buoyancy surface'). As shown in Figure 3.8, this level is higher than the piezometric level.

By the same principle as in Hughes Baildown test, as recovery takes place the rate slows as the top surface of the LNAPL rises past the buoyancy surface. The thickness of mobile product in the ground is calculated from the difference in elevation between the LNAPL in the well before the test and the buoyancy surface elevation.

$$T_G = Tc\ \rho_W/(\rho_W-\rho_L) + H_L \qquad (4.9)$$

where Tc is the buoyancy surface elevation
and H_L is the thickness of the LNAPL Capillary Zone

The thickness of the LNAPL Capillary zone is not given by this method.

In fact since the head at the buoyancy surface will be zero, it would be expected that the thickness would virtually stop increasing. The dominant process now would be the transient imposed by the pumping rather than the well attaining equilibrium and this may well be an order of magnitude slower. Gradually the surface of the mobile LNAPL in the ground and in the well will rise up to its former level.

One possible criticism of this approach is that because of the pressure reduction around the well caused by removing fluid, the whole pressure system may have been shifted downwards while steady-state was being reached. The transient left by this shift would be operating on a similar time-scale as recovery after the buoyancy surface is reached.

4.4.5 Optoelectronic Sensing

This method was developed by Kimberlin *et al* (1989) for determining LNAPL thickness in confined aquifers, where the exaggeration factor can be very large due to the confining pressures encountered. The technique combines a bail-down test with an opto-electronic sensor which detect the inflow of hydrocarbons into the well. The entrance zone over which LNAPL is influxing to the well, which is below the piezometric level in a confined aquifer, reflects the true LNAPL thickness in the aquifer. The sensor works by detecting droplets of oil with LED/photosensor pairs. The presence of oil droplets refract the light away from the photosensors which causes a sound signal to be made from loudspeakers at the surface.

Drawbacks for this techniques are that the borehole logging and construction must be done accurately to determine the exact depth of the confining layer. If the borehole has a gravel pack then the LNAPL will migrate upwards from beneath the confining layer unless the annulus is sealed at the base of the confining layer. In addition the inflow zone is disturbed

by upconing of water during baildown so the inflow zone is smaller than the LNAPL thickness.

4.5 Cone Penetrometer Logs

Cone penetrometer testing is carried out by hydraulically pushing a truck-mounted probe into the ground. Various probes can be attached which continuously measure the properties of the ground as the probe advances. Depending on the size of the truck, penetration can be up to 60 m although this requires favourable ground conditions (unconsolidated sand or clay). The technique is not possible in consolidated rock, bouldery deposits or hard gravels. The technique is reported to achieve a logging rate of over 100 m per day in soft sand deposits.

Advantages of the method are that there are no wastes to dispose of, it is fast, results are available on site and the continuous logging enables a large volume of soil to be tested.

There are two probes available which can potentially detect LNAPLs. These are fluorescence probes and, to a lesser extent, conductivity probes.

4.5.1 Fluorescence Logging

4.5.1.1 Background

The fluorescence of hydrocarbons under ultra violet (UV) light has been commonly used to aid detection of hydrocarbons in soil samples (Hughes *et al*, 1990, Scheinfeld *et al*, 1986). More recently the fluorescent properties of hydrocarbons have been used to measure LNAPLs in the ground during cone penetrometer tests (CPTs) (Wheeler, 1994, Bratton and Bianchi, 1995a, Jacobs, 1997).

The principle behind the fluorescence cone is to emit light from a UV source into the soil through a sapphire window in the cone. The UV light excites the hydrocarbon molecules causing them to emit light of a longer wavelength. For a specified hydrocarbon type and soil type, the intensity of the emitted light is proportional to the concentration of the hydrocarbon. This has been shown in laboratory experiments by Haas (undated). Only the soil/hydrocarbon directly adjacent to the window is measured (since the UV light cannot pass through soil grains).

Two methods have been used, the mercury lamp (ML) cone (also known as the field fluorescence detector (FFD)) and the laser induced fluorescence (LIF) cone. The difference between the two methods is the power of the light source used to irradiate the soil. The LIF has a more powerful laser source and can therefore detect hydrocarbons at much lower concentrations, but is more expensive. Both techniques measure the fluorescence every second or approximately 20 mm during penetration, which provides an effectively continuous log.

The LIF can also determine the type of hydrocarbon present by "fingerprinting". With this technique, the spectrum of light emitted from the hydrocarbon is collected at a range of wavelengths, which gives information on the hydrocarbons present. The spectral analysis can also be a continuous log.

4.5.1.2 Variation with hydrocarbon type

Fluorescence varies with the type of hydrocarbon, with some compounds such as BTEX showing high fluorescence and other compounds such as chlorinated hydrocarbons having a low fluorescence. The fluorescence depends on the presence of aromatic compounds, with aliphatic compounds showing no fluorescence. Fluorescence is also affected by molecular size. Many common LNAPLs are detectable, including petrol, diesel, creosote and motor-oil. A list of compounds detectable by the LIF cone is given in Table 4.1 (after Fugro Ltd), although the list is not exhaustive, so compounds not in Table 4.1 are not necessarily non-fluorescent.

Table 4.1 Compounds Detectable by Laser Induced Fluorescence Cone (after Fugro Ltd)

Compounds		
1-Methyl Naphthalene	Diesel Fuel	Natural Gas Condensate
2-Methyl Naphthalene	Ethylbenzene	Petroleum
Acenaphythylene	Fluorene	Petroleum Distillates
Anthracene	Fuel Oil	Petroleum Raffinates
Asphalt	Hydraulic Fluid	Phenanthrene
Aviation Turbine Fuel	Indeno (1,2,3-c,d) Pyrene	Pyrene
Benzene	JP-4, JP-5 and Jet A Fuel	Tar
Benzo (a) anthracene	Kerosene	Toluene
Benzo (a) pyrene	Liquefied Petroleum Gas	Transformer Oil
Benzo (b) fluoranthene	Mineral Spirits	Turpentine
Chrysene	Motor Oil	Varsol
Creosote	Naphtha Solvents	Xylenes
Dibenzo (a,h) anthracene	Naphthalene	

The fluorescence intensity of each compound also depends on the excitation wavelength, with longer wavelength light exciting the heavier hydrocarbons. The excitation wavelength is longest for the nitrogen laser (337 nm) and this is known not to fluoresce many of the lighter compounds such as benzene, toluene and xylenes (Bratton and Bianchi, 1995b). Further excitation systems were developed using other wavelengths: a 'tuneable dye' laser and an Argon laser system based on Raman spectroscopy techniques were developed. The argon

laser emits at 514 nm and has been used for heavier oils and jet fuel. The original mercury lamp emits at the shortest wavelength (254 to 300 nm) and is the only system able to detect benzene. Details of the various methods of excitation and sources are discussed in Bratton and Bianchi (1995a).

For compounds which display a low fluorescence such as chlorinated solvents (although these are DNAPLs), Raman spectroscopy has been used, which involves excitation with lower frequency (near infra-red light) (Haas and Forney, undated).

4.5.1.3 Calibration

If the compounds in the soil are variable, it is not possible to estimate the relative concentrations of hydrocarbon present using the ML cone (which measures overall fluorescence intensity). However if the compound is reasonably consistent in composition then a clear idea of the relative amounts of LNAPL in the soil can be gained, especially if some soil sampling is also carried out to calibrate the logs.

There may be some dependency of fluorescence with soil type, mineralogy, oxidation, grain size and moisture content (Bratton and Bianchi, 1995b). However, Applied Research Associates (pers com) have stated that there is little variation between clay, sand and gravel and that the main soil factor affecting fluorescence is its organic content. The fluorescence of natural organic compounds in the soil may cause false positive results.

Attempts to calibrate fluorescence logs by laboratory fluorescence measurements of samples with known hydrocarbon concentrations have generally not been successful (Applied Research Associates, pers. com). Therefore, Applied Research Associates recommend site-specific calibration, using samples taken near to the CPT tests.

There are four cases in the published literature collated in this study where fluorescence logs have been compared to soil sampling results. Three of these datasets are shown in on Figure 4.1. Bratton and Bianchi (1995a) plotted soil concentrations against fluorescence intensity using the Nd:YAG laser system on a jet fuel contaminated site. The LIF fluorescence and total petroleum hydrocarbons correlation, plotted on a log-log scale in the paper, shows a reasonably good linear relationship. The data appear far more scattered when plotted on a linear scale, as in Figure 4.1.

A further comparison by Bratton and Bianchi (1995b) showed a poor correlation, with several contradictions between the soil sampling and fluorescence log results (Figure 4.1). These were attributed to differences between the soil sampling locations and logged depths. At several locations, measured TPH concentrations of less than 100 ppm were recorded as contaminated by the LIF probe. This was taken to indicate that detection limits were below

100 ppm. However at two of the locations, high concentrations of TPH in the soil (528 and 1108 ppm) were not detected by the LIF probe.

Earley and Rapp (1995) also compared LIF probe and sampling results, and showed that most positive TPH results also had fluorescence above background using an LIF probe. However these results, shown on Figure 4.1, were very scattered and did not show a clear linear relationship between concentration and fluorescence.

In addition, Fugro have produced data comparing fluorescence to semi-volatile organic carbon (semi-VOC) readings, these data have been replotted as an x-z scatter plot in Figure 4.2. These show a clear relationship with some scatter: all positive semi-VOC readings show above background fluorescence.

4.5.1.4 Detection limits

Detection limits for the fluorescence probe are reported to be below 100 ppm for the LIF nitrogen laser and the mercury lamp (Bratton and Bianchi, 1995b). However this limit will clearly vary with the fluorescence of the hydrocarbon (as discussed above).

Entec UK Ltd has carried out CPT fluorescence logging at a site in Preston containing free-product contamination and an example log is shown in Figure 4.3. Field fluorescence data from Entec's work at Preston showed good correlation between fluorescence and sample analyses, although for most logs only a few samples were taken. The fluorescence readings are in volts because the light received by the detector is amplified by a photomultiplier to produce a voltage proportional to the fluorescence. The fluorescence logs showed an upper detection limit at about 10 volts, as illustrated by the log in Figure 4.3. (Although the nearby trial pit sample from this depth had a concentration of 500 ppm, this was not close enough to the CPT to convert this upper voltage limit accurately into a concentration). This upper detection limit may be met at a concentration less than that of a fully LNAPL-saturated soil (as it has done in Figure 4.2). In this case it would not be possible to accurately delineate zone of fully LNAPL-saturated soil, only zones where LNAPL is higher than the upper concentration limit.

According to Applied Research Associates, this upper limit is due to the setting of the amplifier. If the amplifier gain is reduced, a clearer picture could be obtained for the upper end of the concentration range encountered, however this would increase the detection limit. If it is known that free-product exists at a site, then it may be more important to delineate the free-product thickness accurately so the amplifier gain could be reduced, although this would result in contamination at lower concentrations not being detected.

4.5.2 Conductivity Logs

A further method of detecting LNAPLs during CPTs is with a conductivity sensor cone probe (Erchul, 1990). The LNAPL layer was defined by its low conductivity compared to the water saturated zone. The LNAPL/air interface could not be easily delineated by the conductivity probe, the difference between unsaturated and LNAPL saturated soil being determined by the properties of the soil during the CPT. Erchul (1990) also developed a CPT sensor cone, tested in the laboratory only, for measuring the *in situ* flow rate of LNAPLs.

4.5.3 Aquifer Dipstick

Hampton *et al* (1990) developed a tool for measuring LNAPL presence with a hydrocarbon sensitive indicator strip, attached to steel rods which could be driven about 3 m into the ground. The strip consisted of a dimethylsiloxane-based polymer mixed with a hydrophobic dye. The strip changed colour in the presence of hydrocarbons, the intensity of colour change indicating the concentration of the LNAPL. The strip can be reused as the LNAPL volatilises when left in the air and the dye reverts to a colourless state.

The probe was still in the early stages of development in 1990 and no later reports on this method were found. It is limited to use in shallow unconsolidated aquifers due to the hand-driven rods.

4.6 Downhole Geophysical Logs

4.6.1 General

Downhole geophysical logging is common practice in the oil industry who have used it with great success to determine the presence of hydrocarbons. Although the determination of the thickness of LNAPL spills may at first seem a similar problem to oil exploration drilling, there are major differences.

The first is the scale of the investigation - LNAPL spills are likely to be relatively thin (< 2 m) whilst oil reservoirs are much thicker. Generally oil industry logging tools have a low resolution, greater than 2 m, so these could not determine the presence of a typical LNAPL layer. Although the tools could be modified to give a higher resolution, this would mean that the measurement would be focussed nearer to the borehole wall and would be affected by the borehole construction, and possibly drilling fluid invasion.

The second major difference is that oil industry logging takes place well-away from the water table and is not designed to work at the air/liquid interface. Therefore the tools are not generally suitable for measurements around the water table; the borehole is required to be mud- or foam-filled to maintain contact with the formation.

During the literature search, very little was found on the use of downhole geophysical logging to delineate LNAPLs in groundwater situations, probably because of the reasons given above. Therefore in this Section, the only logging techniques discussed are those where literature has been found describing their application to LNAPL spill problems. This does not include down-hole resistivity logging.

4.6.2 Dielectric Logging

Dielectric logging involves the measurement of the relative permittivity of the formation, which is dependent on the dielectric properties of the solid and the fluid within the pores. An electromagnetic wave is transmitted into the formation and received it after it has travelled through the formation. Amplitude and phase differences between the transmitted and received signal (which relate to the attenuation and travel time of the electromagnetic waves) give information on the dielectric properties of the formation.

The dielectric logging method was developed for the oil industry, where the electromagnetic tool is moved along the sidewalls of open holes in consolidated formations. The principles of electromagnetic logging are discussed in Serra (1986).

For groundwater applications, the formations are likely to be unconsolidated where the boreholes would have to be cased. Logging tools used by the oil industry are likely to have poor resolution due to their large transmitter-receiver spacing, designed for measurement of large hydrocarbon reservoirs rather than the thin layers caused by pollution incidents.

In the only example we have found of this method being used for LNAPL detection (Keech, 1988), logging was done inside an air-filled borehole with non-metallic (eg PVC) casing to allow propagation of the electromagnetic signal through the casing.

The dielectric permittivity of a formation is made up of contributions from the solid and the pore fluid. Keech (1988) compared the dielectric properties of sand with different saturating fluids, and showed that there is a good contrast between LNAPL (low permittivity) and water saturated formation (high permittivity). The dielectric properties of materials are discussed further in Section 5.4.

A portable logging tool was developed by Keech (1988) for use in cased air-filled boreholes. However, the presence of an annulus between the casing and the formation causes unresolvable reflections of the electromagnetic waves from the borehole sidewall. Keech solved this problem by making the annular thickness large (8.75 cm) so that the electromagnetic waves did not penetrate as far as the borehole sidewall. To ensure that the capillary properties of the annulus are similar to those in the formation, the annulus in filled with sand which must be matched using grain size analysis to samples from the formation, with emphasis on samples from around the water table.

The tool used two receivers, one above and one below the transmitter, to measure the difference between the dielectric properties across two adjacent sections of the borehole. The method relies upon the difference in dielectric properties of the LNAPL and water bearing formation to delineate the LNAPL layer (the dielectric constant is not directly measured by this technique). The method proved successful for delineating the water/LNAPL boundary but the LNAPL/air boundary was much less easily distinguished due to the similarity of the dielectric properties. Other field observations were required to confirm the location of the top of the LNAPL layer.

4.6.3 Fast Neutron Thermalisation

This method uses a radioactive source to emit fast neutrons which collide with particle matter, which slows them down (thermalises) them to a velocity where they can be detected by detector (usually BF_3 or ^3He since they have a large neutron capture cross-section). The neutrons are slowed most by hydrogen atoms, which are present in water, hence the technique is used to determine the moisture content in the unsaturated zone (e.g. Unruh *et al*, 1990).

The technique cannot be used to differentiate between LNAPL and water interfaces, because the number of hydrogen atoms in water and LNAPL are similar, but it could be used to detect the air/LNAPL interface. The only reference found for this method was Indergard and Hagan (1991-abstract only), who indicated that they had used a compensated neutron log to estimate the thickness of the LNAPL capillary zone. However, details of the method or its success were not available.

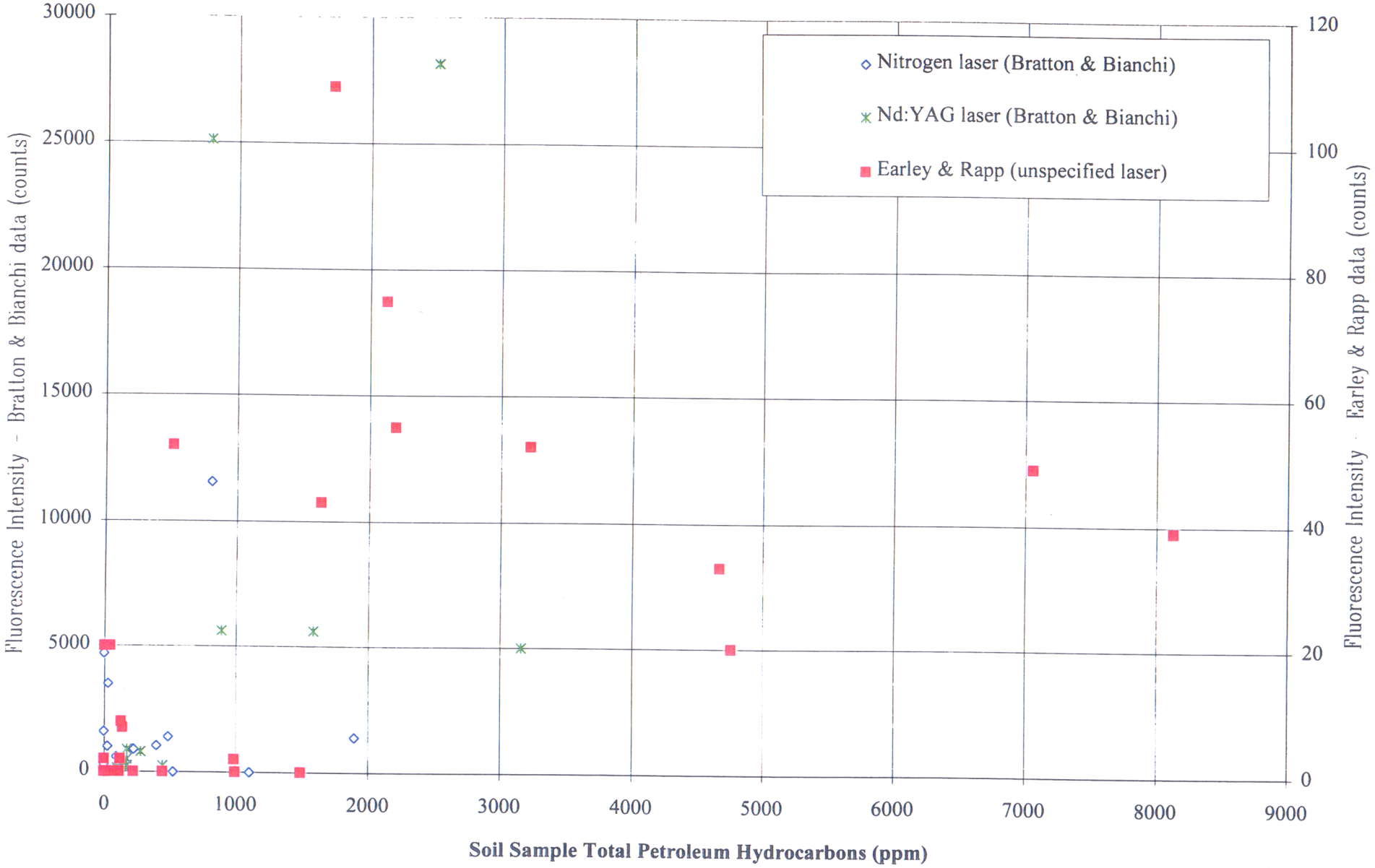

Figure 4.1 Comparison of CPT laser induced fluorescence with total petroleum hydrocarbon in soil

h:\projects\wr\15690\cales\X142.XLS fig4.2

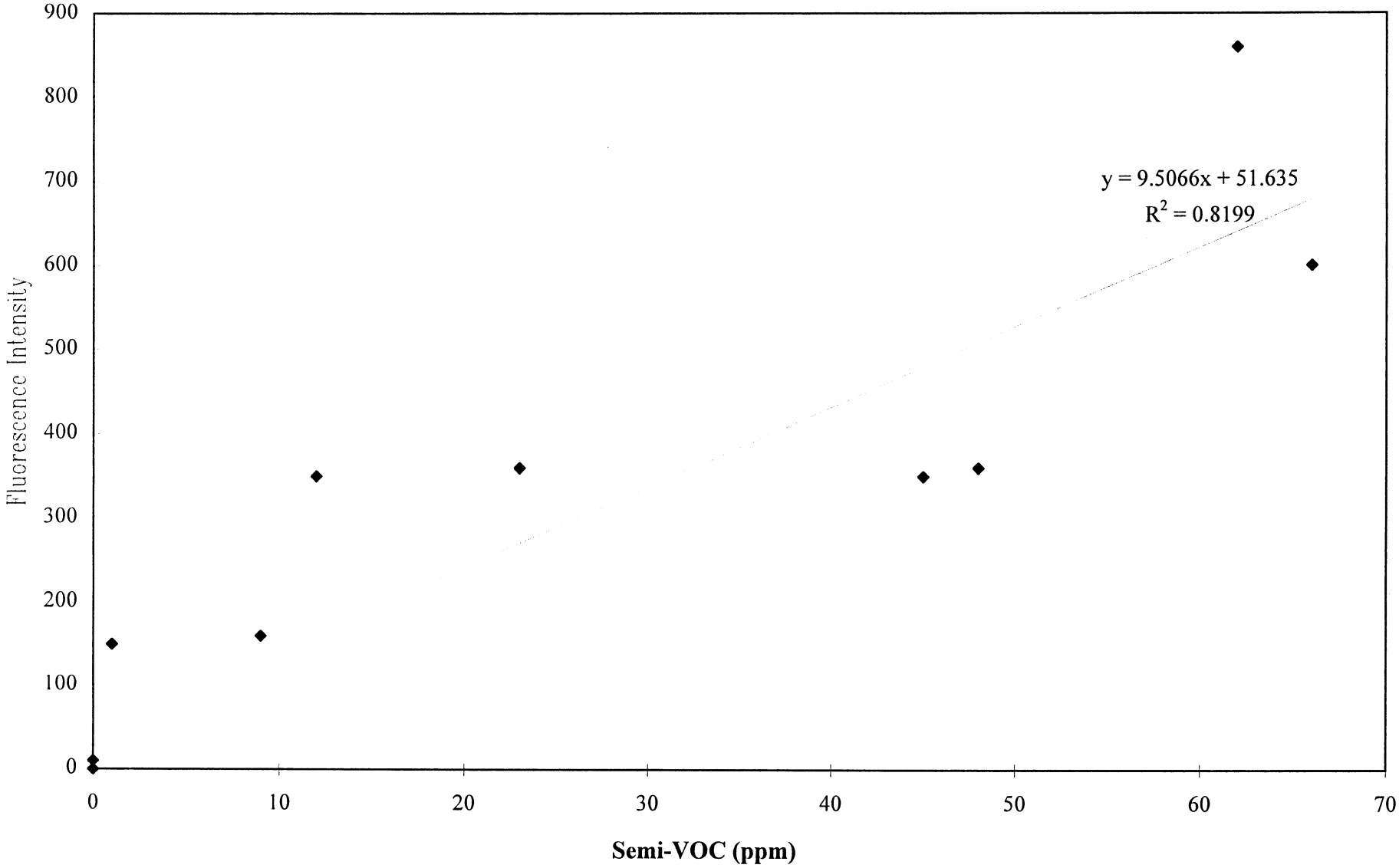

Figure 4.2 Comparison of CPT laser induced fluorescence with semi-volatile organic carbon in soil (data from Fugro Ltd)

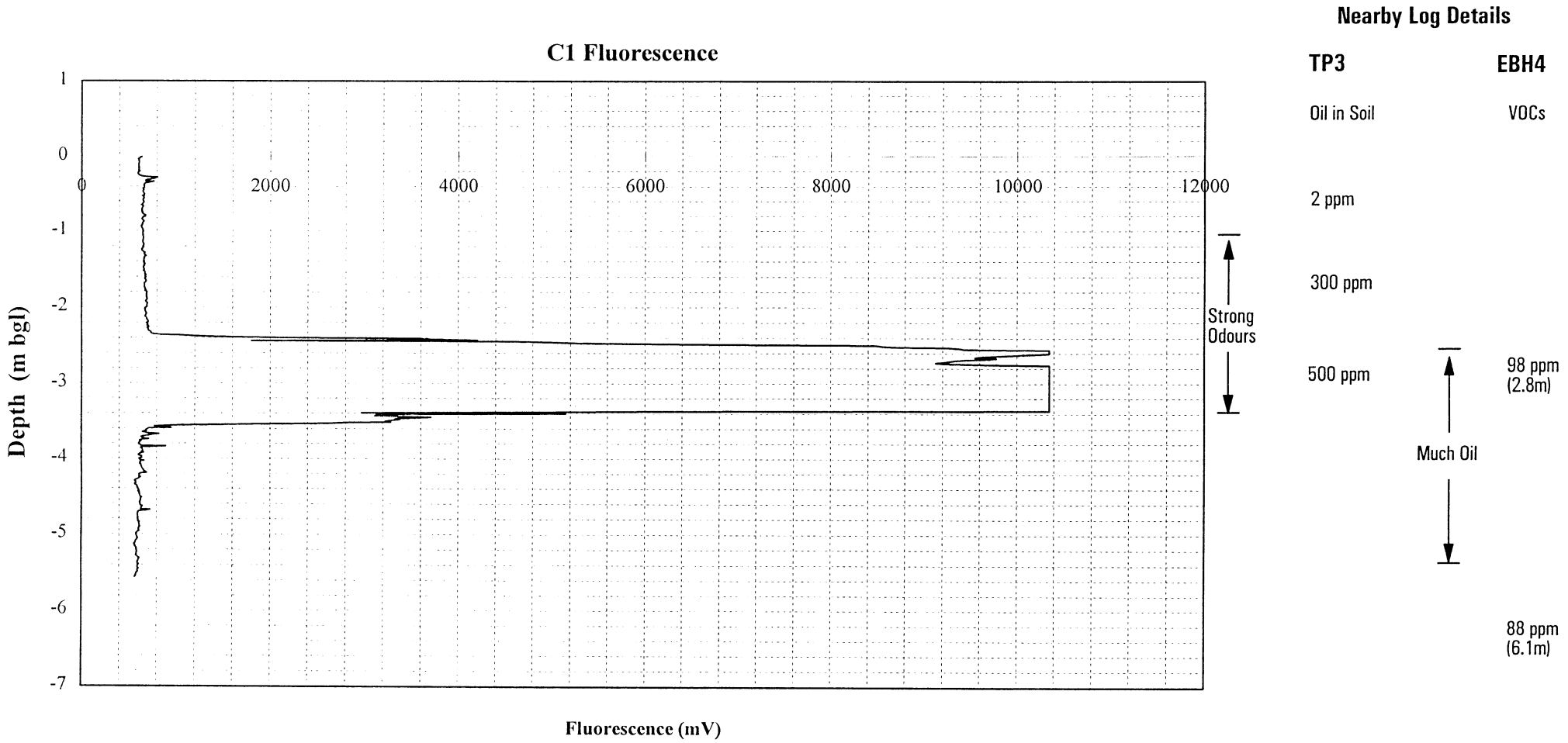

Figure 4.3 Geocone field fluorescence detector log

5. METHODS OF OBTAINING DATA FROM SURFACE

5.1 Introduction

This section reviews non-invasive geophysical survey methods, which can obtain measurements of ground properties from the surface, and their ability to detect and delineate hydrocarbon spills. There are many advantages in using surface geophysical surveys, which are summarised as follows:

- surface surveys are non-invasive, therefore require no waste disposal and have fewer access problems
- they can cover a large area rapidly
- in general, they sample a large volume of ground (i.e. not just spot readings)

The disadvantages are:

- poor spatial resolution, especially vertically
- the interpretation of results can be difficult
- they give no quantitative measurements of LNAPL concentrations
- each survey method will only work under certain ground conditions.

In general, geophysical methods are probably best used in conjunction with invasive sampling to calibrate the geophysical survey results.

Key references specifically discussing their application to detecting hydrocarbons are Olhoeft (1986), who summarised the effectiveness of electromagnetic conductivity, resistivity, induced polarisation and ground penetrating radar, Davis (1990, 1991), who discusses electromagnetic conductivity and resistivity surveys and Leonard *et al* (1997) who discuss ground-penetrating radar.

General textbooks on geophysical surveys are Telford (1976) and Zohdy (1974) which covers groundwater applications.

5.2 Resistivity/Conductivity Surveys

5.2.1 General

Ground resistivity can be either measured using an array of electrodes in contact with the ground, or by using electromagnetic induction, which uses hand-held coils and does not

require ground contact. Although the two methods essentially measure the same property of the ground, electrode arrays measure the resistivity directly, whilst electromagnetic (EM) induction actually measures conductivity, the inverse of resistivity.

These survey methods can detect contaminants if they change the apparent resistivity of the formation. The resistivity of a formation is usually increased by hydrocarbon based contaminants, although this may not be the case if the hydrocarbon has undergone significant degradation. Resistivity values for various materials, collated by Andres and Canace (1984) are given in Table 5.1.

Table 5.1 Resistivity Values for Selected Materials (after Andres and Canace, 1984)

Material	Resistivity (ohm.m)
Clays[a]	1-100
Alluvium and Sands[a]	10-800
Loose Sands[b]	10^3-10^5
Sandy Soils[b]	7×10^2-7×10^3
Quartz[c]	10^{12}-10^{14}
Petroleum[c]	10^9-10^{16}

[a] Telford *et al* (1976), [b] Kollert (1969), [c] Gearhart Industries inc.

Olhoeft (1986) presents resistivity values for various sand and clay mixtures saturated with air, water, benzene and methanol. These are shown in Figures 5.1 and 5.2.

Some authors (Saunders *et al*, 1983, and Saunders and Germeroth, 1985) have derived a linear relationship between the resistivity of the ground and the thickness of the LNAPL layer, for a relatively homogeneous formation. This is discussed further in Section 5.2.3.

Although most hydrocarbon compounds increase the resistivity of the formation, this is usually only by a small amount compound to background variation in freshwater aquifers, especially if the hydrocarbon layer is thin. If any inorganic contaminants are also present, these will increase the conductivity and generally mask the effect of the hydrocarbons. According to Olhoeft (1986), the resistivity/conductivity methods are most effective where the LNAPL is not accompanied by inorganic contaminants or where LNAPLs react with clays, greatly reducing their normally high conductivity.

Background resistivity is greatly affected by the presence of underground objects such as buried services which can create large anomalies and mask the effect of the hydrocarbons. Resistivity surveys are therefore not possible in many urban environments.

In general the electrode array method is better for depth profiling, whilst EM surveys are better for areal mapping (Olhoeft, 1986). Also the electrode array method is quicker, since multiple measurements are taken from one array between electrodes at different spacings. For both methods the depth of investigation is dependent on the geometry and spacing of the electrodes or coils and receivers. The methods both show poorer resolution with increasing depth.

Since conductivity = 1/resistivity, a small reduction in conductivity will mean a large increase in resistivity. Therefore, for non-conductive ground conditions, such as clean sands, using an electrode array would show up high resistivity anomalies better than an EM survey.

5.2.2 Resistivity Surveys

Resistivity surveys are carried out using an array of electrodes on the ground surface and passing current between the electrodes whilst measuring the voltage across them. The depth of investigation depends on the electrode spacing and geometry. There are two basic methods: vertical sounding, which measures the variation in resistivity with depth, and lateral profiling which measures lateral variation in apparent resistivity over a quasi-constant depth. The depth of measurement for a given electrode spacing can vary with ground conditions - if there is a deep conductive layer, the apparent resistivity will be measured deeper than if the conductive layer was shallower.

For vertical soundings, the detectability of a layer of contrasting resistivity to the surrounding formation is dependent on its relative depth (= layer thickness (m)/depth (m bgl)). As a rule of thumb, if the layer has a thickness less than 10% of its depth below ground, it will not be detectable.

The technique has been commonly used for the detection of contaminants which raise the conductivity of the groundwater, but less often to determine the presence of resistive contaminants such as LNAPLs. The earliest report of this method use in detecting hydrocarbons is Holzer (1976), who delineated a subsurface oil-spill. Holzer reported limited success due to the thinness of the oil layer and cultural interferences (such as buried pipelines).

Daily *et al* (1995) carried out a well-controlled experiment to determine the capabilities of this method for detecting hydrocarbons. Daily *et al* (1995) used a laboratory experiment in a large sand tank to determine the feasibility of using electrical resistance tomography to delineate spills and monitor air-sparging operations. A controlled gasoline spill in the tank was found to cause an increase in resistivity, although this was small in comparison to the natural inhomogeneities in the sediments (non-layered river bed silts and sands). A clear picture of the gasoline spill was only possible by subtracting the resistivity image taken prior to the spill. The extent of air-sparging (regions where air-bubbles had displaced pore water) was also only

detectable as a resistive anomaly once the background resistivity anomalies had been subtracted. They concluded that the method is not useful unless there is little background variation since prior measurements of the resistivity at a site are unlikely to be available.

De Limia *et al* (1995) reported mapping a high resistivity anomaly associated with LNAPL free product. The survey was carried out in a sandstone aquifer, described to be of relatively uniform resistivity. However, accurate delineation of the spill in terms of thickness or areal extent was not attempted.

Two further references were found which detected low resistivity anomalies associated with an LNAPL spill. Banks *et al* (1997) used resistivity to map the extent of an oil contaminated site in Latvia, although at this site, which had been used for fuel storage since 1941, the contamination showed up as areas of low resistivity due to the presence of inorganic contamination resulting from oil degradation. The oil degradation reaction produces CO_2 and consumes O_2. The CO_2 was found to enhance weathering of carbonates and silicates raising the electrical conductivity of the groundwater. The consumption of oxygen promotes reducing conditions which increase concentrations of dissolved iron.

Andres and Canace (1984) successfully used both lateral and vertical profiling to delineate a thick (up to 1.25 m) LNAPL spill (jet fuel), in relatively homogenous strata. The contamination was a low resistivity anomaly due to the presence of the aqueous foam used to put out the fire after the spill. The lateral profiles indicated the extent of the plume but could not distinguish the boundaries very precisely. The vertical soundings could not accurately measure the depth and thickness of the LNAPL layer but showed differing characteristic profiles for uncontaminated and contaminated locations.

5.2.3 Electromagnetic Conductivity Surveys

An electromagnetic survey measures the conductivity of the ground by inducing a magnetic field in the ground. It uses a transmitter coil, which uses alternating current (AC) to create a primary magnetic field, which generates small electric currents in the ground. A receiver coil measures both the primary and secondary magnetic fields in the ground. The coil spacing and AC frequency is set such that the ratio of primary to secondary fields is proportional to the terrain conductivity. The apparent resistivity (the reciprocal of conductivity) is given by the following equation derived from ohm's law (McNeill, 1980):

$$\rho = \frac{1}{2}\pi f \mu_0 s\left(\frac{H_p}{H_s}\right) \qquad (5.1)$$

where ρ is the apparent resistivity in ohm m
f is the frequency of the electromagnetic field (Hz=s^{-1})
μ_0 is the magnetic permeability of free space (4.1×10^{-7} H/m)
s is the transmitter to receiver spacing (m)
H_p is the intensity of the primary magnetic field (H), and
H_s is the intensity of the secondary magnetic field (H).

Electromagnetic survey methods can detect contaminants if they change the apparent resistivity of the formation. The depth at which resistivity is measured depends upon the coil spacing and the coil orientation, with greater spacing focusing at greater depths. A depth of 30 m can be achieved with a two-man operated system with 40 m coil spacings. A vertical coil orientation receives most of its response from the near surface (Davis, 1991, Saunders, 1985). The horizontal coil orientation receives a major part of its response from a depth of approximately 0.4 times the transmitter-receiver distance.

There is some literature on the use of EM surveys to detect LNAPL spills.

Saunders *et al* (1993) and Saunders and Germeroth (1985) used EM surveys to detect LNAPL spills at three sites, including a large jet fuel spill at Newark Airport New Jersey. They used terrain conductivity measurements to predict LNAPL thicknesses. They derived an approximately linear relationship between LNAPL thickness and terrain conductivity using LNAPL thicknesses in monitoring wells (Figure 5.3). However it appears that in both papers the exaggeration factor in the monitoring wells was not taken into account so this relationship may be unreliable or at least less useful. However, Saunders and Germeroth (1985) followed up the EM survey with the installation of 35 new wells and found a 90% agreement between predicted and observed borehole hydrocarbon thickness.

Davis (1991) used EM to detect coal tar contamination, which was then confirmed by the drilling of monitoring boreholes. There were complications due to concurrent sulphur and ionic contamination. In his comparison of total extractable hexane and EM conductivity, the contaminated areas mostly showed lower conductivity than the uncontaminated areas (Figure 5.4). The summary by Davis concluded that the EM survey was a useful technique for determining the lateral extent of a hydrocarbon contaminant.

5.3 Induced Polarisation (Complex Resistivity)

Induced polarisation (IP) or complex resistivity measures how the resistivity of the ground, when measured by applying an alternating current (AC), is dependent on the frequency of the current applied. Measurements can be made by two methods:

i) measuring the variation of ground resistivity with the frequency of AC applied

ii) by passing a direct current through the ground, which generates a potential field in the ground, and measuring the decay of the field when the current is turned off.

The IP effect is the result of electrochemical energy storage in the ground during the transmission of current. This energy is released when the current is switched off. The IP or chargeability of the ground depends on the electrolyte content of the porewater, permeability, clay content and saturation. High IP effects are also caused by some minerals such as sulphides, some oxides, graphite and coal.

If a contaminant causes chemical reactions in the ground, then it may be detectable using IP (Olhoeft, 1986). Reactions which can be observed are mainly inorganic oxidation/reduction and cation exchange reactions, but reactions between hydrocarbons and clays have been observed using IP both in the laboratory and in the field (Olhoeft, 1986). A hydrocarbon can react with clays and reduce their ion exchange capacity. This would reduce their IP effect or chargeability, causing a negative anomaly. As it is a chemical reaction that is being detected, very small amounts of organics may be detected. However, not all organic compounds will react with clays.

Levitskaya and Sternberg (1996) have reviewed complex resistive properties of sedimentary rocks of various lithologies, porosities and pore fluids (including hydrocarbons and saline fluids). Their review of research (mainly carried out in the USSR) describes the complex dielectric permittivity behaviour of the rocks, which is the variation in dielectric permittivity with the frequency of the electromagnetic field applied. The complex resistivity (ρ^*) is related to the complex dielectric permittivity (ε^*) by a simple equation

$$1/\rho^* = i\omega\varepsilon^* \qquad (5.2)$$

where ω is the angular frequency ($= 2\pi f$) (s^{-1})
f is the frequency of the electric field.

Olhoeft (1986) reports that induced polarisation has been used with success at a contaminated site contaminated by both organics and inorganics, where the organic plume was mapped using IP and the inorganic plume mapped using EM. The IP technique was also recommended by R. Ogilvy of BGS. However, further case studies involving LNAPLs were not found. The IP method has more commonly been used for mineral prospecting or determination of clay content.

5.4 Ground Penetrating Radar

Ground penetrating radar uses the propagation of electromagnetic energy to measure changes in dielectric permittivity in the ground. A short pulse of electromagnetic energy is transmitted by an antenna placed on the ground. Waves are reflected in the ground and detected by a receiver a short distance away.

The dielectric permittivity is a measure of the polarity of a medium. The dielectric constant of a formation (ε_r) is a dimensionless constant which is the ratio of its dielectric permittivity compared to the dielectric permittivity of free space. The transmission speed of electromagnetic waves within a medium is determined by its dielectric permittivity and also its magnetic permeability (which remains fairly constant in the absence of certain iron minerals for porous media):

$$v = 1/(\mu\varepsilon)^{1/2} \qquad (5.3)$$

where v is the velocity of electromagnetic waves in the medium (m/s)
μ is the magnetic permeability of the medium (H/m)
ε is the dielectric permittivity of the medium, = $\varepsilon_r\varepsilon_0$ (Farads/m)
ε_r is the dielectric constant of the formation[]
and ε_0 is the dielectric permittivity of free space (= 8.854×10^{-12} Farads/m)

The dielectric constant of a porous medium is made up of contributions from the solid and the pore fluid. The dielectric properties of sand with different saturating fluids, from Keech (1988), are summarised in Table 5.2. It can be seen that there are large differences in the relative permittivities of LNAPL- and water-saturated formation, but that oil- and air-saturated formations have similar properties.

Table 5.2 Dielectrical Properties (after Keech, 1988)

Material	Dielectric Constant (dimensionless)	Dielectric Constant of Sand with 30% Porosity saturated with fluid (dimensionless)
Water	78	17.2
Hydrocarbon	2.4	3.9
Air	1.0	3.2
Sand	4.6	
Clay + water	-	60*

* from Olhoeft (1986)

Hydrocarbons generally cause a large reduction in the dielectric permittivity of the ground (Leonard *et al* 1997, Olhoeft, 1986) as would be expected from the properties given by Keech, 1988 (Table 5.2). Olhoeft (1986) presents dielectric constants for various sand and clay mixtures saturated with water, air, benzene and methanol. These are shown in Figures 5.5 and 5.6, which illustrates the high permittivity of water-saturated samples compared to air and benzene saturated samples. Methanol-saturation reduces the permittivity to a lesser extent than benzene.

Levitskaya and Sternberg (1996) have reviewed complex dielectric properties of sedimentary rocks of various lithologies, porosities and pore fluids (including hydrocarbons and saline fluids) as discussed in Section 5.3.

The depth of investigation depends on the transmitter - receiver spacing, but is also limited by the depth of penetration of the electromagnetic energy. The penetration depth of the electromagnetic waves depends on the attenuating properties of the ground and the frequency of the waves. The higher the frequency, the greater the attenuation

Electromagnetic energy is attenuated most if the ground has a high conductivity, due to clay or water content, or by inhomogeneity (changes in the electrical properties of the formation). In clayey soils, penetration is typically only about 1 m. Olhoeft (1986) reports penetration up to 30 m in dry, clay-free sand and gravel deposits, but with the addition of 5% clay this reduces to less than 2 m. In sandy soils, a penetration depth of about 4 m is usual.

The resolution is controlled by the wavelength of the electromagnetic waves, a higher frequency giving better resolution, and is not dependent on the depth of investigation. Resolution is typically 10 cm for 100 MHz, at depths of up to 30 m in clay-free sands (Olhoeft, 1986). The technique has often been used in archaeological investigations because of the ability to map detail at high resolution.

Olhoeft (1986) reports that the technique was used to measure the presence of LNAPLs on the surface of the water table at a site in Bemidji where an EM survey had proved unable to map the petroleum spill. At a second site the GPR showed the location of a creosote plume below the water table due to the presence of altered soil mineralogy from clay-organic reactions.

Bermejo *et al* (1997) report the discovery of an LNAPL plume using GPR, although the GPR actually identified a zone of ionic contamination in the groundwater beneath the LNAPL (caused by biodegradation of the LNAPL) rather than the LNAPL itself.

Leonard *et al* (1997) describe GPR surveys at several sites including a petrol stations, and oil refinery and a chemical plant. They demonstrated an acceptable correlation with soil gas measurements in delineating contamination. They have also used the technique to map out subsurface features, by detailed analysis of the radargrams to identify refraction hyperbolae.

A software package, RADPRO™ has been developed which is an automated 3D visualisation tool (developed by Shell Research, Geo-Services International and Liverpool University).

5.5 Seismic

Seismic refraction surveys involve the measurement of the propagation of seismic waves in the subsurface. The method can detect interfaces or gradational changes in the speed of sound waves, which are generated at the surface. This method is used often in the oil industry for detecting large structural features. The interface between gas and liquid is detectable but the difference in sound speed between water-saturated and LNAPL-saturated formation is likely to be small. No examples of its use in detecting LNAPL spills have been found, since they are generally too small for this method to work, the smallest vertical resolution being a quarter of a wavelength (about 2 m in wet unconsolidated sands, 10 m in dry sands). In small scale investigations the method is limited to the measurement of geological structure and water table location.

5.6 Comparisons

A summary of the advantages and disadvantages of the methods described in this section is given in Table 5.3.

Table 5.3 Comparison of Non-Invasive Survey Methods

Method	Property Measured	Advantages	Disadvantages	Successful Case Studies Published?
Resistivity Survey	EC	Need homogeneous ground conditions, better for thick LNAPL spill		Yes
Conductivity Survey	EC	Need homogeneous ground conditions, better for thick LNAPL spill		Yes
Induced Polarisation	Frequency dependence of EC	Hydrocarbons can be detected if they react with clays	Requires presence of clays	Yes but few
Ground Penetrating Radar	Dielectric Permittivity	Hydrocarbons and water show contrasting permittivity	Cannot use in clays	Yes
Seismic	Velocity of sound waves		Very poor resolution, not possible to measure thin layers of hydrocarbon	No

Note: EC = Electrical Conductivity

All of the surface survey methods reviewed here are qualitative in terms of measuring hydrocarbon thickness. Although there are more case studies for LNAPL delineation involving the use of resistivity/conductivity methods, these appear to be of limited use unless the ground conditions are extremely homogeneous. They are likely to be most successful in delineating a low resistivity anomaly which would be produced if there is concurrent ionic contamination or if the hydrocarbon is highly degraded.

Induced polarisation (IP) and Ground Penetrating Radar (GPR) look to be much more promising techniques although there are few case studies, especially for IP. These two methods are complementary in terms of their geological limitations: GPR cannot be used where there are clays, whilst IP cannot be used if there are no clays. IP and GPR are usually used as a targetted follow up to other investigations as they are too costly and slow to survey large areas.

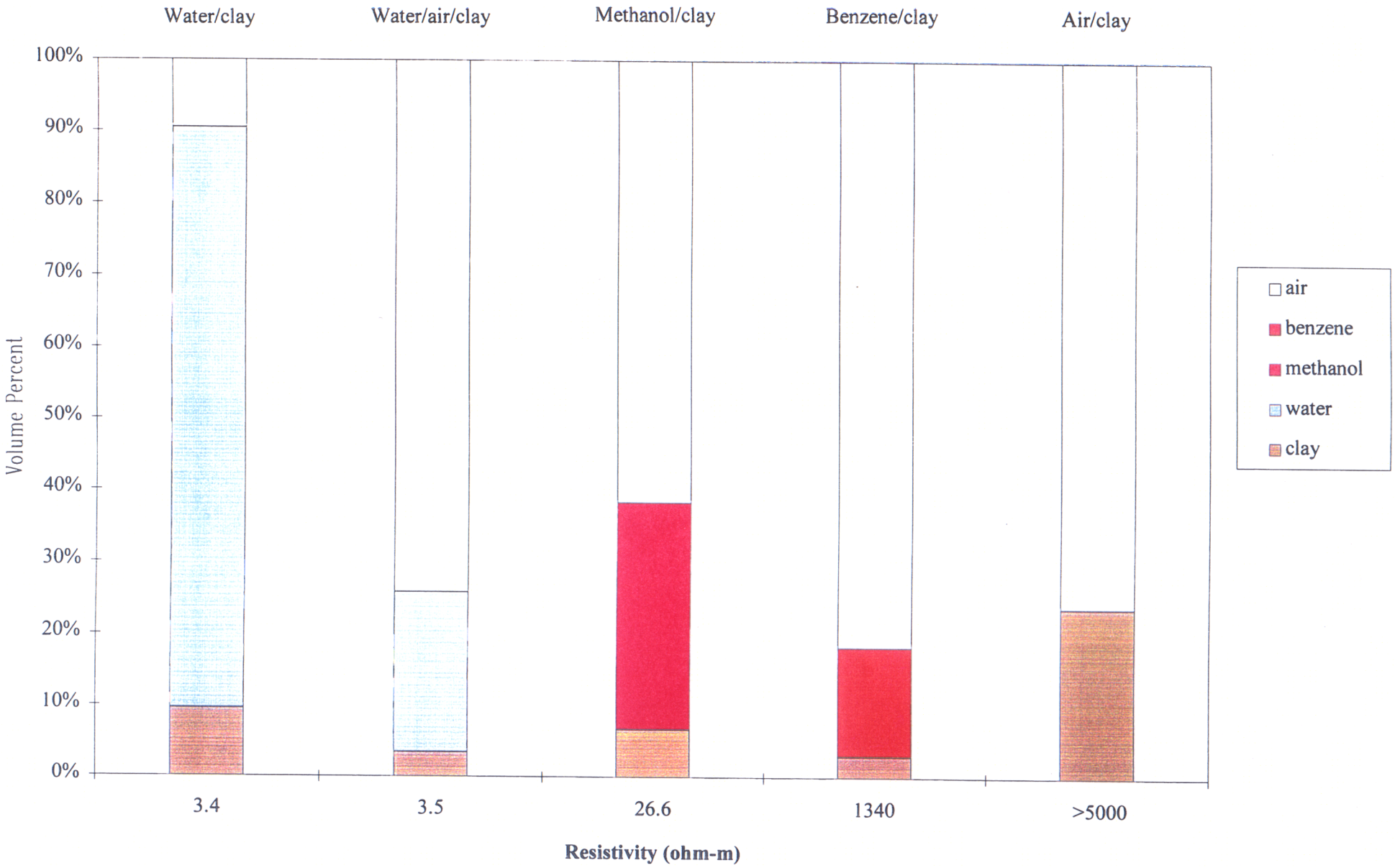

Figure 5.1 Variation of clay resistivity with various saturating fluids (data derived from Olhoeft (1986))

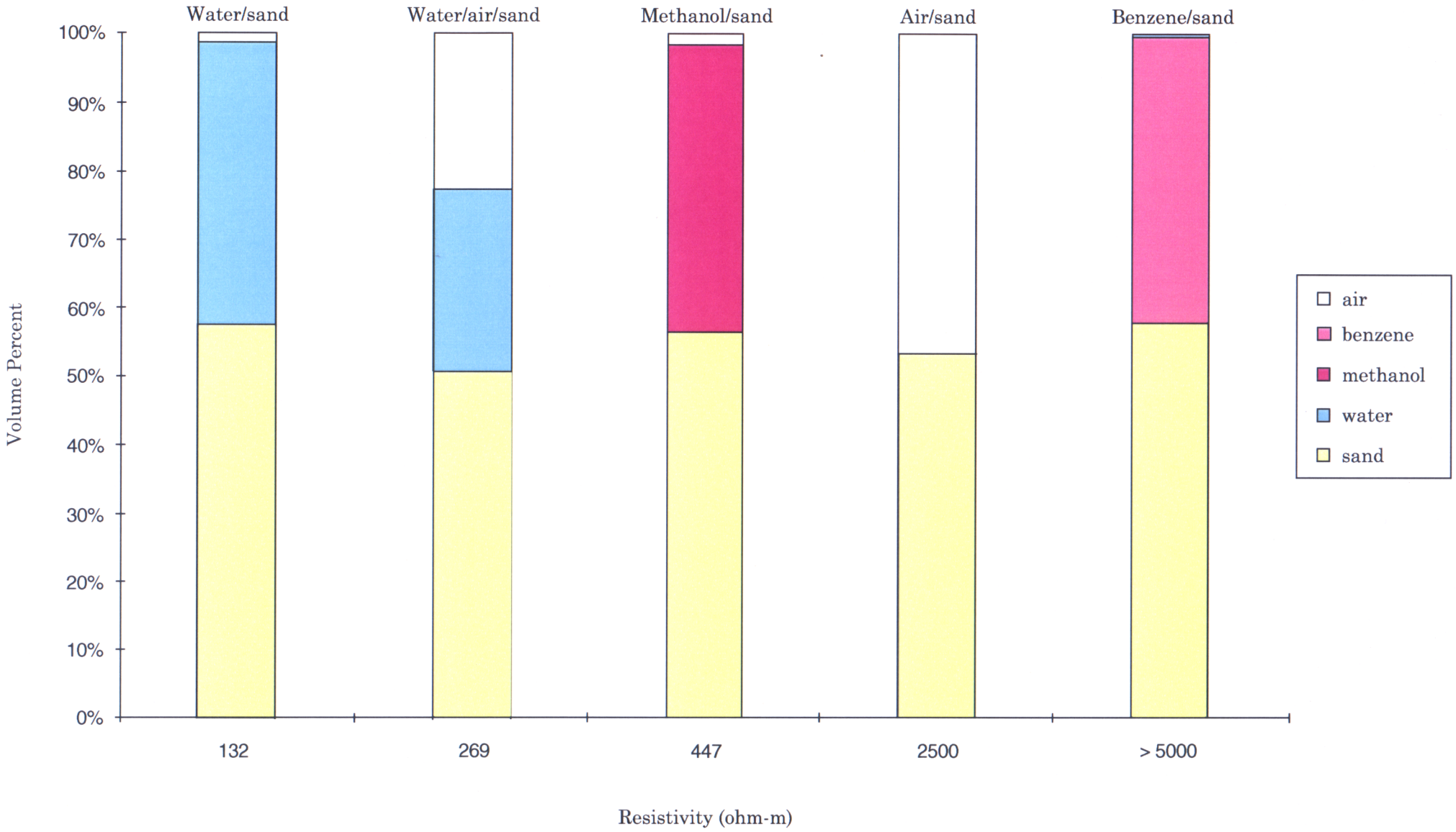

Figure 5.2 Variation of sand resistivity with various saturating fluids (data derived from Olhoeft (1986)

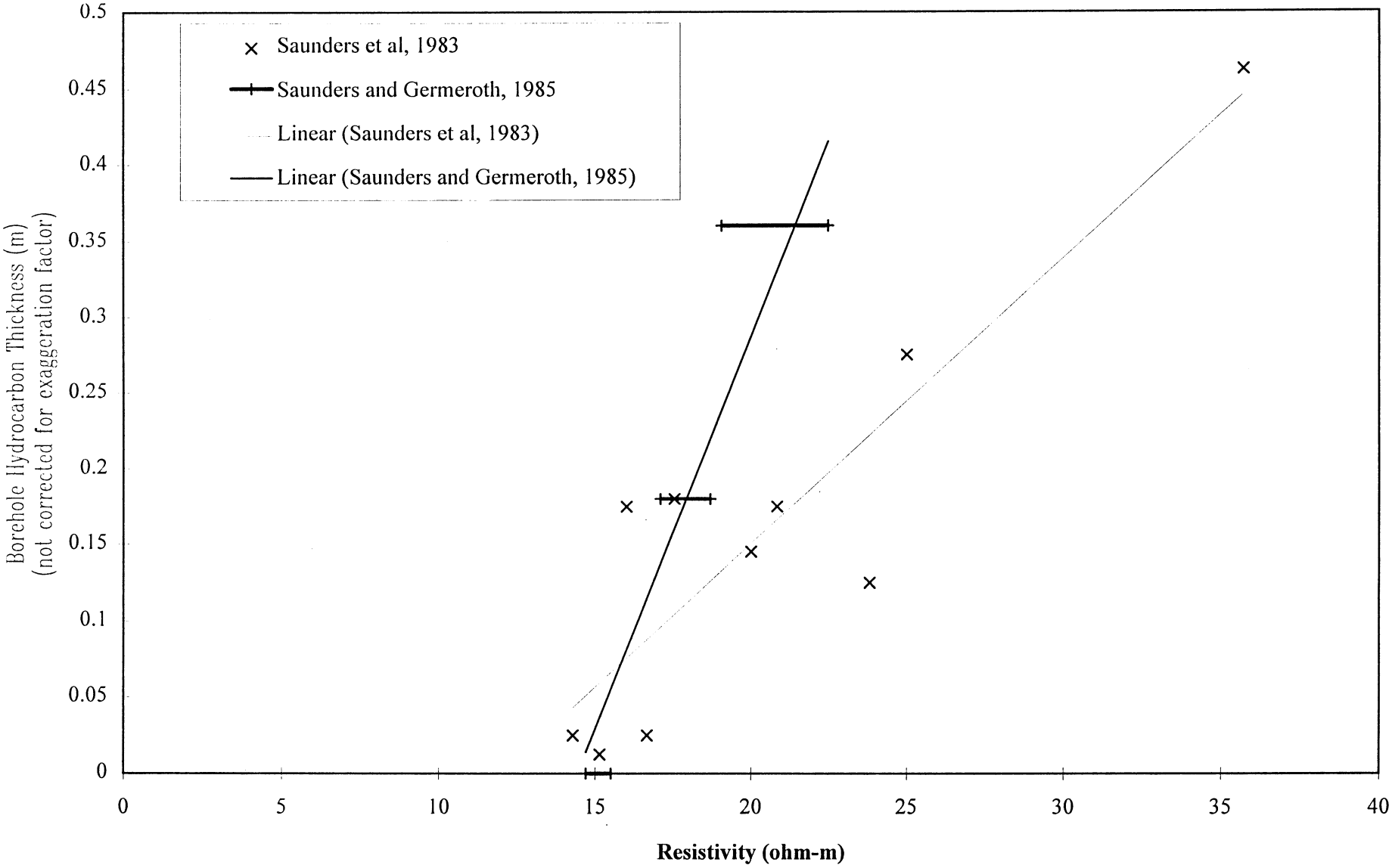

Figure 5.3 A comparison of borchole LNAPL thickness and resistivity

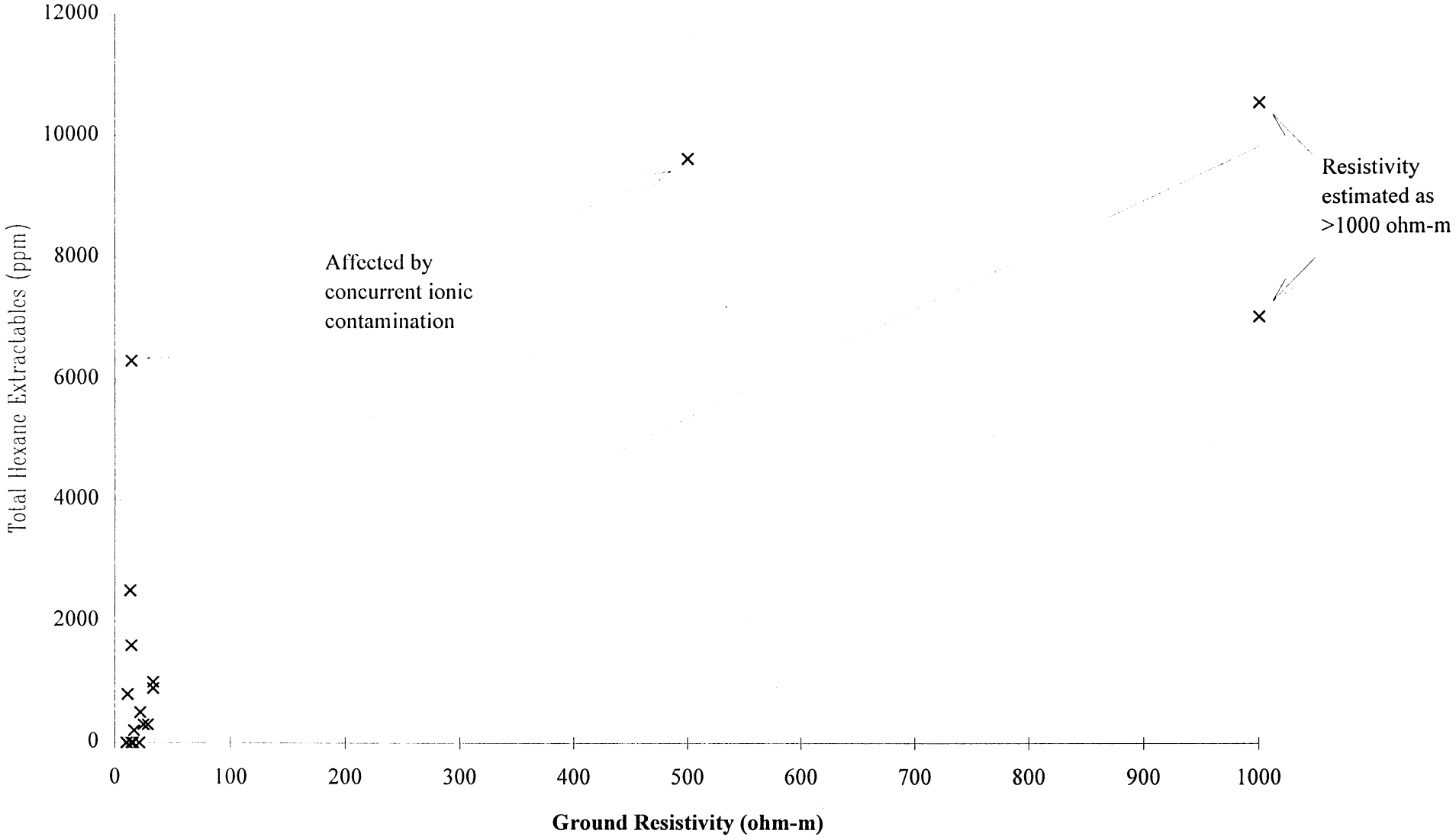

Figure 5.4 Comparison of total hexane extractables in soil and ground resistivity (data from Davies 1991)

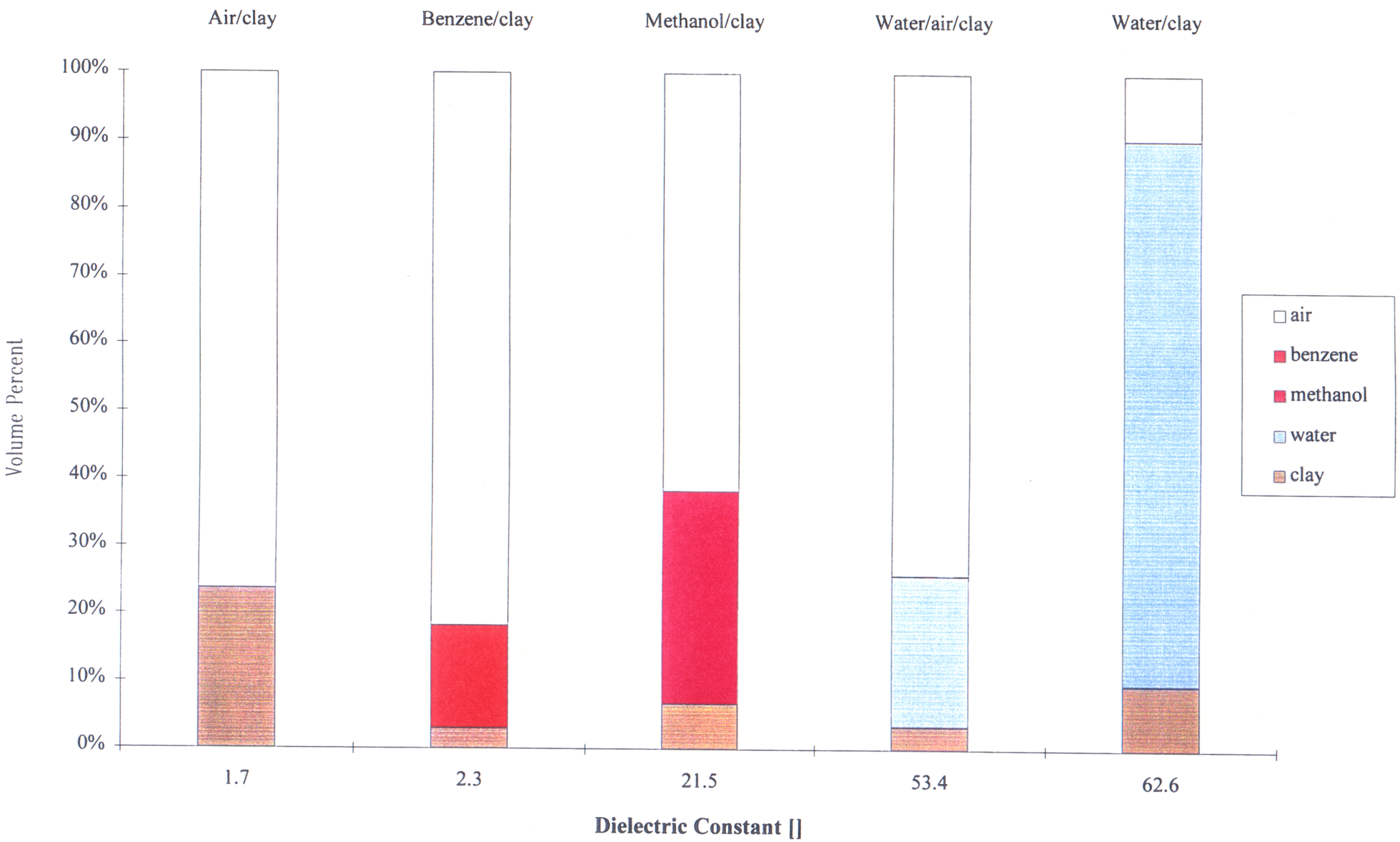

Figure 5.5 Variation of clay permittivity with various saturating fluids (data derived from Olhoeft (1986)

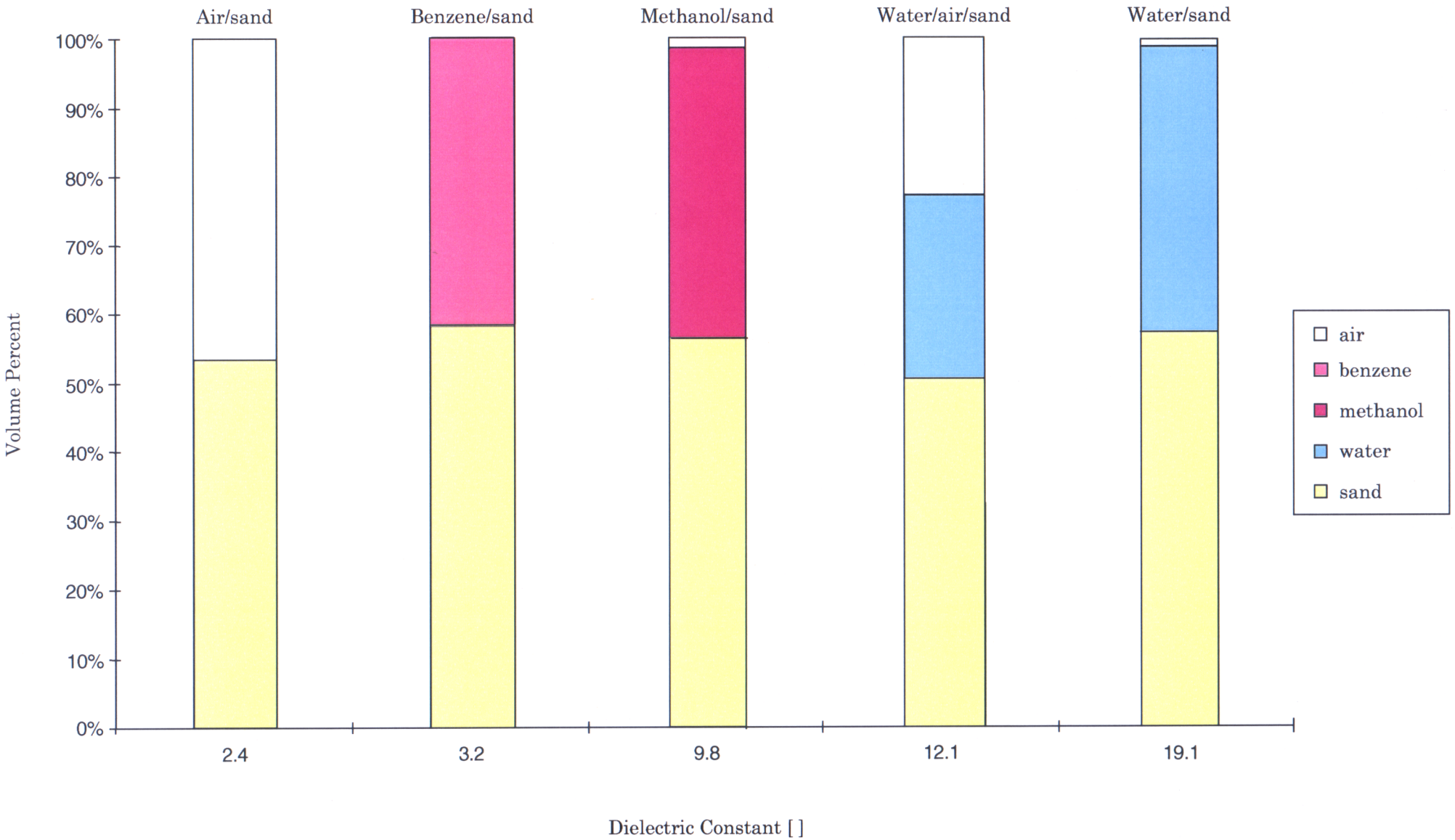

Figure 5.6 Variation of sand permittivity with various saturating fluids (data derived from Olhoeft (1986)

6. METHODS OF EXTRAPOLATING TO TOTAL VOLUME

6.1 Introduction

This Section reviews methods of using the spot-measurement data acquired in a site investigation to estimate the total volume of a LNAPL in the ground. The basis of each interpolation method is first briefly described. The methods are then compared using a practical assessment based on a theoretical problem. This examines the accuracy and precision of results that are obtainable, and how this is affected by sample density and sampling strategy. This exercise is carried out using the software SURFER which is a highly regarded contouring package.

Although the emphasis in this Section is on the determination of free-product volume, the interpolation methods also apply to dissolved concentration data.

6.2 Statement of Problem

The identification of optimum methods of calculating contaminant in place requires a clear statement of the problem. The 'optimum' can probably be defined only in terms of the key constraints; therefore these must also be identified.

6.2.1 Problem

The problem can be defined as follows: given a finite number of point observations of a measure of plume content, determine the total content of the plume. Plume content may be defined in terms of thickness observed in boreholes or probe-holes in the case of free product (after correction for the exaggeration factor if necessary), in which case the total content is its volume. It may be defined in terms of concentration of dissolved material, in which case the total content is the mass of dissolved material. Neither of these measures of content at a point are in terms of volume of geological material. Therefore they must be scaled by the porosity. In general the porosity will vary independently of the measure of content, and therefore the expression for the plume volume is

$$V = \iiint C\phi \, dxdydz \qquad (6.1)$$

where C is concentration
ϕ is porosity

where the integral is taken over a sufficiently large volume to include the whole of the plume.

6.2.2 Constraints

Key practical issues are:

- required accuracy and precision of result,
- level of sampling effort.

It would be expected that there is a trade-off between these. However, different aspects may be more important at different times. In terms of managing emergency response, extent of contamination may have overriding importance, whereas for costing remediation, plume volume may be more important. Sampling suffers from logistical constraints at nearly all sites; the extent to which these can be overcome is affected by priorities.

6.2.3 Issues

The problem stated above is readily tractable for a plume of mathematically defined shape, where the value of C is defined at all x, y, z. These plumes may be integrated directly in some cases, or numerically in all cases. For known functions, any errors in numerical integration are quantifiable.

In a real situation, the plume shape is not defined by a known mathematical function and therefore the value of C is not known everywhere, but only at the sampling points. Additionally, the measured value of C is subject to error, and the outer surface of the plume is probably poorly defined by the available sample points. As a consequence of the nature of geological materials, it is probable that the true shape of the plume is arbitrarily complex, determined by the heterogeneity of the geological material. For the same reason, the three-dimensional distribution of porosity will be very complex and poorly known.

Approaches to the problem involve the determination of a function that approximates to the true plume, and then integrating this plume numerically. Although some techniques lead to a plume description that could be integrated analytically, there is little advantage in this - the possible increase in accuracy is slight, compared with significant loss of ease of use. In SURFER this procedure is known as 'gridding' and involves defining the function at the points of a rectangular grid. In SURFER, there are many different ways of defining the grid from a given set of data points, and these interpolation methods are discussed in Section 6.3.

After gridding has taken place, producing contours from the grid in SURFER is straightforward and requires no further choice in the method of contouring. Similarly, calculating the volume from the grid is relatively simple and can be done either using the Trapezoidal Rule or Simpson's rule. Areas of negative values in a grid can arise from several of the interpolation methods although clearly this cannot occur in reality. If negative volume is included in the calculation it can lead to an underestimation of spill volume. If the positive

volume only is required, as would be the normal case for an LNAPL spill, only the Trapezoidal rule is available to calculate this in SURFER.

The function must decrease to zero at the edge of the plume and remain at zero beyond the edge of the plume, unless the integration can be restricted to the plume volume only. This correction can be partially achieved in SURFER by setting a 'lower surface' of $C = 0$. SURFER will then calculate the 'positive volume' which only includes areas where $C > 0$.

6.2.4 Nature of Plume

Plumes of free LNAPL typically have an areal extent large compared with their thickness. The content is defined by measured thickness and therefore is intrinsically variable in two dimensions rather than three. Effective porosity is a three-dimensional variable and therefore the product of the two should be integrated in three dimensions. However, it is usual to assume that porosity is constant with depth, resulting in a simpler expression which need be integrated in the x-y plane only.

Concentration of dissolved contaminant varies in three dimensions. This is frequently ignored since the data are difficult and expensive to collect. On other occasions vertical averages are made.

Throughout the rest of the discussion, variation in the vertical direction will be ignored.

The shapes of free and dissolved product plumes differ, especially near the edge. The edge of a free product plume is controlled by pore entry effects and there is a clear separation between areas containing no contaminant and those containing contaminant - the transition is sharp, at least while the plume is advancing. The question arises as to whether the intrinsic shape of a free product plume can be used in definition of the best determination method.

The edge of a dissolved solute plume is defined by diffusive and dispersive processes and is asymptotic. There is no clear boundary.

Measurements may only be available for apparent LNAPL thickness in boreholes, uncorrected for the exaggeration effect. In this case, a differential method of determining the true thickness in the formation has been suggested by Littlefield *et al* (1984) although this requires starting recovery pumping of LNAPL prior to the estimation of total volume. The method involves monitoring the amount of recovered product accurately and contouring the apparent thickness in the boreholes before and after pumping. The relationship between apparent volume in the ground and pumped volume can be extrapolated to determine the actual volume in the ground.

6.2.5 Oil Industry Approach

Determination of the volume of free-phase hydrocarbons is a routine task within oil exploration. However, there are significant differences between hydrocarbon reservoirs and oil-spills in aquifers. Oil reservoirs are typically large, with horizontal extents of several thousand metres, and thick, in excess of one metre. Oil reservoirs, almost by definition, have a readily identifiable upper surface controlled by geology. Given the areal extent this can be considered well mapped by geophysics supplemented by borehole control. The lower boundary is defined from borehole geophysics, again with adequate accuracy given the thickness. A major uncertainty is porosity distribution. This can be addressed with control from very frequent core samples, extended by conditional simulators which contain knowledge of sedimentary architecture (e.g. STORM).

For an oil spill located on the water table, it is likely that neither the top nor the bottom surface are easily located. Given this uncertainty, collecting the considerable amount of data for conditional simulation of porosity is inappropriate.

6.3 Review of Methods

6.3.1 Types of Method

Methods fit into two groups: function fitting, and weighting. Into the first group can be placed Thiessen polygons, Delaunay triangulation, and Trend surfaces. These methods lead to functions which are defined everywhere and could be integrated directly - although in practice 'Gridding' is the easiest way to integrate (and is the method used by SURFER). In the second group are Kriging, conditional stochastic simulation and various machine contouring algorithms. These methods lead to a grid of data. In addition hand contouring is considered.

These methods are considered briefly to assess their ability to cope with the identified issues: edge determination, variability in the plume, measurement error, repeatability, accuracy and precision.

In terms of measurement error, some methods 'honour' the data and others do not. A method which honours the data will force the grid to match the data exactly at each data point. A method which does not honour data points will have some degree of error at each data point. The fitting of the function to the data involves minimising the error at each datapoint.

Most methods which honour data also allow smoothing functions to be applied which allow the method not to honour the data. The approach not honouring data is more applicable to data which include a large number of readings with significant errors. Two general characteristics of LNAPL measurement data are that it is usually relatively sparse - depending on a borehole or probe-hole for each reading, and secondly, that it is fairly accurate. If 0.5 m of product exist in the ground at a borehole, then it is a good idea to ensure that the fitted

function is 0.5 m at that location. Therefore it is sensible to restrict analysis to methods that honour the data.

Another consideration is how the edge of the plume is defined. This factor is most important where there are few zero measurements. In some cases the zero contour may not be defined and the plume size would be infinite. If there are no zero data, a decreasing trend in measurements could result in a zero contour. However in a real situation, additional boreholes would be probably be required to define the extent of the plume.

6.3.2 Function Fitting

6.3.2.1 Thiessen Polygons

The method represents the data by a piecewise constant function, defined for polygonal tiles. The tiling pattern is related to Delaunay triangulation, in that the tile sides are the perpendicular bisectors of the sides of corresponding Delaunay triangles.

- All data points are honoured explicitly and there is no allowance for statistical error.
- The algorithm for generating the tile pattern is simple, robust and repeatable.
- The edge of the plume is undefined in the absence of an adequate cover of zero content data points all around the plume. In the presence of zero data points, the plume edge is defined as half way between pairs of zero points and those showing measurements. This line is likely to fluctuate around the true zero contour, rather than to follow it.

This method is available in SURFER as 'Nearest Neighbour'.

6.3.2.2 Delaunay Triangulation

The method represents the data by a piecewise linear function, defined over triangular tiles. The tiling pattern is complementary to Thiessen polygons as described in Section 6.3.2.1.

- All data points are honoured explicitly and there is no allowance for statistical error.
- The algorithm for generating the tile pattern is simple, robust and repeatable.
- The edge of the plume is undefined in the absence of an adequate cover of zero content data points all around the plume. In the presence of zero data points, the plume edge is defined as joining these points.

6.3.2.3 Trend Surfaces

The method represents the data by a continuous polynomial function of arbitrary degree n provided that there are at least $(0.5n^2+1.5n+1)$ data points. If only the minimum number of data points is present, all data points are honoured. However, surfaces of high degree tend to fluctuate considerably between data points. If the degree is less than two, it is not possible for there to be a closed zero contour.

- The degree of fit of the surface can be computed
- The algorithm is robust and repeatable, but the choice of degree is arbitrary
- The edge of the plume can be defined objectively by determining the curve along which the function predicts zero content, but this may not be a closed shape. Beyond this zero contour, the fitted function predicts unphysical contents.

6.3.3 Weighting

6.3.3.1 Kriging

The method computes weighted values at arbitrary points, usually a regular grid. Extensions of the method perform the volume integral directly.

The method uses a knowledge of the spatial variability of the data to compute the Best Linear Unbiased Estimator to weight the data for gridding or integration. It is necessary to determine the spatial variability as a separate step. This step is not necessarily entirely objective.

- Data require additional manipulation if they are not stationary, i.e. the mean is not constant throughout the domain.
- The method works best with fairly large datasets collected on a fairly regular basis. Clusters of data points can lead to errors.
- The method honours all data points
- An estimate of relative statistical reliability is obtained, both for gridded points. The uncertainty in the volume integral can be calculated. From an extension of the method, an estimate of uncertainty reduction by acquiring additional data is possible.
- The edge of the plume is not determined by the method.

6.3.3.2 Other Contouring Algorithms

The methods work by estimating values on a regular grid. A large number of weighting functions area available, with different biases. A prime objective in algorithm development has been to produce contours the look reasonably similar to hand contours, whilst using minimum CPU time. The volume is determined by integrating the resulting grid numerically.

- The choice of algorithm is subjective and can influence the results considerably. Given an algorithm and parameters, the result is repeatable.

- Most algorithms perform badly when the data do not fit an approximately quadratic surface on the scale of a few data points.

- Algorithms do not in general honour data points. Forcing the honouring of data points tends to result in unlikely 'bulls-eye' contours.

- In the absence of zero content control points around the plume, algorithms perform badly near the edge of the data.

The methods available in SURFER include the following:

1. Inverse Distance Weighting (Radial Basis Functions). At each point in the grid the nearest points are averaged, weighting them by $1/r^n$ where r is the distance away. The power, n, number of points sampled and search method can all be varied. This method is fast but is very susceptible to the Bull's Eye' effect.

2. Minimum Curvature. An elastic plane is fitted to the data in such a way as it keeps within the 'Maximum Residual' value of each reading but with as smooth a grid as possible. This method does not honour the data.

3. Shepard's Method. This method uses an inverse distance weighted least squares method (Surfer manual). The use of local least squares is meant to reduce the bull's eye appearance of the contours generated from this gridding method. The method is described fully by Shepard (1968).

6.3.3.3 Hand Contouring

- This method is subjective and may be difficult to repeat

- The method is prone to bias

- The method allows for the input of considerable conceptual understanding (but this may be self-delusion!)

- The method allows for the definition of zero contour, although this may not be well founded.

- It is possible to generate results from very sparse data.

- All data points may be honoured.

- Estimates of accuracy and precision are subjective only.

To integrate the volume, areas within contour lines must be measured, either by planimetry or square counting, and then the areas multiplied by values and a weighted total produced. Weighting may be by the trapezium rule or the more complex Simpson's rule. The methods are easier to use if the contour interval is regular.

For ease of volume calculation, computer generated contours could be manipulated by adding fictional points (e.g. a zero point in a low permeability region) so the volume could then be integrated by the computer. Essentially, this is a similar process to manipulating hand-drawn contours to fit in with conceptual understanding. However this should be done with care, ensuring that all assumptions made in the volume calculation are clearly stated, and that the generated contours are still match the conceptual understanding.

6.4 Practical Assessment

An exhaustive assessment of methods of plume volume estimation would be a wide-ranging and time-consuming exercise. We therefore limit our assessment to estimations made using methods and tools (software) which are very widely used. From this limited exercise on a single distribution of LNAPL, it is not possible to identify one method which will always give the most accurate plume volume. Each method's performance depends on which dataset it is used on. The exercise then is to compare the contours and volume calculation errors arising from these widely-used methods, to give a general guide to their performance.

As a test of alternative methods, a hypothetical plume of known volume and known spatial coverage has been generated. The effect of different sampling strategies and interpolation methods on the estimation of the volume and area has been investigated. In the short time available for this exercise, we take no account of variations in porosity, thereby simplifying the problem considerably. The PC-industry standard contouring software SURFER has been used to perform most of the calculations.

6.4.1 Hypothetical Plume

The LNAPL plume used in this exercise is derived by taking a horizontal 'slice' through a sphere of 100 m radius, at a level such that the maximum height of the plume is 1 m, and it is circular in plan. A real plume is unlikely to have this degree of symmetry and therefore we remove the 'south-western' quadrant of the plume. This provides a test of the ability of methods to cope with a plume that is irregular. In concept, this removed area might represent a volume of low permeability strata.

The hypothetical plume has a volume of 235 m^3, and covers an area of 469 m^2. The radius of the contaminated area is 14.1 m.

Sampling Strategies

We consider a domain of 100 m by 100 m. As a primary test of the contouring algorithms within SURFER, we generate a plume from a set of observations spaced at 2 m centres. This is clearly an unrealistic sampling grid, but it gives an indication of the ability of the routines to reproduce the known plume.

Moving on to more realistic sampling strategies, for a domain and 'hot-spot' of the sizes used here, Department of Environment guidelines (Nottingham Trent University, 1994) recommend approximately 20 boreholes in a 'herringbone' pattern to guarantee hitting the hot-spot. For convenience, we use 25, spaced approximately at 20 m intervals. We assume that the location of the centre of the plume is known, and that one borehole is placed there.

The coarse herringbone pattern results in only one borehole intercepting the plume (as would be expected from the guidelines). We then superimpose another herringbone grid, at approximately 5 m centres, around the 'hot-spot'. This results in a total of 49 sampling points with 6 intersecting the plume.

Alternatives to this 'nested' herringbone pattern assume no knowledge of the plume centre location, with all sampling points moved 5 m to the east and the north (i.e. diametrically away from the 'missing' part of the plume), or 5 m to the west and the north.

We also consider a pattern of sampling points drawn from a real investigation in a congested urban area in which access was severely limited. This meant that boreholes could not be drilled in optimum places, resulting in a random element in placing, typical of 'real-life' situations. The spread of sampling points was scaled to fit between ± 45 m, and alternatively between ± 20 m.

For each of the above strategies, we use two gridding options within SURFER, namely kriging and triangulation. Default parameters are used in all cases. The interpolation is

produced to a 50 by 50 m grid and the final integration made using the Trapezoidal Rule (which is a robust and reliable numerical integration method).

Table 6.1 summarises the results of this exercise and the contours and volume calculations are in Appendix A. Volumes are calculated above the $z = 0$ level. This means that any extrapolated measurements that are less than zero are not included. As a solution to the 'edge effect' (the definition of the zero contour where few zero data exist) this appears to solve the problem, since any method producing a result which does not fall away to zero is likely to go negative at distance (since the measurements are decreasing). Any method which is subject to a different trend at infinity should be used with caution and may require "trimming" of the area.

Table 6.1 Comparison of Estimated Plume Volumes for a Range of Sampling Strategies

Dataset name	Description of Sampling Strategy	No of Hits	Interpolation Method	Contour shape	Positive volume (m^3)	Area of Plume (above z=0.0) (m^2)	VOLUME ERROR	AREA ERROR
ACTUAL	Calculation		Calculation		235	469		
TRUE2M	2m by 2m discretisation over whole domain (2601 points)	~120	Kriging	Good, some zero frills	252	898	7.3%	91.4%
TTRUE2M	2m by 2m discretisation over whole domain (2601 points)	~120	Triangulation	Very good	252	584	7.3%	24.5%
HER5	Simple 5x5 herringbone with known plume centre (25 points)	1	Kriging	Circular, since only one point encounters plume	439	2423	86.8%	416.7%
THER5	Simple 5x5 herringbone with known plume centre (25 points)	1	Triangulation	Poor, asymmetric hexagon	400	1344	70.6%	186.6%
HER5NST	5x5 simple herringbone with known plume centre, nested 5x5 herringbone from -20 to +20 (49 points)	6	Kriging	Slight indentation in null quarter	263	2256	12.1%	381.0%
THER5NST	5x5 simple herringbone with known plume centre, nested 5x5 herringbone from -20 to +20 (49 points)	6	Triangulation	Quite good	252	798	7.3%	70.1%
HER5NST3	5x5 simple herringbone with unknown plume centre, nested 5x5 herringbone from -20 to +20 (49 points), all points offset by x=+5, y=+5 (i.e. to NE)	7	Kriging	Indent in SW good shape but not big enough	225	1129	-4.2%	140.7%
THER5NT3	5x5 simple herringbone with unknown plume centre, nested 5x5 herringbone from -20 to +20 (49 points), all points offset by x=+5, y=+5 (i.e. to NE)	7	Triangulation	Not bad, thin 'drip' to south	222	1020	-5.6%	117.5%
HER5NST4	5x5 simple herringbone with unknown plume centre, nested 5x5 herringbone from -20 to +20 (49 points), all points offset by x=-5, y=+5 (i.e. to NW)	6	Kriging	Zero contour bulges to E and S	274	1606	16.8%	242.5%
THER5NT4	5x5 simple herringbone with unknown plume centre, nested 5x5 herringbone from -20 to +20 (49 points), all points offset by x=-5, y=+5 (i.e. to NW)	6	Triangulation	Poor, bulges to E and S	367	1510	56.5%	222.0%
LLRAN1	Site locations scaled to fit between -45m to +45m in both x and y	4	Kriging	Very poor	392	3291	66.9%	601.7%
TLLRAN1	Site locations scaled to fit between -45m to +45m in both x and y	4	Triangulation	Poor, large bulge to NE	356	1710	51.8%	264.6%
LLRAN2	Site locations scaled to fit between -20m to +20m in both x and y	15	Kriging	Good within plume, large -ve areas in extrapolated areas	228	804	-2.7%	71.5%
TLLRAN2	Site locations scaled to fit between -20m to +20m in both x and y	15	Triangulation	Good, SURFER cuts off contours in NE	204	640	-13.2%	36.5%
LLRAN2A	Site locations scaled to fit between -20m to +20m in both x and y	15	Informed kriging, (nested Gaussian variogram)	Good	240	825	2.3%	75.9%

NB All grid domains are $(100m)^2$

*** Refers to filenames in Appendix A**

6.4.2 Interpolation Strategies

For this exercise, a particular dataset was selected from the various sampling scenarios devised. The one thought to be most typical of a real-life investigation was the herring-bone strategy with 6 boreholes encountering LNAPL. The edges of the plume are well-delineated in this case.

Eight types of interpolation methods were used on this dataset, seven of which were available in SURFER, the last method being hand-contouring. Several of the interpolation methods depend on 'data search' settings. The value assigned to each point on the grid is calculated from nearby data points. The data points used are defined by the radius to be searched, the maximum number of data points used and other optional factors such as anisotropy, searching in selected quadrants etc. The grid used for the calculations in Table 6.2 is 45 by 45 m unless otherwise stated and the integration method is again the Trapezoidal Rule.

The hand contouring was done independently by three senior hydrogeologists, who were told only that the data points were measurements of LNAPL thickness. The total volume was estimated from the contours using a planimeter and the Trapezoidal Rule. The area between each two contours is multiplied by the midpoint value and the total added.

The results of this exercise are summarised in Table 6.2 and the contours and volume calculations are in Appendix A. There are five methods which calculated the volume with less than 10% error. These were triangulation, inverse distance (using nearest 4 data points), kriging (using nearest 4 data points), hand contouring and nearest neighbour methods. Of these, the kriging and inverse distance methods depend on the 'data search' settings, with other data search settings producing poorer results. The volumes from the hand contours ranged from 4.6 to 14.1% error.

6.4.3 Comments on Results

The hypothetical plume used in this exercise is quite a 'difficult' shape to contour, particularly because of the sharp plume edges resulting from removal of a quarter of the circular plume. We would therefore expect most techniques to over-estimate the volume and area for this reason at least.

It is noteworthy that all examples resulted in over-estimation of plume area, and most examples resulted in over-estimation of plume volume. Use of these techniques could therefore be considered to be conservative for real situations. Where precise estimates of plume volume, and particularly plume area are required, care should be taken to critically review the default calculations. The only method which came close in estimating the plume area was the nearest neighbour method with an error of 1%. All the other methods over

estimated the area, with errors of between 74.5 and 1440.5%. However, the estimation of plume area is not usually the main aim of contouring LNAPL thickness data.

Triangulation and nearest neighbour techniques perform well for this exercise, primarily because there is no smoothing of a fitted surface beyond the zero data points causing the generation of negatively valued areas. These techniques are robust and do not require many decisions about data search options.

From Table 6.1, where both triangulation and kriging were applied to several different datasets, default plume volume calculations for triangulation are slightly better than kriging (for the same data support), and default plume area calculations are generally much better. Unsurprisingly, better results were obtained where more data points were available from within the plume itself.

With the inverse distance method, when all data points were used during gridding, the results were much poorer than when only the nearest 4 data points were used (107% error). Similarly, with kriging, using all data gave worse results than just using the nearest 4 data points, although the maximum error using kriging was only 12.1%. Several different sizes of grid were tried using kriging, which made only slight differences to the calculated volume.

The best shaped contours were from the inverse distance and triangulation methods, whilst kriging produced odd artifacts around the edges. Shepard's method, polynomial trend surface and the minimum curvature methods produced a lot of above zero regions away from the plume. The nearest neighbour method produced polygonal contours, as would be expected since it is analogous to doing Theissen Polygons.

Hand contouring compares well to the automated methods and had a sensible edge definition. This test was done using no prior site knowledge. If a site has known geological controls, this method would be probably preferable to automated methods which cannot take these into account.

Kriging over the whole domain has some problems, in that large areas of negative values are generated. This may be at least partly overcome by using a log transformation of the sampled data, but this was not done for the purposes of this exercise. Restricting the kriging to a smaller domain produces a better representation of plume area and volume. Kriging is likely to work better in the absence of large areas of zero value, for example where several hot-spots exist on a contaminated land site, rather than for a specific plume. The default variogram model built into SURFER does not get the most out of the data, being a linear variogram apparently based on data variance at relatively large separations: small scale spatial correlations are therefore not well accounted for.

Polynomial regression was experimented with, using different orders of equations to describe the trend surface. The lowest order, a quadratic surface, showed a simple circular pattern. None of the polynomial equations showed the indentation feature in the south western quadrant. There was little difference in the volumes calculated using higher (3, 4 and 5) order equations - all are overestimates, due to the grid becoming positive towards the edges of the domain. For the 4th order equation, the domain was reduced in size to remove the edge effects, and only this result (the best from this method) is shown in Table 6.2.

SURFER does not provide functionality either for displaying the experimental variogram, or for variogram modelling, which could be used to investigate the spatial structure of the data in more detail. As an example, the plot presented in Appendix A (referred to as LLRAN2A) shows the result of kriging over a restricted domain using a nested Gaussian variogram model derived from an analysis of the experimental variogram. The resulting plume is the 'best' reproduction of the hypothetical plume, although the effort required to do this is considerable and requires some familiarity with geostatistical techniques.

6.4.4 Summary

Table 6.3 shows the performance of the various sampling strategies and interpolation methods tried in terms of percentage error in volume. However it should be noted that good performance against a specific problem does not imply good performance against all problems. There is also the possibility that a poor predictor is good 'by luck' in this particular problem. The conclusions and recommendations from these results are given in Section 7.

Table 6.2 Comparison of Estimated Plume Volumes for a Range of Interpolation Methods

Dataset name*	Interpolation Method	Contour shape	Positive volume (m^3)	Area of Plume (above z=0.0) (m^2)	VOLUME ERROR	AREA ERROR
ACTUAL	Calculation		234.8	469		
JHER5NST	Inverse Distance to Power of 2 ($^1/r^2$), search nearest 4 data points	Very good	249.5	978	6.3%	108.5%
CHER5NST	Kriging $(85m)^2$ domain) search nearest 4 data	Plume shape good, but above zero artifacts over large area	249.8	2739	6.4%	484.0%
ZHER5NST	Triangulation	Quite good	252.1	818	7.4%	74.5%
NHER5NST	Nearest Neighbour (Theissen Polygons), search 60.1m radius	Slightly odd shape	252.8	465	7.7%	-0.9%
NRU/MJS/RWNS	Hand Contouring plus integration with planimeter, average results from 3 senior hydrogeologists	Good	256.4	539	9.2%	14.9%
HER5NST2	Kriging $(70m)^2$ domain, search all data	Slight indentation in null quarter	262.8	945	11.9%	101.6%
KHER5NST	Kriging $(85m)^2$ domain, search all data	Not bad, odd shaped edges	262.9	1089	12.0%	132.2%
HER5NST	Kriging $(100m)^2$ domain, search all data	Slight indentation in null quarter	263.2	2256	12.1%	381.0%
MHER5NST	Minimum Curvature (max residual = 0.001)	Not bad, a lot of positive area away from plume	288.1	3858	22.7%	722.6%
PCHR5NST	Polynomial Trend Surface of Order 4, $(65m)^2$ domain	Very symmetrical, goes up steeply at edges of grid so domain size reduced	294.2	2120	25.3%	352.1%
AHER5NST	Shepard's Method, search all data	Not bad, a lot of positive area at edge of grid	323.4	6672	37.7%	1322.5%
IHER5NST	Inverse Distance to Power of 2, search all data	Not bad, but does not reach zero	486.8	7225	107.3%	1440.5%
SHER5NST	Shepard's Method, search nearest 4 data points	Contour shape totally wrong, grid range -7 to +5 m	1241.9	2179	428.9%	364.5%

NB All grid domains are $(85m)^2$ unless otherwise stated

All datasets from the sampling strategy: 5x5 simple herringbone with known plume centre, nested 5x5 herringbone from -20 to +20 (49 points) (6 hits)

*** Refers to filenames in Appendix A**

Table 6.3 Summary of Sampling Strategies and Interpolation Methods

Sampling Strategy	2m by 2m discretisation over whole domain	Simple herringbone, known plume centre	Nested herringbone, known plume centre	Nested herringbone, unknown plume centre	Nested herringbone, unknown plume centre, all points offset to NW	'Random' locations (scaled to 85m)	'Random' locations (scaled to 40m)
Interpolation Method	**Volume Error (%)**						
Nearest Neighbour (Theissen Polygons)			7.7%				
Triangulation, $(85m)^2$ domain			7.4%				
Triangulation, $(100m)^2$ domain	7.3%	70.6%	7.3%	-5.6%	56.5%	51.8%	-13.2%
Kriging, $(100m)^2$ domain, search all data	7.3%	86.8%	12.1%	-4.2%	16.8%	66.9%	-2.7%
Kriging, $(70m)^2$ domain, search all data			11.9%				
Kriging, $(85m)^2$ domain, search all data			12.0%				
Kriging, $(85m)^2$ domain search nearest 4 data			6.4%				
Informed Kriging, nested Gaussian variogram							2.3%
Inverse Distance $(1/r^2)$, search nearest 4 data points			6.3%				
Inverse Distance $(1/r^2)$, search all data			107.3%				
Hand Contouring, average results from 3 senior hydrogeologists			9.2%				
Minimum Curvature (max residual = 0.001)			22.7%				
Shepard's Method, search all data			37.7%				
Shepard's Method, search nearest 4 data points			428.9%				
Polynomial Trend Surface of Order 4, $(65m)^2$ domain			25.3%				

less than 10% error

less than 20% error

7. CONCLUSIONS AND RECOMMENDATIONS

7.1 Determination of True Free Phase LNAPL Thickness

7.1.1 Conclusions

The conclusions of the study on the theoretical aspects of LNAPL occurrence and its relationship with thicknesses observed in the wells are:

- The Zilliox Equation appears to be vindicated by sand tank data with the additional comment that sub-critical ingress appears to occur in reality. Sub-critical ingress implies that as soon as LNAPL is present at the top of the water capillary zone, a thickness of LNAPL will move into the well. The LNAPL thickness in the borehole, D, is given by:

$$D = p_{LW}/g(\rho_W-\rho_L) - p_{AL}/\rho_L g \qquad \text{(from equation 3.5)}$$

where
p_{LW} is the LNAPL-water displacement pressure (N/m^2)
p_{AL} is the air-LNAPL displacement pressure (N/m^2)
ρ_W is the density of water (kg/m^3)
ρ_L is the density of LNAPL (kg/m^3)

  Thereafter the thickness in the well will always exceed the thickness in the ground by this quantity, D.

  In practice, transient effects complicate the situation, and there may not be enough time for this thickness to be attained due to short term drainage of the larger pores around the borehole. Frequently, in the field, boreholes appear to exist in steady-state with 1 or 2 cm of LNAPL, which is not consistent with the theory. This may be because the LNAPL layer is simply not mobile enough to fill the borehole at very thin thicknesses.

- The more advanced formulae available do not contradict the sharp interface version as such, but extend it. The pressure curves are the same as the sharp interface theory - it is only the saturation curves that have been modified. In terms of volume of LNAPL they provide a means of estimating the additional LNAPL occurring above the top of the LNAPL capillary zone and subtracting off the volume of water that occurs above the top of the water capillary zone. The Brooks-Corey formulation is recommended not because it is necessarily the most accurate, but because it is easy to use in practice since it provides an explicit formula and only requires one more parameter to be estimated. This parameter is λ, the pore-size distribution index.

- Although the formula is generally accepted, the use of it in calculation is difficult because of the problems in estimating the two displacement pressures p_{LW} and p_{AL}. Methods of estimating the missing parameters have been developed by various authors.

  If the surface tension and density of the LNAPL is known, the following formula can be derived but has not been experimentally verified:

$$T_G = T + \frac{H_C \rho_W}{\sigma_{AW}} \left[\frac{\sigma_{AL}}{\rho_L} - \frac{\sigma_{LW}}{\rho_W - \rho_L} \right] \tag{3.11}$$

  where T_G is the actual thickness in the ground (m)
  T is the observed thickness in the borehole (m)
  H_C is the height of the top of the capillary zone above piezometric level (m)
  σ_{AL} is the surface tension between air and LNAPL (N/m)
  σ_{AW} is the surface tension between air and water (72.5×10^{-3} N/m)
  σ_{LW} is the surface tension between LNAPL and water (N/m)

  If density only is known, then this more approximate empirical equation could be used:

$$T_G = T + 0.3\ H_C\ \rho_W/\rho_L\ - 0.5\ H_C\ \rho_W/(\rho_W-\rho_L) \tag{4.7}$$

  The estimation of the water capillary zone can be done on the basis of the table in Bear (1979) or one of the available formulae.

  It is unfortunate that more work has not been carried out in sand tanks investigating the validity of these equations. There are ways of calculating water capillary zones from particle size analyses. The measurement of the density and surface tensions of a sample of LNAPL from the field in a laboratory would not be difficult. Equation (3.11) seems to have potential but the verification of it using sand tanks has not been carried out. However, in general there is no easy way to determine true LNAPL thickness in the ground from simple measurements in open boreholes.

7.1.2 Recommendations

In deciding how to monitor an LNAPL spill, some consideration must be given to what is the most useful measurement to make. This may be either the mobile or the total LNAPL thickness in the ground or the volume of LNAPL per unit area. If remediation using a skimmer pump is planned, an estimate of the mobile LNAPL thickness would be useful, whereas if soil removal is to be considered then the total contaminated thickness would be required. To convert to total volume per unit area an estimate of storage is required. In this

case the more advanced Brooks-Corey formula could be used to include residual LNAPL in the unsaturated zone.

The most reliable way of estimation of the LNAPL thickness in the ground is sampling of the ground. Essentially this method produces the 'correct' result and is the test against which other methods should be verified. In general the ground in at least one borehole should be thoroughly sampled to act as a calibration check.

Sampling need not involve high technology. We would recommend either coring, or if this drilling method is unacceptable, regular U100 samples. These can be visually examined on site if the LNAPL is easy to detect (if there is a colour contrast with the soil for example) or sent to laboratories or a combination of both. The expense of laboratory analysis means that it will be worth using on-site logging where possible and UV light can make this process more reliable.

The down-hole geophysics methods do not appear to be reliable on the whole with the exception of laser fluorescence. This last technique requires probe holes and therefore is only suitable for unconsolidated materials.

7.2 Surface Geophysics

All of the surface survey methods are qualitative in terms of measuring hydrocarbon thickness but may be able to give good indications of lateral extent. Although there are more case studies involving the use of resistivity/conductivity methods, these appear to be of limited use unless the ground conditions are extremely homogeneous. They may more useful in detecting other low resistivity anomalies associated with the spill such as concurrent inorganic contamination and degradation products.

Induced Polarisation (IP) and Ground Penetrating Radar (GPR) look to be more promising techniques for detecting hydrocarbons, although there are few case studies, especially for IP. These two methods are complementary in terms of their geological limitations: GPR cannot be used where there are clays, whilst IP is unlikely to give useful results if there are no clays present. These two methods are relatively slow and expensive, and are therefore usually targetted, rather than surveying the whole site.

A surface geophysical survey would be appropriate if the lateral extent of the LNAPL at a site was unknown. Given the right geological conditions, a surface survey can help determine the approximate lateral extent and may be of use in determining where the LNAPL is thickest. The results would be very useful in siting boreholes in appropriate locations and would reduce the number of boreholes necessary to monitor the spill. This is particularly important if there are access problems or if drilling would entail a high risk of spreading the contamination. However there are many factors working against the success of non-invasive surveys.

7.3 Cost Comparison

The method chosen to measure the LNAPL obviously will depend on the degree of accuracy required and the resources available. The relative costs and accuracy of the methods are compared in Table 7.1. The costs given are approximate and were estimated for a 1 ha site with five 15 m deep boreholes. Note that the geophysical surveys provide information over a much larger area than the five spot measurements.

Clearly some methods provide a single observation whereas others provide an installation which can be used for monitoring. Table 7.1 indicates whether the measurements are carried out once or if they are repeatable. The investigation should balance the need for future monitoring and the need for a detailed single observation.

Table 7.1 Cost and Accuracy of Methods

Method		Relative Accuracy	Cost (1997 prices)	Notes
CPT Fluorescence	Mercury lamp	High	£2000-4000	Once
	Laser		£3000-6000	
Shell and auger drilling* and U100 sampling every 0.5 m	(visual)	High	£6000-12 000	Once
	(lab. analysis)		£8500-17 000	
Coring* and sampling every 0.5 m	(visual)	V. High	£9000-18 000	Once
	(lab. analysis)		£11 000-22 000	
Shell and auger drilling, installation of screen + dipping and corrections to borehole LNAPL thickness		Medium	£9000-18 000	Repeat observations for £1000
Shell and auger drilling, installation of screen + baildown tests		V. Low	£9500-19 000	Repeat observations for £1300
Surface Geophysical Surveys:				Once
Resistivity (6100 m spreads)		V. Low	£2000-4000	
EM conductivity (2 m grid)		V. Low	£1000-2000	
Ground Penetrating Radar (2 m grid)		Low	£3000-6000	
Induced Polarisation (600 line-m)		Low	£3500-7000	

* Installation of screen an extra £2500-6000

7.4 Extrapolation to Total Volume

7.4.1 Conclusions

Our conclusions are based on the practical assessment carried out in Section 6 on the performance of various sampling strategies and interpolation methods. The main criteria for success are good contour shape and low error in calculated volume. It should be noted that good performance against a specific problem does not imply good performance against all problems. There is also the possibility that a poor predictor is good 'by luck' in this particular problem.

For the problem used in the practical assessment, most of the methods gave an overestimate of plume volume, which is preferable since it is conservative. This is as expected for this problem where a portion of the plume was removed - for other problems the methods may underestimate the volume.

Our conclusions are:

- Triangulation and nearest neighbour methods are good for their ability to define edges, honour the data points and calculate the volume fairly accurately. They are robust and the nearest neighbour method has a reasonable estimate of area. Nearest neighbour 'contours' look poor since they represent Theissen polygons.

- Kriging performs to reasonable precision for volume calculation and is not heavily dependent on data search specifications. However, in general kriging produces poor contours with edge artefacts. The negative artefacts can be removed from the volume calculation by defining a zero surface.

- The accuracy of inverse distance methods in calculating the volume is dependent on the data search specification. These methods may result in 'bulls-eye' contours.

- Hand-contouring methods did not perform significantly worse than any other method in calculating the volume and produced sensible contour shapes.

- Statistical variogram analysis was the most accurate method on the test case for volume calculation, although the effort required to do this is considerable and requires some familiarity with geostatistical techniques.

7.4.2 Recommendations

LNAPL thickness data obtained from site investigations are likely to be sparse and so it is sensible to use a method which honours the data points. Given that LNAPL product plumes are likely to form relatively simple shapes, complex methods fitting the data to non-linear

trend surfaces are not likely to perform better than linear interpolation. The following recommendations are based on these observations, and the results of the practical assessment in Section 6.3:

If an automated contouring package such as SURFER is to be used, then linear methods (such as triangulation and Theissen Polygons) are recommended for volume calculations for the following reasons

- data points are honoured
- the methods are simple and robust
- definition of plume edge is sensible
- they do not result in convoluted edges or non-zero artefacts away from the plume

For many sites the expected LNAPL distribution will depend on known geological variations or knowledge of how and where the leak occurred. In this case, hand-contouring which allows these factors to be taken into account is recommended. Automatic contouring could be done in addition for comparison.

For sites with large amounts of good quality data, more elaborate methods could be used, possibly using 'informed kriging' to get the most out of the data. For most site investigations, data are unlikely to be of sufficient quantity to make this method worthwhile.

8. REFERENCES

The references are listed in Table 8.1. This represents the list of all references obtained by the project plus occasional references not obtained but nevertheless referred to. As such it may contain references that have not been referred to in this report.

Author	Publ. Date	Title	Source	Copy
Abdul AS, Kia SK and Gibson TL	1989	Limitations of Monitoring Wells for the Detection and Quantification of Petroleum Products in Soils and Aquifers	Proceedings of the 3rd National Outdoor Action Conference on Aquifer Restoration, Ground Water Monitoring and Geophysical Methods, 1989, pp357 372	y
Andres KG and Canace R	1984	Use of Electrical Resistivity Technique to Delineate a Hydrocarbon Spill in the Coastal Plain Deposits of New Jersey	Proceedings of the 1984 NWWA/API Conference on Petroleum Hydrocarbons and Organic Chemicals in Groundwater: Prevention, Detection and Restoration, pp188-197	y
Annable MD	1994	Field Scale Tracer Test in a Shallow, Sand and Gravel Aquifer Contaminated with a Complex LNAPL	EOS 75, Vol 44, p252 (Supplement)	y
Baker GS, Clement WP	1995	Amplitude and Phase Variations with Offset in Ground Penetrating Radar for Identifying Dense and Light Non-Aqueous Phase Liquid Contaminants	Geol. Soc. America, 1995 Annual Meeting	n
Ballestero TP, Fiedler FR and Kinner NE	1994	An Investigation of the Relationship between Actual and Apparent Gasoline Thickness in a Uniform Sand Aquifer	Ground Water, Vol 32, No 5, pp708-718	y
Banks D, Baulins L, Lacis A, Sichovs G and Misund A	1997	How to Map Hydrocarbon Contamination of Groundwater for Organics without Analysing for Organics	D. Banks, Norwegian Geological Survey (presented at NATO workshop, Vilnius, Lithuania, to be published by Kluwer) 16pp	y
Bear J	1979	Dynamics of Fluids in Porous Media	Dover Publications Inc., Mineola	y
Benson AK, Payne KL and Stubben MA	1997	Mapping Groundwater Contamination Using DC Resistivity and VLF Geophysical Methods - A Case Study	Geophysics, Vol 62, No 1, pp80-86	
Bermejo JL, Sauck WA and Atekwana, EA	1997	Geophysical Discovery of a New LNAPL Plume at the Former Wurtsmith AFB, Oscoda, Michigan	Ground Water Monitoring Review, Fall 1997, pp131-137	y
Blake SB (Geraghty and Miller)	1991	Hydrocarbon Thickness and Bail Tests (draft)	Pers. com.	y
Blake SB and Hall RA	1984	Monitoring Petroleum Spills with Wells: some Problems and Solutions.	Proceedings of the 4th National Symposium on Aquifer Restoration and Groundwater Monitoring, 1984, pp305-310	y
Bratton WL and Bianchi JC	1995a	LNAPL Site Characterisation using Optical Sensors and Cone Penetrometers	Geocone commercial information, 20pp	y
Bratton WL, Bratton JL and Shinn JD	1995b	Direct Penetration Technology for Geotechnical and Environmental Site Characterisation	Geoenvironment 2000, Proceedings of a Speciality Conference Sponsored by the Geotechnical Engineering and Environmental Eng. Div. ASCE, 1995, p105-122	y
Brewster ML, Annan AP, Greenhouse JP, Kueper BH, Olhoeft GR, Redman JD and Sander KA	1995	Observed Migration of a Controlled DNAPL Release by Geophysical Methods	Ground Water, Vol 33, No 6, pp977-987	y
Brookes RH and Corey AT	1966	Properties of Porous Media affecting Fluid Flow	J. Irrig. Drain. Div. Am. Soc. Civ. Eng. Vol 92, No IR2, pp61-88	y
Busby DB, Lenhard RJ and Rolston DE	1995	An Investigation of Saturation-Capillary Pressure Relations in Two- and Three-Fluid Systems for Several NAPLs in Different Porous Media	Ground Water, Vol 33, No 4, pp570-578	y
Chaffee WT and Weimar RA	1983	Remedial Programs for Groundwater Supplies Contaminated with Gasoline	Proc. of the 3rd Nat. Symposium on Aquifer Restoration and Groundwater Monitoring, 1983, Ohio, pp39-46	n
Christy and Gillespie	1996	Direct Image Soil Conductivity System and Membrane Interface Probe (MIP)	Direct Push Days 1996, Direct Sensing Workshop, obtained from Fugro Ltd, 19pp	y
Cohen RM et al	1992	Evaluation of Visual Methods to Detect LNAPL in Soil	Ground Water Monitoring Review, Fall 1992, pp132-141	y

Author	Publ. Date	Title	Source	Copy
Cummings TR and Twenter FR	1986	Asessment of Groundwater Contamination at Wurtsmith Air Force Base, Michigan, 1982-85	USGS Water Resources Investigations Report 86-4188, Lansing MI, 110pp	n
Daily W et al 1995	1995	Electrical Resistance Tomography Experiments at the Oregon Graduate Institute	Applied Geophysics, No 33, pp227-237	y
Davis JO	1990	Quantification of Ionic and Hydrocarbon-type Contaminants with Geophysical Resistivity Surveys and Drill hole Sample Data	Proceedings of the 5th Canadian/American Conference on Hydrogeology, 1990 p261	y
Davis JO	1991	Depth Zoning and Specialised Processing Methods for Electromagnetic Geophysical Surveys to Remote Sense Hydrocarbon Type Contaminants	Proceedings of the 5th National Outdoor Action Conference on Aquifer Restoration, Ground Water Monitoring and Geophysical Methods, 1991, pp905 913	y
De Limia OAL, Sato HK and Porsami MJ	1995	Imaging Industrial Contaminant Plumes with Resistivity Techniques	Journal of Applied Geophysics, Vol 34, pp93-108	y
De Pastrovich TL et al	1979	Protection of Groundwater from Oil Pollution	CONCAWE Report No 3/79, Den Haag	y
Domenico PA and Schwartz FW	1990	Physical and Chemical Hydrogeology	Wiley, Canada	y
Durnford D et al	1991	LNAPL Distribution in a Cohesionless Soil: a Field Investigation and Cryogenic Sampler	Ground Water Monitoring Review, Summer 1991, pp115-121	y
Earley K and Rapp K	1995	A Case Study Comparing the use of Laser Induced Fluorescence with Cone Penetrometer Testing to more Conventional Screening Methods	Proceedings of the 4th International Symposium on Field Screening for Hazardous Wastes and Toxic Chemicals (1995), 21pp	y
Eckberg D and Sunada DK	1984	Non-steady Three Phase Immiscible Fluid Distribution in Porous Media	Water Resources Research, Vol 20, pp1891-1897	y
Erchul RA	1990	A Conductivity Cone Penetrometer to Detect Contaminant Plume Flow Rate	Proceedings of the 4th National Outdoor Action Conference on Aquifer Restoration, Ground Water Monitoring and Geophysical Methods, 1990, pp419 428	y
Essaid HI, Herkelrath WN and Hess KM	1993	Simulation of Fluid Distributions Observed at a Crude Oil Spill Site incorperating Hysteresis, Oil Entrapment and Spatial Variability of Hydraulic Properties	Water Resources Research, Vol 29, No 6, pp1753-1770	y
Farr AM, Houghtalen RJ and McWhorter DB	1990	Volume Estimation of Light Non-Aqueous Phase Liquids in Porous Media	Ground Water, Vol 28, No 1, pp48-56	y
Fetter CW	1993	Contaminant Hydrogeology	MacMillan, New York	y
Fugro Ltd	1997		Personal communication	
Gearhart Industries Inc.		Formation Evaluation Data Handbook	Gearhart Industries Inc. and Wireline Services, Fort Worth, Texas, 100pp	
Gruszczenski TS	1987	Determination of a Realistic Estimate of the Actual Formation Product Thickness using Monitor Wells: a Field Bailout Test	Proceedings of the 1987 NWWA/API Conference on Petroleum Hydrocarbons and Organic Chemicals in Groundwater: Prevention, Detection and Restoration, pp235-253	y
Haas, JW	?	Fuel Fluorescence Detector, Feasibility Study Report	EIC laboratories, Inc, Norwood MA 22pp	y
Haas, JW and Forney RW	?	Nonaqueous Phase Liquids: Searching for the Needle in the Haystack	EIC Laboratories Inc, Norwood MA 7pp	y
Hall RA, Blake SB and Champlin SCet al	1984	Determination of Hydrocarbon Thickness in Sediments using Borehole Data.	Proceedings of the 4th National Symposium on Aquifer Restoration and Groundwater Monitoring, 1984, pp300-304	y

Author	Publ. Date	Title	Source	Copy
Hampton DR and Miller PDG	1988	Laboratory Analyses of the Relationship between Actual and Apparent Product Thickness in Sands	Proceedings of the 1988 NWWA/API Conference on Petroleum Hydrocarbons and Organic Chemicals in Groundwater: Prevention, Detection and Restoration, pp157-181	y
Hampton DR, Wagner RB and Heuvelhorst HG	1990	A New Tool to Measure Petroleum Thickness in Shallow Aquifers	Proceedings of the 4th National Outdoor Action Conference on Aquifer Restoration, Ground Water Monitoring and Geophysical Methods, 1990, pp27-141	y
Hardisty PE and Johnston PM	1993	Characterisation of Occurrence and Distribution of LNAPL in Fractured Rocks	Ground Water Management, No 17, pp113	n
Hess KM et al	1992	Determination of Subsurface Fluid Contents at a Crude Oil Spill Site	J. Contam. Hydrol, Vol 10, pp75-96	y
Holzer TL	1976	Application of Ground Water Flow Theory to a Sub-surface Oil Spill	Ground Water, Vol 14, No3, pp138-145	n
Hughes JP, Sullivan CR and Zinner RE	1988	Two Techniques for Determining the True Hydrocarbon Thickness in an Unconfined Sandy Aquifer	Proceedings of the 1988 NWWA/API Conference on Petroleum Hydrocarbons and Organic Chemicals in Groundwater: Prevention, Detection and Restoration, pp291-314	y
Hult MF	1984	Groundwater Contamination by Crude Oil at the Bemidji Minnesota Research Site	USGS Toxic Waste- Groundwater Contamination Study, USGS Water Resources Investigation Report No 84-4188 107pp	n
Hult MF	1984	Non-Disruptive Measurement of Organic Fluid Thickness in the Shallow Subsurface	Proceedings of the Conference on Petroleum Hydrocarbons and Organic Chemicals in Groundwater, 1984 ?NOT FOUND BY NGWA	n
Hunt WT, Weigand JW and Trompeter	1989	Free Gasoline Thickness in Monitoring Wells Related to Groundwater Elevation Change	Proceedings of the Conference on New Techniques for Quantifying the Physical and Chemical Properties of Heterogeneous Aquifers, US NWWA, Texas pp671-692	y
Huntley D, Hawk RN and Corley HP	1994	Nonaqueous Phase Hydrocarbon in a Fine-Grained Sandstone: 1. Comparison between Measured and Predicted Saturations and Mobility	Ground Water, Vol 32, No 4, pp626-634	y
Huntley D, Wallace JW and Hawk RN	1994	Nonaqueous Phase Hydrocarbon in a Fine-Grained Sandstone: 2. Effect of Local Sediment Variability on the Estimation of Hydrocarbon Volumes	Ground Water, Vol 32, No 5, pp778-783	y
Indergard LM and Hagan F	1991	Geophysical and Bail-down Test Investigation of Capillary Fringe Free Phase Hydrocarbons	Ground Water 29, No 5, pp755	y
Jacobs P	1997	Putting a Light on Contamination - the Investigation of Hydrocarbon Contaminated Land using Real Time in Situ Probing Techniques	Ground Engineering, Jan/Feb 1997 p23	y
Johnson RL, McCarthy KA, Perrott M and Hinman N	1989	Direct Comparison of Vapor-, Free-Product- and Aqueous-Phase Monitoring for Gasoline Leaks from Underground Storage Systems	Proceedings of the 1989 NWWA/API Conference on Petroleum Hydrocarbons and Organic Chemicals in Groundwater: Prevention, Detection and Restoration, pp605-615	y
Keech DA	1988	Hydrocarbon Thickness in Groundwater by Dielectric Well Logging	Proceedings of the 1988 NWWA/API Conference on Petroleum Hydrocarbons and Organic Chemicals in Groundwater: Prevention, Detection and Restoration, pp275-289	y
Kemblowski MW and Chiang CY	1990	Hydrocarbon Thickness Fluctuations in Monitoring Wells	Ground Water, Vol 28, No 2, pp244-252	y
Kemblowski MW and Chiang CY	1988	Analysis of the Measured Free Product Thickness in Dynamic Aquifers	Proceedings of the 1988 NWWA/API Conference on Petroleum Hydrocarbons and Organic Chemicals in Groundwater: Prevention, Detection and Restoration, pp183-205	y

Author	Publ. Date	Title	Source	Copy
Kimberlin DK and Trimmel ML	1988	Utilisation of Optoelectric Sensing to Determine Hydrocarbon Thicknesses within Confined Aquifers.	Proceedings of the 1988 NWWA/API Conference on Petroleum Hydrocarbons and Organic Chemicals in Groundwater: Prevention, Detection and Restoration, pp255-274	y
Klainer SM, Goswami K, Le Goullon D, Dandge DK, Thomas JR and Eccles L	1988	Monitoring of Gasoline Vapor and Liquid by Fiber Optic Chemical Sensor	Proceedings of the 1st International Symposium on Field Screening for Hazardous Wastes and Toxic Chemicals (1988) pp25-29	y
Kollert R	1969	Ground Water Exploration by the Resistivity Method	Geophysical Memorandum 3/69, Abem, Sweden, 7 pp	n
Konasewich DE, Gerencher E and Morin KA	1989	Confidential report, data in Davis 1991		n
Lambson M and Jacobs P	1995	The Use of the Laser Induced Fluorescence Cone for Environmental Investigations	CPT'95, Linköping, Sweden, 6pp	y
Lenhard RJ and Parker JC	1987	Estimation of Free Hydrocarbon Volume from Fluid Levels in Monitoring Wells	Ground Water, Vol 28, No 1, pp57-67	y
Lenhard RJ and Parker JC	1990	Discussion of 1990 Ground Water papers	Ground Water, Vol 28, No 5, pp800-801	y
Leonard DW, Erikson AS, Booth S, Nguyen VT, Quick MJ, Zhang D, Al-Nuamy W and Huang Y	1997	Hydrocarbon Contamination and Features Mapping using GPR	Geo-Services International, Witney, Oxfordshire, commercial information, 4pp	y
Leverett MC	1941	Capillary Behaviour in Porous Solids	Trans. Am. Inst. Min. Metall. Pet. Eng, No 142, pp152-169	y
Levitskaya TM and Sternberg BK	1996	Polarization Processes in Rocks 1.Complex Dielectric Permittivity Method	Radio Science Vol 31, No 4, pp755-779	y
Littlefield KV, Wehler NE and Heard RW	1984	Identification and Removal of Hydrocarbons from Unconsolidated Sediments Affected by Tidal Fluctuations	Proceedings of the 1984 NWWA/API Conference on Petroleum Hydrocarbons and Organic Chemicals in Groundwater: Prevention, Detection and Restoration, pp316-322	n
Lohman SW	1972	Ground Water Hydraulics	USGS Professional Paper 708, 70pp	n
Lundy DA	1988	Conceptual Model of Transient Accumulations of Liquid Phase Hydrocarbons in Wells Resulting from Water Table Fluctuations	Trans Am Geophys. Union, Vol 69, Part 44, pp1213	y
Marinelli F and Durnford D	1996	LNAPL Thickness in Monitoring Wells Considering Hysteresis and Entrapment	Ground Water, Vol 34, No 3, pp405-414	y
Mavis FT and Tsui TP	1939	Percolation and Capillary Movements of Water through Sand Prisms	Bull. 18, Univ. of Iowa, Studies in Eng, Iowa City	y
McNeill JD	1980	Electromagnetic Terrain Conductivity Measurements at Low Induction Numbers	Geonics Ltd, Technical Note TN-6, Ontario	n
Mishra S, Parker JC and Singhal N	1989	Estimation of Soil Hydraulic Properties and their Uncertainty from Particle Size Distribution Data	Journal of Hydrology Vol 108, pp1-18	y
Nottingham Trent University	1994	Sampling Strategies for Contaminated Land, CLR Report No. 4	Dept. of Environment Contaminated Land Research Department	y
Olhoeft GR	1986	Direct Detection of Hydrocarbon and Organic Chemicals with Ground Penetrating Radar and Complex Resistivity	Proceedings of the 1986 NWWA/API Conference on Petroleum Hydrocarbons and Organic Chemicals in Groundwater: Prevention, Detection and Restoration, pp284-305	y

Author	Publ. Date	Title	Source	Copy
Oostrom M	1994	An Experimental and Numerical Study of LNAPL and DNAPL Movement in the Subsurface	EOS 75, Vol 44, pp254 (Supplement)	y
Parker JC, Katyal AK, Zhu JL and Mishra S	1990	Estimation of Spill Volume from Monitoring Well Networks	Proceedings of the 4th National Outdoor Action Conference on Aquifer Restoration, Ground Water Monitoring and Geophysical Methods, 1990, pp233-1243	y
Pharr DY, McKenzie JK and Hickman AB	1992	Fingerprinting Petroleum Contamination using Synchronous Scanning Fluorescence Spectroscopy	Ground Water, Vol 30, No 4, pp484-489	y
Polubarinova-Kochina PY	1962	Unsteady Seepage with Interface (in Russian)	Dokl. Nauk, SSSR, Moscow, 66, p173-176	n
Rose W and Bruce WA	1949	Evaluation of Capillary Character in Petroleum Reservoir Rock	Journal of Petroleum Technology, Trans Am. Inst. Mining Eng, Vol 1, No 5, Sect.3	n
Saunders WR and Germeroth RM	1985	Electromagnetic Measurements for Subsurface Hydrocarbon Investigations.	Proceedings of the 1985 NWWA/API Conference on Petroleum Hydrocarbons and Organic Chemicals in Groundwater: Prevention, Detection and Restoration, pp310-321	y
Saunders WR, Castle RW and Foget CR	1983	Delineation of Subsurface Petroleum Spills using Terrain Conductivity Measurements	Proceedings of the 1983 Oil Spill Conference, API/EPA/US coast guard, pp415-417	y
Scheinfeld RA, Robertson JB and Schwendeman TG	1986	Underground Storage Tank monitoring: Observation Well Based Systems	Ground Water Monitoring Review, Fall 1986, pp49-55	y
Schiegg HO	1984	Considerations on Water, Oil and Air in Porous Media	Water Science and Technology, Vol 17, pp467-476	y
Senn RB and Johnson MS	1987	Interpretation of Gas Chromatographic Data in Subsurface Hydrocarbon Investigations	Ground Water Monitoring Review, Winter 1987, pp58-63	y
Serra O	1986	Fundamentals of Well-Log Interpretation	Developments in Petroleum Science 15B, Elsevier, Amsterdam	y
Shepard D	1968	A Two Dimensional Interpolation Function for Irregularly Spaced Data	Proc 23rd Nat Conf, ACM, pp 517-523	n
Soukup WG and Schleuing LE	1996	A Comparison of NAPL Field Screening Techniques at Three Hazardous Waste Sites	Proceedings of the 10th National Outdoor Action Conference on Aquifer Restoration, Ground Water Monitoring, Geophysical methods and Soil Treatment, 1996, pp51-62	y
Steffy DA	1994	Response of LNAPL Pore Pressure to a Dynamic Water Table	EOS 75, Vol 44, pp254 (Supplement)	y
Stotz TM, Hillyer MJ and Hughes JP	1990	Monitoring and Statistical Analysis of Liquid Hydrocarbon during Remedial Action	Proceedings of the 1990 NWWA/API Conference on Petroleum Hydrocarbons and Organic Chemicals in Groundwater: Prevention, Detection and Restoration, pp179-194	y
Sullivan CR, Zinner RE and Hughes JP	1988	The occurrence of Hydrocarbon on an Unconfined Aquifer and Implications for Liquid Recovery	Proceedings of the 1988 NWWA/API Conference on Petroleum Hydrocarbons and Organic Chemicals in Groundwater: Prevention, Detection and Restoration, pp135-156	y
Telford WM	1976	Applied Geophysics	Cambridge University Press, New York, 860pp	n
Testa SM and Paczkowski MT	1989	Volume Determination and Recoverability of Free Hydrocarbon	Ground Water Monitoring Review, Vol 9, Part 1, pp120-128	y
Theis TL, Collins AG, Monsour SG, Pavlostathis SG and Theis CD	1991	Analysis of Total Polyaromatic Hydrocarbon using Ultraviolet-Fluorescence Spectroscopy	Proceedings of the 2nd International Symposium on Field Screening for Hazardous Wastes and Toxic Chemicals (1991), pp805-809	y
van Dam J	1967	The migration of Hydrocarbons in a Water Bearing Stratum	The Joint Problems of the Oil and Water Industries, P Hepple Ed, pp23-54	n
van Genuchten MT	1980	A Closed Form Equation for Predicting the Hydraulic Conductivity of Unsaturated Soils	Soil Sci. Am J, Vol 44, pp892-898	y

Author	Publ. Date	Title	Source	Copy
Waddill DW and Parker JC	1997	Simulated Recovery of Light Non-Aqueous Phase Liquid from Unconfined Heterogeneous Aquifers	Ground Water, Vol 35, No 6, pp938-947	y
Wagner RB, Hampton DR and Howell JA	1989	A New Tool to Determine the Actual Thickness of Free Product in a Shallow Aquifer	Proceedings of the 1989 NWWA/API Conference on Petroleum Hydrocarbons and Organic Chemicals in Groundwater: Prevention, Detection and Restoration, pp45-59	y
Wallace JW and Huntley D	1992	Effect of Local Sediment Variability on the Estimation of Hydrocarbon Volumes	Proceedings of the 6th National Outdoor Action Conference on Aquifer Restoration, Ground Water Monitoring and Geophysical Methods, 1991, pp273 284	n
Weiss G	1980	Hazardous Chemical Data Book	Noyes Data Corp., Park Ridge NJ	n
Wheeler P (Fugro)	1994	Screen Test- a US Developed System for Rapid in situ Evaluation of Hydrocarbon Contamination	Ground Engineering, Dec 1994, p26	y
Wright DL, Olhoeft GR and Watts RD	1984	Ground-Penetrating Radar Studies on Cape Cod	Proc. of NWWA/EPA Conf. on Surface and Borehole Geophysical Methods in Ground Water Investigations, 1984, p666-680	y
Yaniga PM	1984	Hydrocarbon Retrieval and Apparent Hydrocarbon Thickness Interrelationships to Recharging/Discharging Aquifer Conditions	Proceedings of the 1984 NWWA/API Conference on Petroleum Hydrocarbons and Organic Chemicals in Groundwater: Prevention, Detection and Restoration, pp299-329	y
Zilliox L and Muntzer P	1975	Effects of Hydrodynamic Processes on the Development of Ground-Water Pollution: Study on Physical Models in a Saturated Porous Medium	Progress in Water Technology, Vol 7, Nos 3/4, pp561-568	y
Zohdy AAR, Eaton GP and Mabey DR	1974	Application of Surface Geophysics to Groundwater Investigations	USGS Techniques of Water Resources Investigations	y

APPENDIX A

PRACTICAL ASSESSMENT OF SAMPLING STRATEGIES AND INTERPOLATION METHODS

(51 Pages)

Entec

GRIDDING METHOD: SHEPARD'S METHOD, SEARCH ALL DATA
DATASET: NESTED HERRINGBONE
FILENAME: AHER5NST.SRF

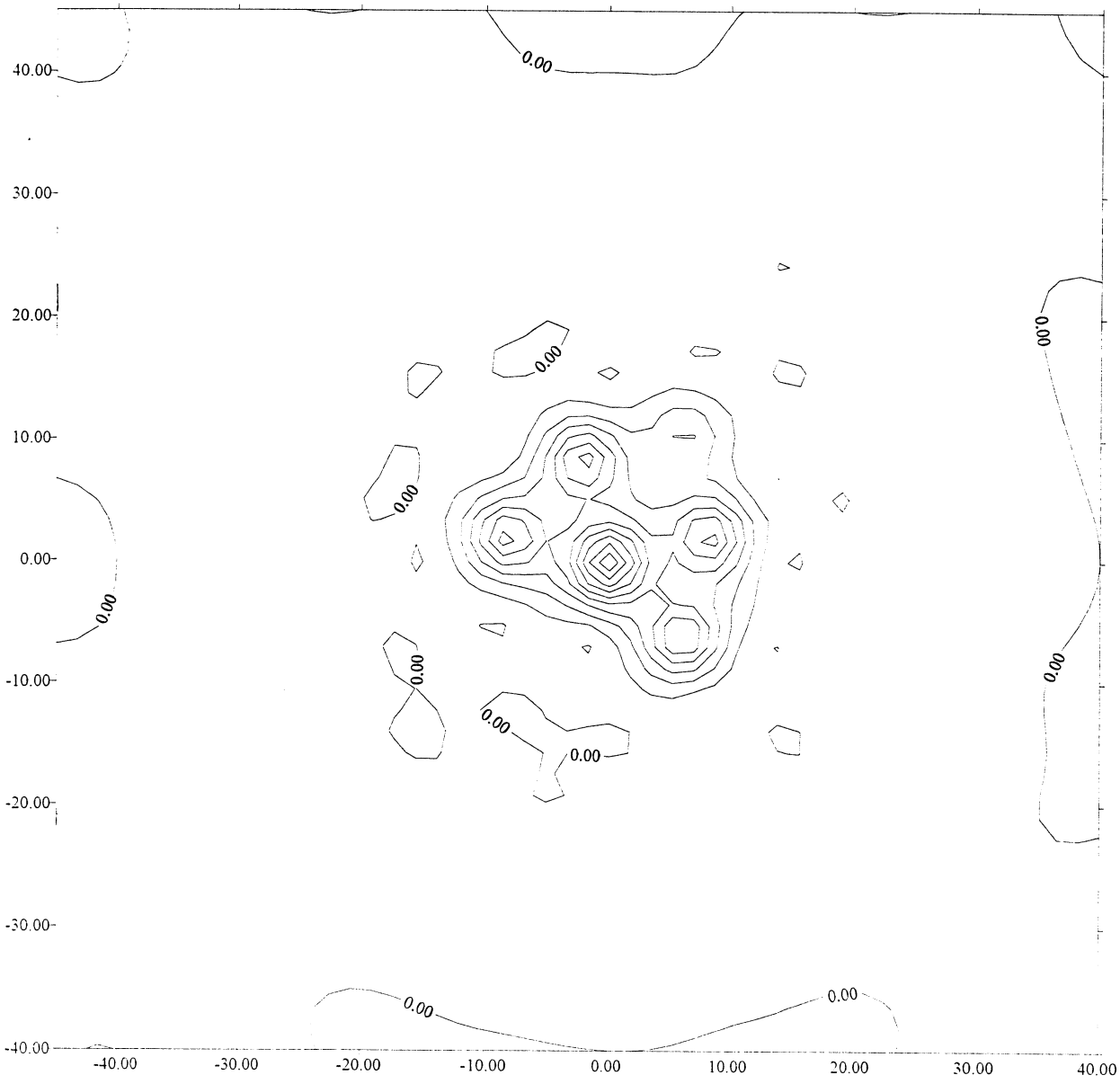

GRIDDING METHOD: KRIGING, SEARCH NEAREST 4 DATA, DEFAULT (LINEAR) SETTINGS
DATASET: NESTED HERRINGBONE
FILENAME: CHER5NST.SRF

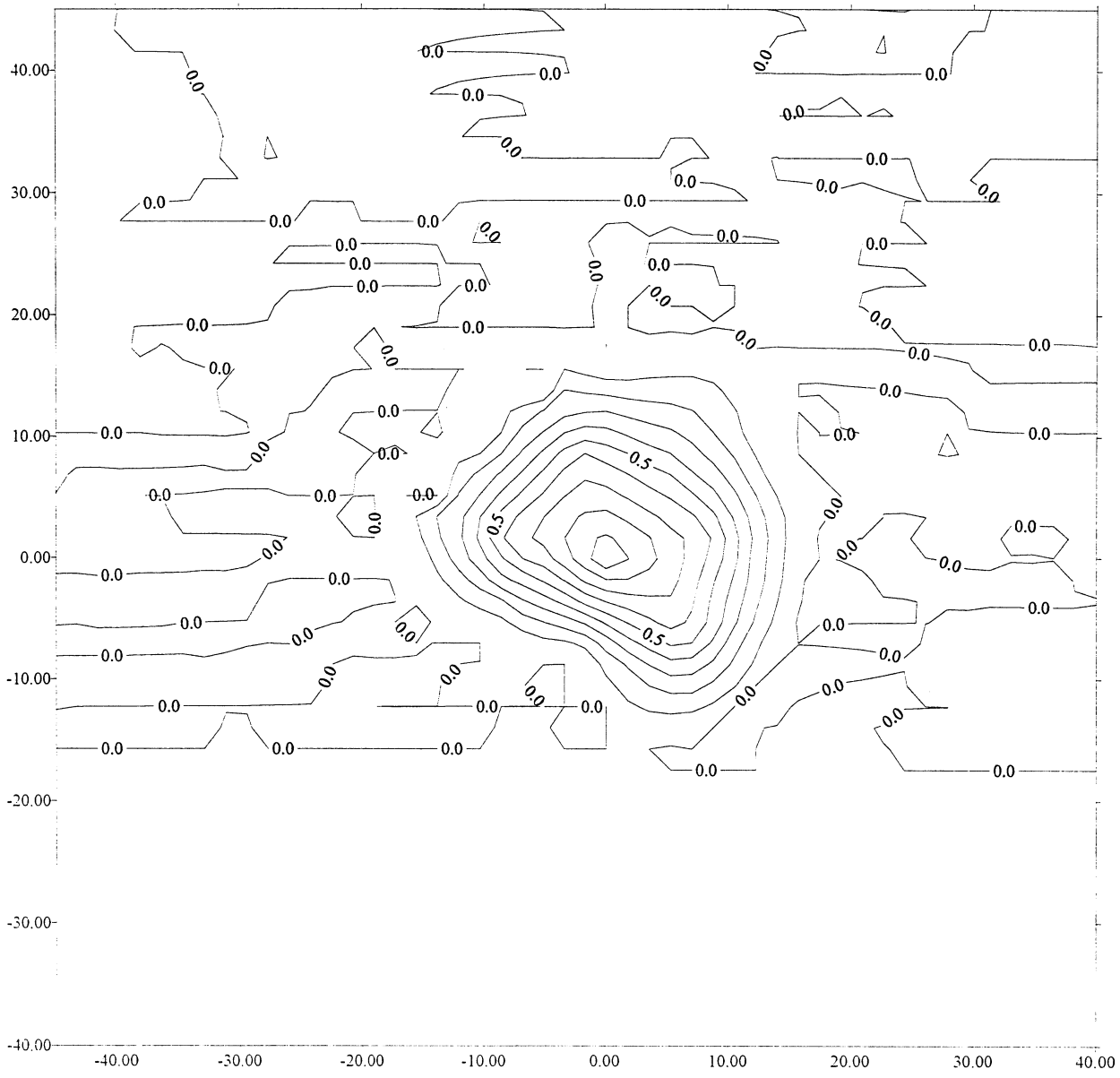

GRIDDING METHOD: KRIGING, SEARCH NEAREST 4 DATA,
DEFAULT (LINEAR) SETTINGS
DATASET: NESTED HERRINGBONE
==========

VOLUME COMPUTATIONS

UPPER SURFACE
Grid File: H:/PROJECTS/WR/15000/15690/CALCS/X132/CHER5NST.GRD
Grid size as read: 50 cols by 50 rows
Delta X: 1.73469
Delta Y: 1.73469
X-Range: -45 to 40
Y-Range: -40 to 45
Z-Range: -0.0435324 to 0.98693

LOWER SURFACE
Level Surface defined by Z = 0

VOLUMES
Approximated Volume by
Trapezoidal Rule: 249.813
Simpson's Rule: 249.765
Simpson's 3/8 Rule: 249.556

CUT & FILL VOLUMES
Positive Volume [Cut]: 250.322
Negative Volume [Fill]: 0.509784
Cut minus Fill: 249.813

AREAS
Positive Planar Area
(Upper above Lower): 2739.15
Negative Planar Area
(Lower above Upper): 4485.85
Blanked Planar Area: 0
Total Planar Area: 7225

Positive Surface Area
(Upper above Lower): 2741.1
Negative Surface Area
(Lower above Upper): 4485.86

GRIDDING METHOD: KRIGING, DEFAULT SETTINGS
DATASET: SIMPLE HERRINGBONE, PLUME CENTRE KNOWN
FILENAME: HER5.SRF

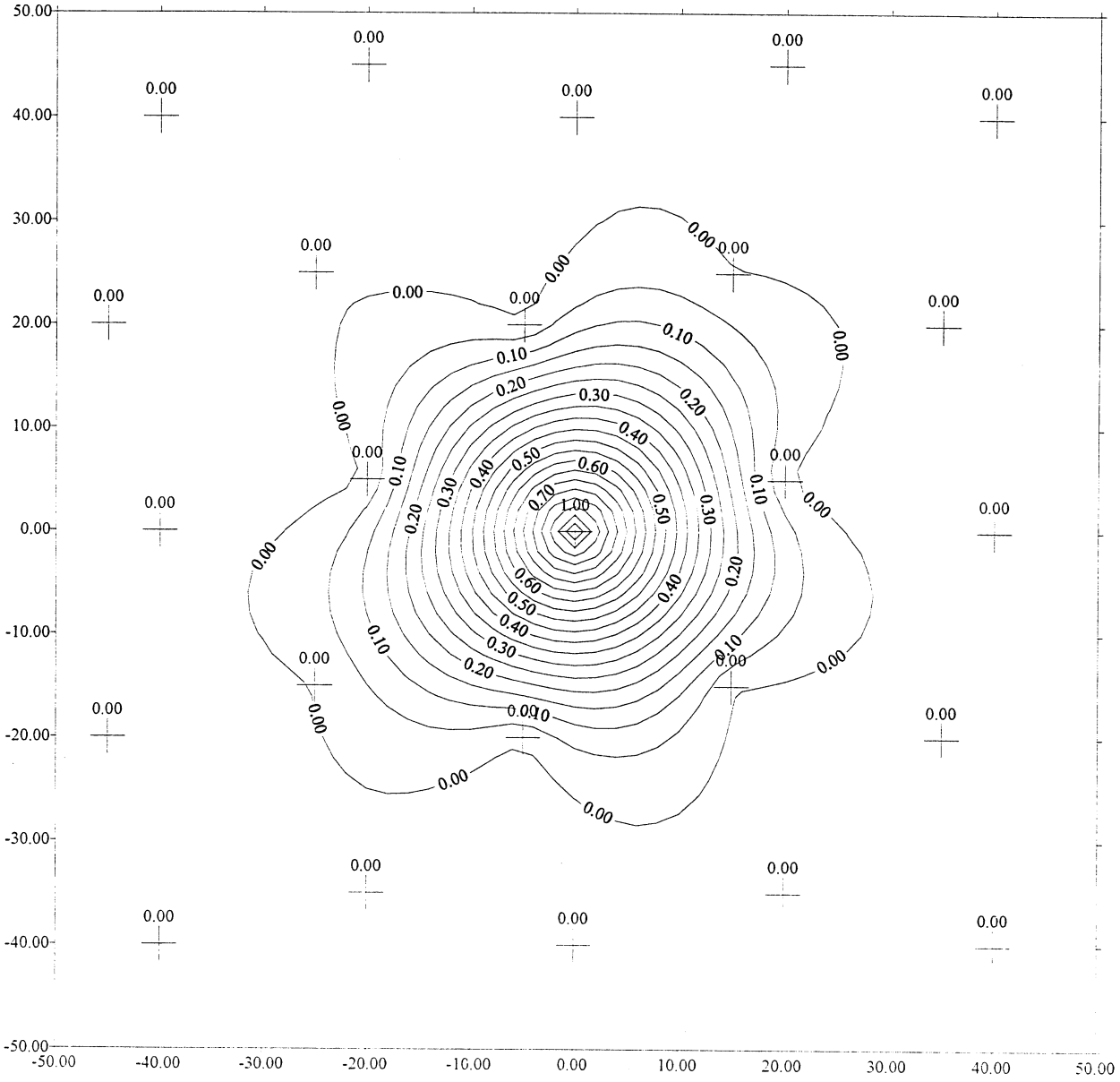

GRIDDING METHOD: KRIGING, DEFAULT SETTINGS
DATASET: SIMPLE HERRINGBONE, PLUME CENTRE KNOWN
==========

VOLUME COMPUTATIONS

UPPER SURFACE
Grid File: H:/PROJECTS/WR/15000/15690/CALCS/X132/HER5.GRD
Grid size as read: 51 cols by 51 rows
Delta X: 2
Delta Y: 2
X-Range: -50 to 50
Y-Range: -50 to 50
Z-Range: -0.0196348 to 1

LOWER SURFACE
Level Surface defined by Z = 0

VOLUMES
Approximated Volume by
Trapezoidal Rule: 397.478
Simpson's Rule: 397.71
Simpson's 3/8 Rule: 397.653

CUT & FILL VOLUMES
Positive Volume [Cut]: 438.546
Negative Volume [Fill]: 41.068
Cut minus Fill: 397.478

AREAS
Positive Planar Area
(Upper above Lower): 2423.26
Negative Planar Area
(Lower above Upper): 7576.74
Blanked Planar Area: 0
Total Planar Area: 10000

Positive Surface Area
(Upper above Lower): 2424.4
Negative Surface Area
(Lower above Upper): 7576.75

GRIDDING METHOD: KRIGING, DEFAULT SETTINGS
DATASET: NESTED HERRINGBONE
FILENAME: HER5NST.SRF

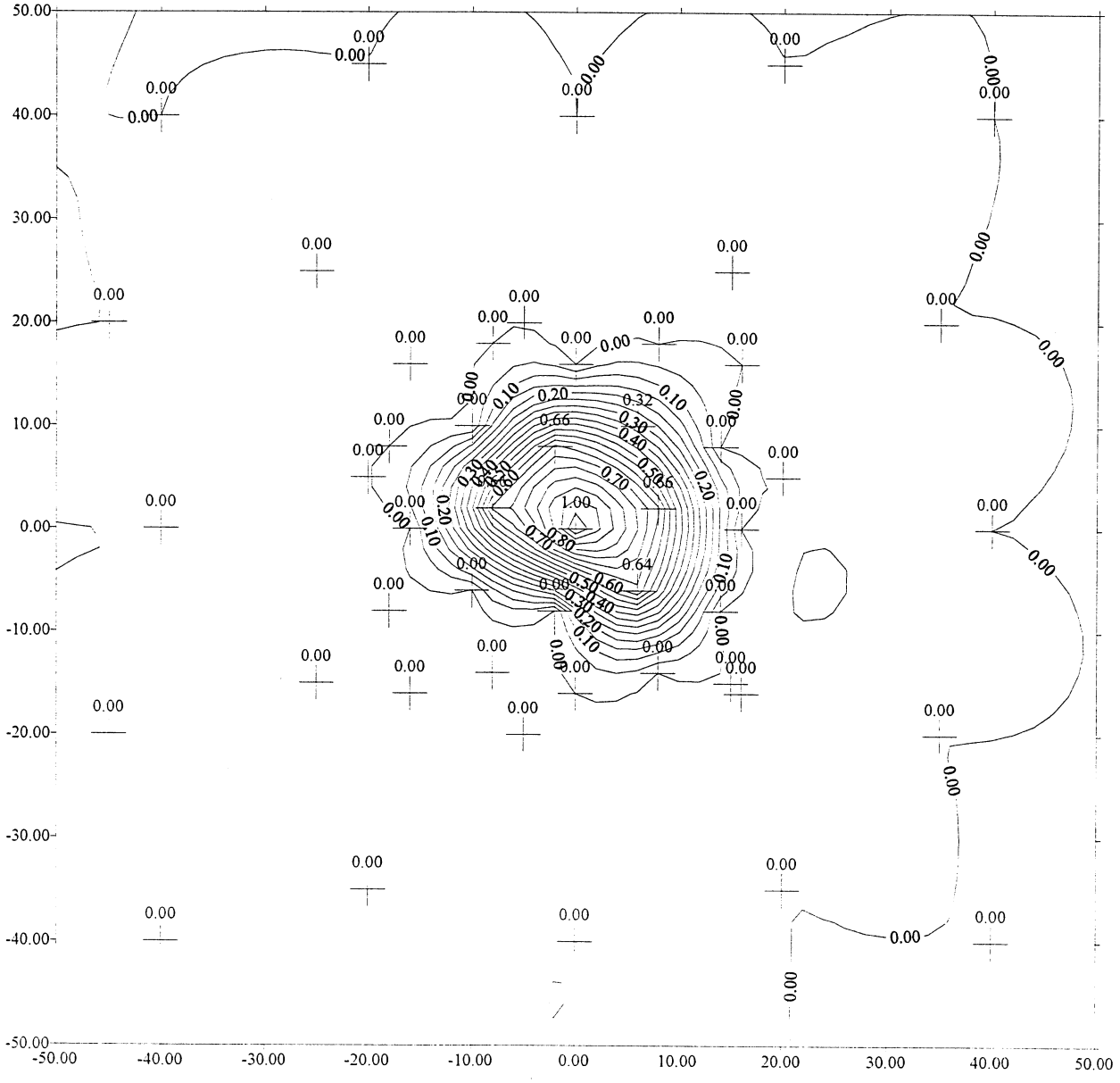

GRIDDING METHOD: KRIGING, DEFAULT SETTINGS
DATASET: NESTED HERRINGBONE
==========

VOLUME COMPUTATIONS

UPPER SURFACE
Grid File: H:/PROJECTS/WR/15000/15690/CALCS/X132/HER5NST.GRD
Grid size as read: 51 cols by 51 rows
Delta X: 2
Delta Y: 2
X-Range: -50 to 50
Y-Range: -50 to 50
Z-Range: -0.0532855 to 1

LOWER SURFACE
Level Surface defined by Z = 0

VOLUMES
Approximated Volume by
Trapezoidal Rule: 200.69
Simpson's Rule: 200.831
Simpson's 3/8 Rule: 201.052

CUT & FILL VOLUMES
Positive Volume [Cut]: 263.193
Negative Volume [Fill]: 62.5028
Cut minus Fill: 200.691

AREAS
Positive Planar Area
(Upper above Lower): 2255.93
Negative Planar Area
(Lower above Upper): 7744.07
Blanked Planar Area: 0
Total Planar Area: 10000

Positive Surface Area
(Upper above Lower): 2257.9
Negative Surface Area
(Lower above Upper): 7744.09

GRIDDING METHOD: KRIGING, DEFAULT SETTINGS, EDGE EFFECTS REMOVED
DATASET: NESTED HERRINGBONE
FILENAME: HER5NST2.SRF

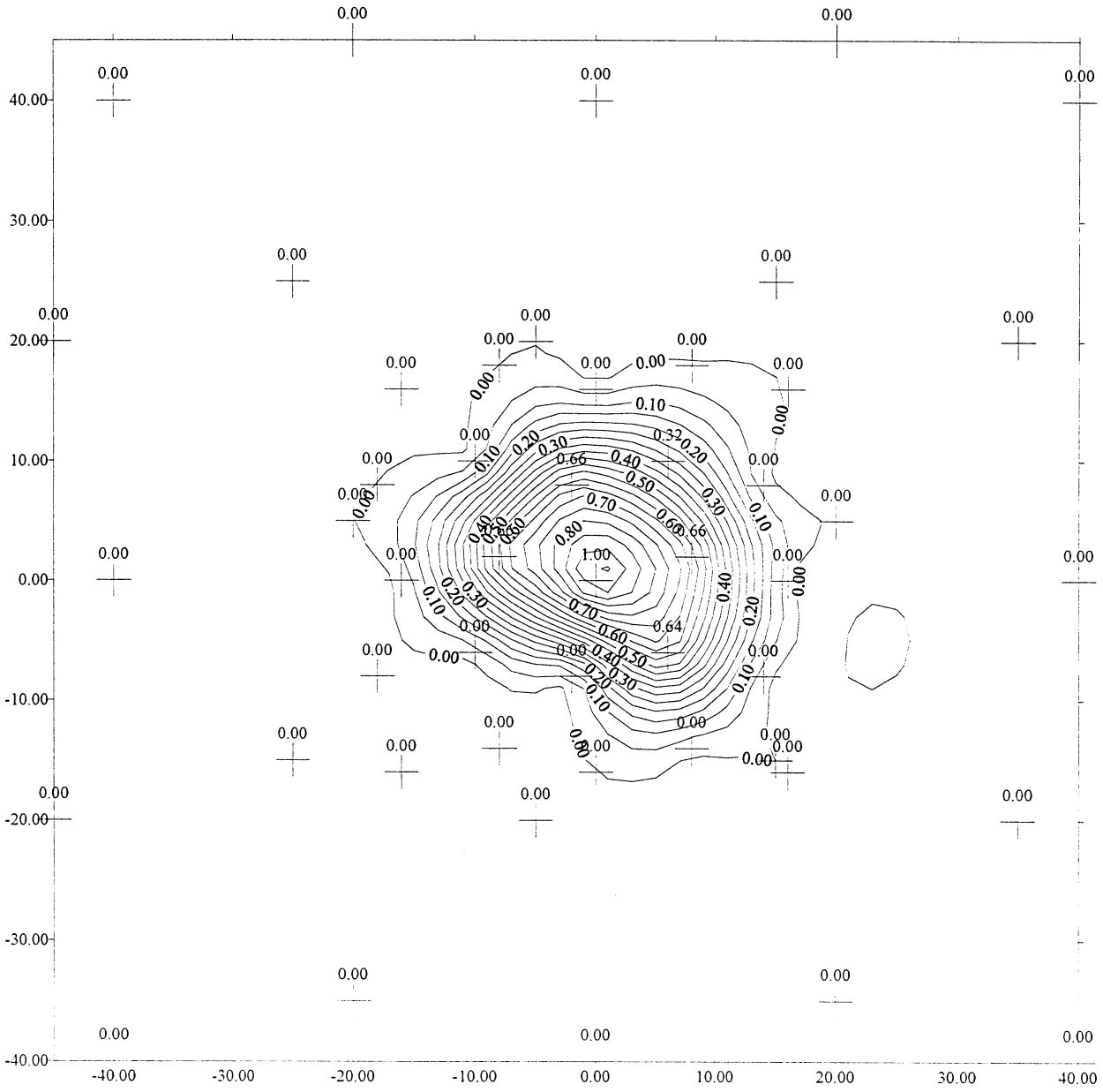

GRIDDING METHOD: KRIGING, DEFAULT SETTINGS,
EDGE EFFECTS REMOVED
DATASET: NESTED HERRINGBONE
==========

VOLUME COMPUTATIONS

UPPER SURFACE
Grid File: H:/PROJECTS/WR/15000/15690/CALCS/X132/HER5NST2.GRD
Grid size as read: 36 cols by 36 rows
Delta X: 2
Delta Y: 2
X-Range: -35 to 35
Y-Range: -35 to 35
Z-Range: -0.0538135 to 0.955653

LOWER SURFACE
Level Surface defined by Z = 0

VOLUMES
Approximated Volume by
Trapezoidal Rule: 209.043
Simpson's Rule: 208.943
Simpson's 3/8 Rule: 208.721

CUT & FILL VOLUMES
Positive Volume [Cut]: 262.763
Negative Volume [Fill]: 53.7201
Cut minus Fill: 209.043

AREAS
Positive Planar Area
(Upper above Lower): 945.418
Negative Planar Area
(Lower above Upper): 3954.58
Blanked Planar Area: 0
Total Planar Area: 4900

Positive Surface Area
(Upper above Lower): 947.291
Negative Surface Area
(Lower above Upper): 3954.61

GRIDDING METHOD: KRIGING, DEFAULT SETTINGS
DATASET: NESTED HERRINGBONE, PLUME CENTRE UNKNOWN
SAMPLING POINTS OFFSET TO NE
FILENAME: HER5NST3.SRF

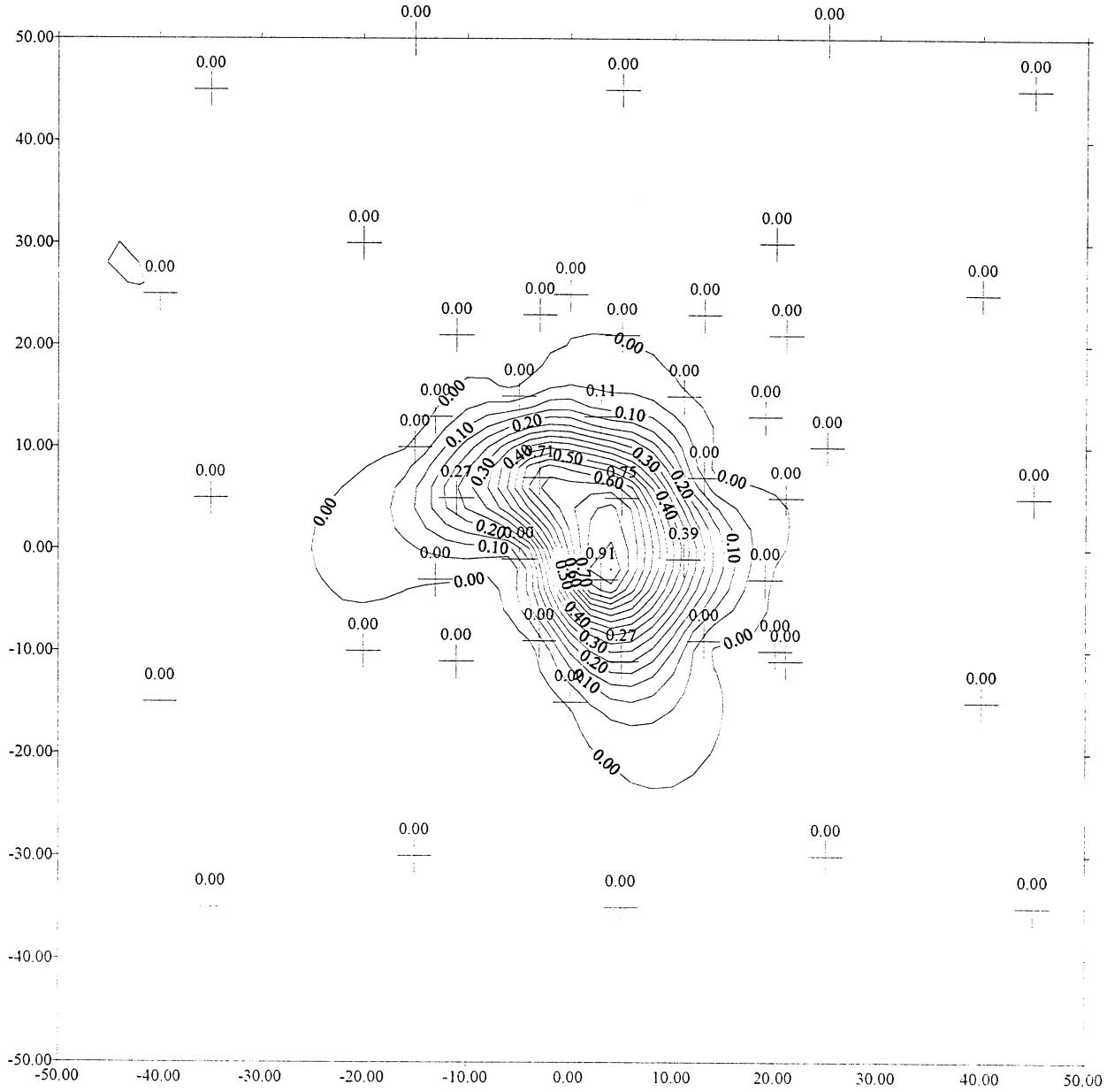

GRIDDING METHOD: KRIGING, DEFAULT SETTINGS
DATASET: NESTED HERRINGBONE, PLUME CENTRE UNKNOWN
==========

VOLUME COMPUTATIONS

UPPER SURFACE
Grid File: H:/PROJECTS/WR/15000/15690/CALCS/X132/HER5NST3.GRD
Grid size as read: 51 cols by 51 rows
Delta X: 2
Delta Y: 2
X-Range: -50 to 50
Y-Range: -50 to 50
Z-Range: -0.0360776 to 0.851571

LOWER SURFACE
Level Surface defined by Z = 0

VOLUMES
Approximated Volume by
Trapezoidal Rule: 187.285
Simpson's Rule: 187.29
Simpson's 3/8 Rule: 187.102

CUT & FILL VOLUMES
Positive Volume [Cut]: 224.913
Negative Volume [Fill]: 37.6279
Cut minus Fill: 187.285

AREAS
Positive Planar Area
(Upper above Lower): 1129.11
Negative Planar Area
(Lower above Upper): 8870.89
Blanked Planar Area: 0
Total Planar Area: 10000

Positive Surface Area
(Upper above Lower): 1130.7
Negative Surface Area
(Lower above Upper): 8870.9

GRIDDING METHOD: KRIGING, DEFAULT SETTINGS
DATASET: NESTED HERRINGBONE, PLUME CENTRE UNKNOWN
SAMPLING POINTS OFFSET TO NW
FILENAME: HER5NST4.SRF

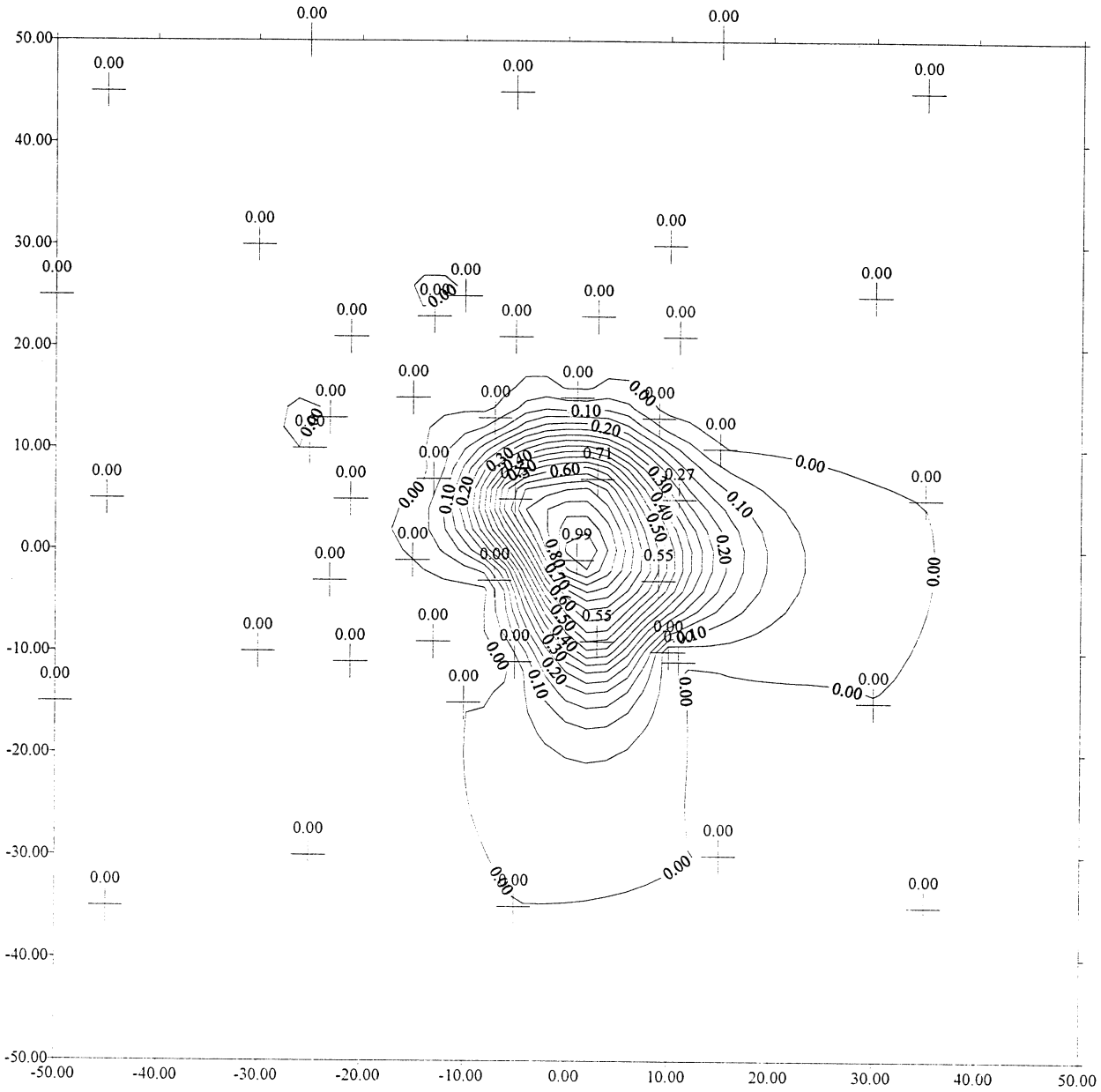

GRIDDING METHOD: KRIGING, DEFAULT SETTINGS
DATASET: NESTED HERRINGBONE, PLUME CENTRE UNKNOWN
SAMPLING POINTS OFFSET TO NW
==========

VOLUME COMPUTATIONS

UPPER SURFACE
Grid File: H:/PROJECTS/WR/15000/15690/CALCS/X132/HER5NST4.GRD
Grid size as read: 51 cols by 51 rows
Delta X: 2
Delta Y: 2
X-Range: -50 to 50
Y-Range: -50 to 50
Z-Range: -0.0337222 to 0.944392

LOWER SURFACE
Level Surface defined by Z = 0

VOLUMES
Approximated Volume by
Trapezoidal Rule: 239.174
Simpson's Rule: 239.346
Simpson's 3/8 Rule: 239.248

CUT & FILL VOLUMES
Positive Volume [Cut]: 274.252
Negative Volume [Fill]: 35.078
Cut minus Fill: 239.174

AREAS
Positive Planar Area
(Upper above Lower): 1606.45
Negative Planar Area
(Lower above Upper): 8393.55
Blanked Planar Area: 0
Total Planar Area: 10000

Positive Surface Area
(Upper above Lower): 1608.27
Negative Surface Area
(Lower above Upper): 8393.57

GRIDDING METHOD: INVERSE DISTANCE TO POWER OF 2
SEARCH ALL DATA
DATASET: NESTED HERRINGBONE
FILENAME: IHERNST.SRF

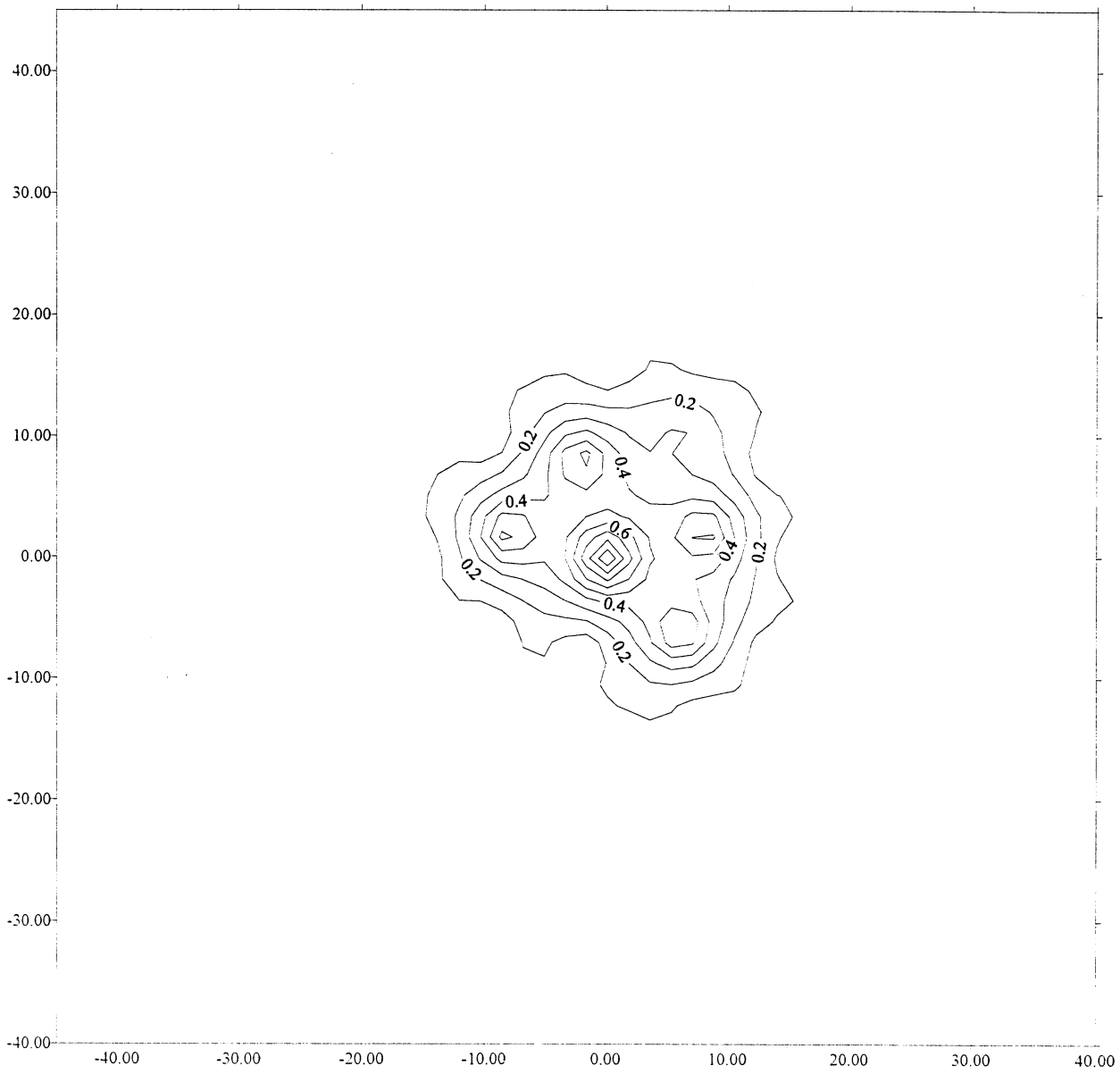

GRIDDING METHOD: INVERSE DISTANCE TO POWER OF 2
DATASET: NESTED HERRINGBONE
==========

VOLUME COMPUTATIONS

UPPER SURFACE
Grid File: H:/PROJECTS/WR/15000/15690/CALCS/X132/IHER5NST.GRD
Grid size as read: 50 cols by 50 rows
Delta X: 1.73469
Delta Y: 1.73469
X-Range: -45 to 40
Y-Range: -40 to 45
Z-Range: 3.63357E-042 to 0.997426

LOWER SURFACE
Level Surface defined by Z = 0

VOLUMES
Approximated Volume by
Trapezoidal Rule: 485.789
Simpson's Rule: 485.707
Simpson's 3/8 Rule: 485.51

CUT & FILL VOLUMES
Positive Volume [Cut]: 485.786
Negative Volume [Fill]: 0
Cut minus Fill: 485.786

AREAS
Positive Planar Area
(Upper above Lower): 7225
Negative Planar Area
(Lower above Upper): 0
Blanked Planar Area: 0
Total Planar Area: 7225

Positive Surface Area
(Upper above Lower): 7226.89
Negative Surface Area
(Lower above Upper): 0

GRIDDING METHOD: INVERSE DISTANCE TO POWER OF 2,
SEARCH ALL DATA
DATASET: NESTED HERRINGBONE
==========

VOLUME COMPUTATIONS

UPPER SURFACE
Grid File: H:/PROJECTS/WR/15000/15690/CALCS/X132/IHER5NST.GRD
Grid size as read: 50 cols by 50 rows
Delta X: 1.73469
Delta Y: 1.73469
X-Range: -45 to 40
Y-Range: -40 to 45
Z-Range: 3.63357E-042 to 0.997426

LOWER SURFACE
Level Surface defined by Z = 0

VOLUMES
Approximated Volume by
Trapezoidal Rule: 485.789
Simpson's Rule: 485.707
Simpson's 3/8 Rule: 485.51

CUT & FILL VOLUMES
Positive Volume [Cut]: 485.786
Negative Volume [Fill]: 0
Cut minus Fill: 485.786

AREAS
Positive Planar Area
(Upper above Lower): 7225
Negative Planar Area
(Lower above Upper): 0
Blanked Planar Area: 0
Total Planar Area: 7225

Positive Surface Area
(Upper above Lower): 7226.89
Negative Surface Area
(Lower above Upper): 0

GRIDDING METHOD: INVERSE DISTANCE TO POWER OF 2, SEARCH NEAREST 4 DATA
DATASET: NESTED HERRINGBONE
FILENAME: JHERNST.SRF

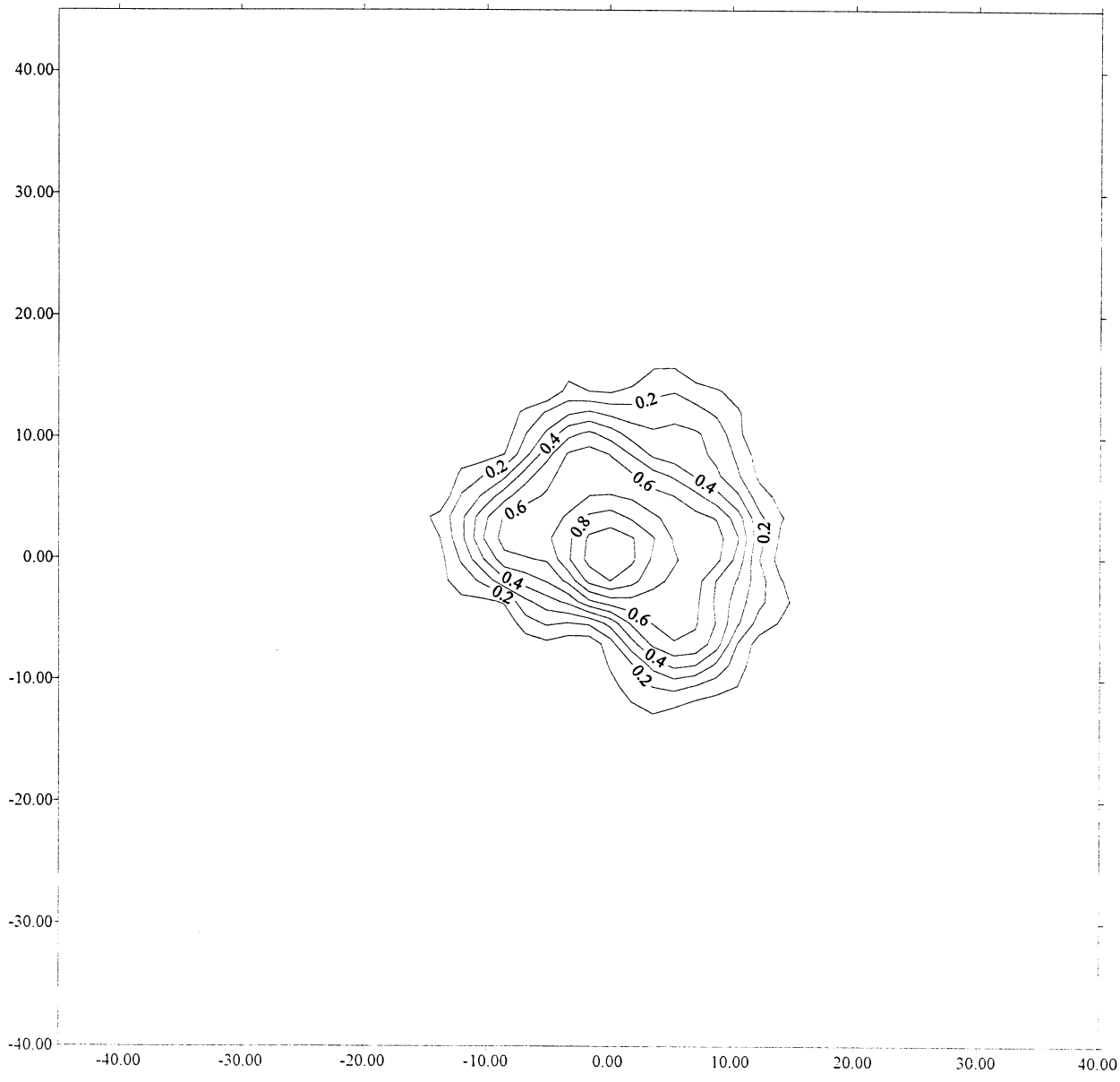

GRIDDING METHOD: INVERSE DISTANCE TO POWER OF 2,
SEARCH NEAREST 4 DATA
DATASET: NESTED HERRINGBONE
==========

VOLUME COMPUTATIONS

UPPER SURFACE
Grid File: H:/PROJECTS/WR/15000/15690/CALCS/X132/JHER5NST.GRD
Grid size as read: 50 cols by 50 rows
Delta X: 1.73469
Delta Y: 1.73469
X-Range: -45 to 40
Y-Range: -40 to 45
Z-Range: 0 to 0.999475

LOWER SURFACE
Level Surface defined by Z = 0

VOLUMES
Approximated Volume by
Trapezoidal Rule: 249.511
Simpson's Rule: 249.521
Simpson's 3/8 Rule: 249.569

CUT & FILL VOLUMES
Positive Volume [Cut]: 249.511
Negative Volume [Fill]: 0
Cut minus Fill: 249.511

AREAS
Positive Planar Area
(Upper above Lower): 977.978
Negative Planar Area
(Lower above Upper): 6247.02
Blanked Planar Area: 0
Total Planar Area: 7225

Positive Surface Area
(Upper above Lower): 980.47
Negative Surface Area
(Lower above Upper): 6247.02

GRIDDING METHOD: KRIGING, SEARCH ALL DATA
DATASET: NESTED HERRINGBONE
FILENAME: KHERNST.SRF

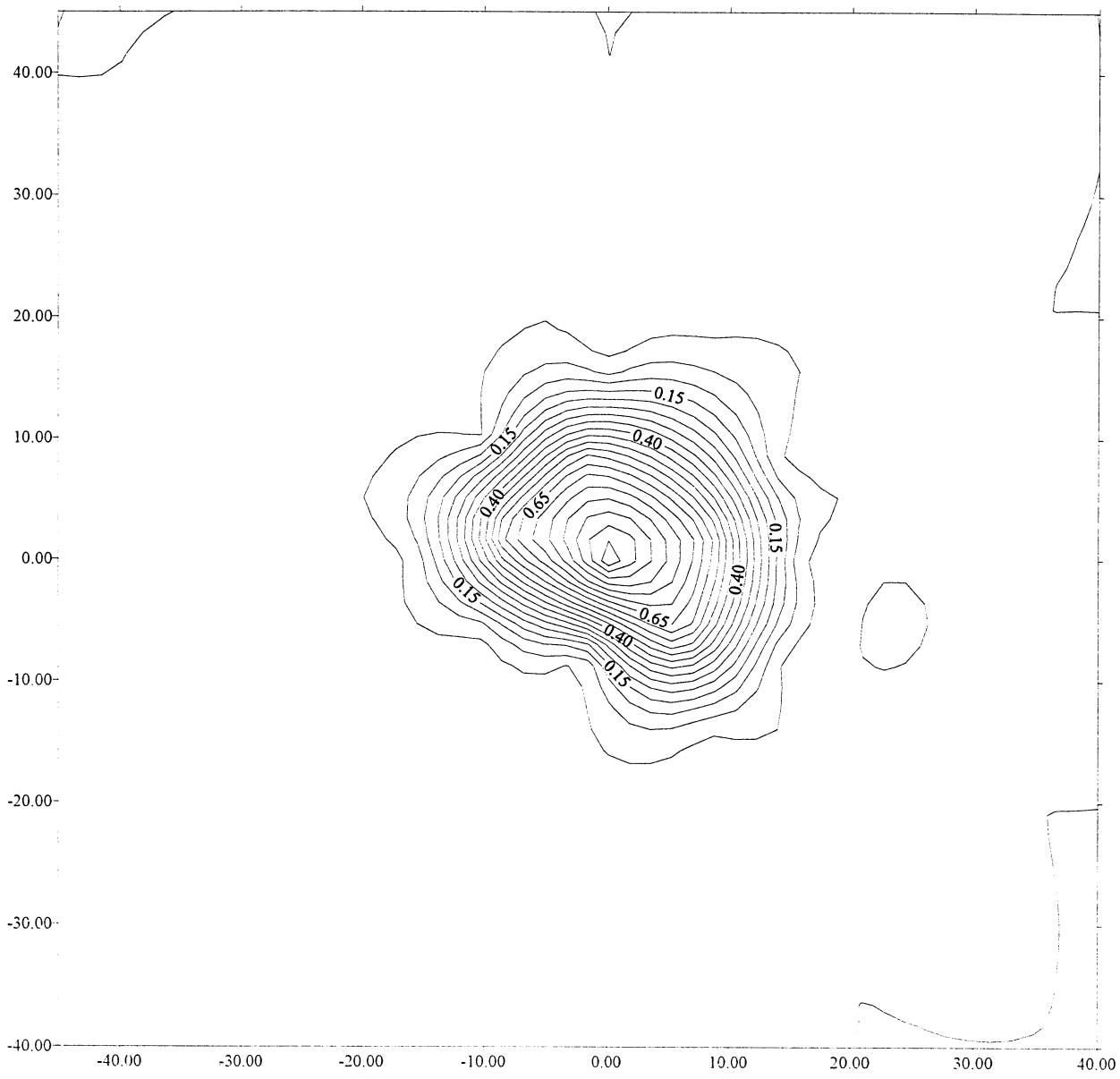

GRIDDING METHOD: KRIGING, SEARCH ALL DATA
DATASET: NESTED HERRINGBONE
==========

VOLUME COMPUTATIONS

UPPER SURFACE
Grid File: H:/PROJECTS/WR/15000/15690/CALCS/X132/KHER5NST.GRD
Grid size as read: 50 cols by 50 rows
Delta X: 1.73469
Delta Y: 1.73469
X-Range: -45 to 40
Y-Range: -40 to 45
Z-Range: -0.0537181 to 0.989199

LOWER SURFACE
Level Surface defined by Z = 0

VOLUMES
Approximated Volume by
Trapezoidal Rule: 201.599
Simpson's Rule: 201.528
Simpson's 3/8 Rule: 201.49

CUT & FILL VOLUMES
Positive Volume [Cut]: 262.9
Negative Volume [Fill]: 61.301
Cut minus Fill: 201.599

AREAS
Positive Planar Area
(Upper above Lower): 1089.25
Negative Planar Area
(Lower above Upper): 6135.75
Blanked Planar Area: 0
Total Planar Area: 7225

Positive Surface Area
(Upper above Lower): 1091.16
Negative Surface Area
(Lower above Upper): 6135.77

GRIDDING METHOD: KRIGING, DEFAULT SETTINGS
DATASET: RANDOM SAMPLING POINTS (SITE SCALED TO -45 TO +45)
FILENAME: LLRAN1.SRF

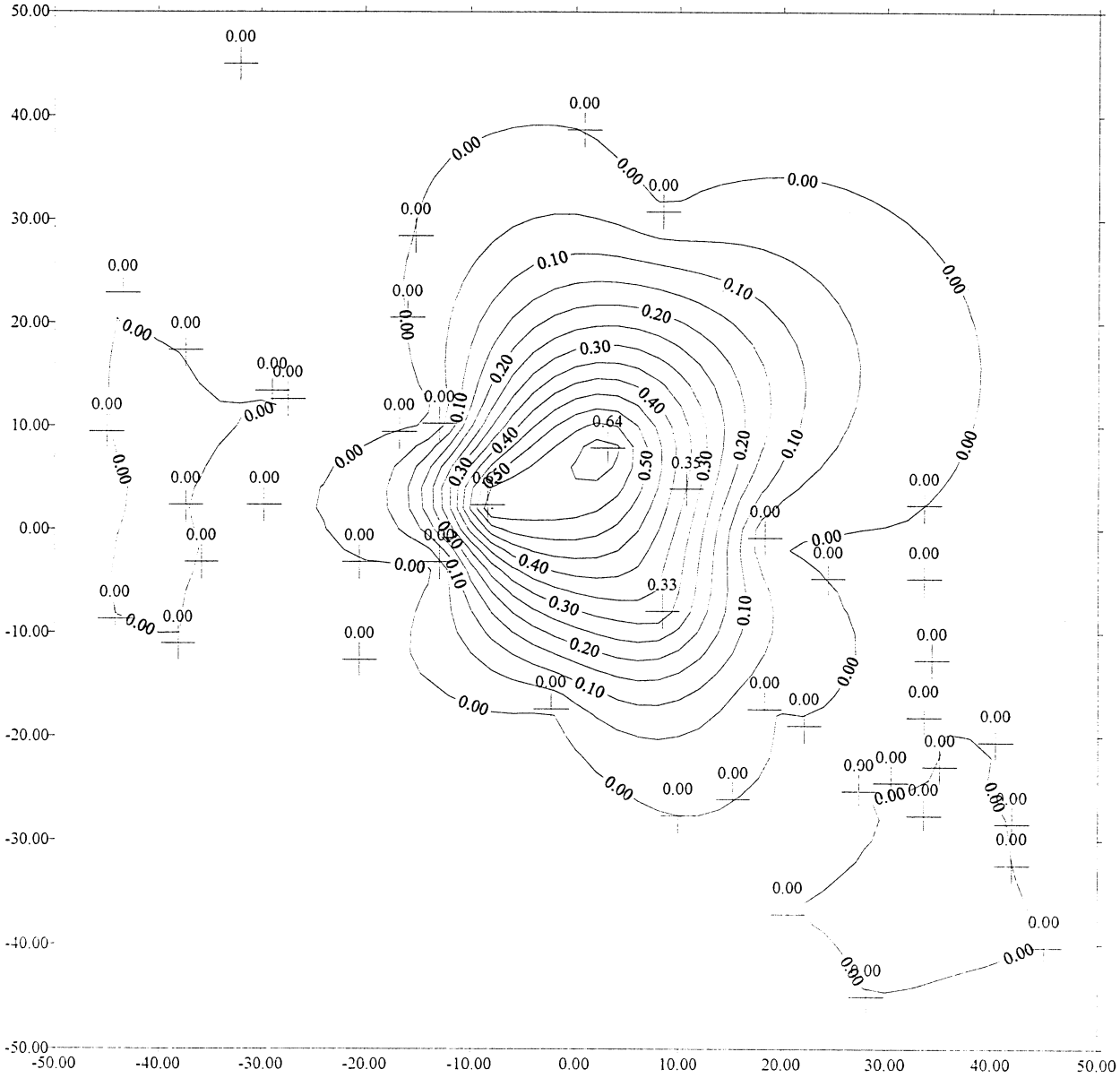

GRIDDING METHOD: KRIGING, DEFAULT SETTINGS
DATASET: RANDOM SAMPLING POINTS (SITE SCALED TO -45 TO +45)
==========

VOLUME COMPUTATIONS

UPPER SURFACE
Grid File: H:/PROJECTS/WR/15000/15690/CALCS/X132/LLRAN1.GRD
Grid size as read: 51 cols by 51 rows
Delta X: 2
Delta Y: 2
X-Range: -50 to 50
Y-Range: -50 to 50
Z-Range: -0.0455909 to 0.621882

LOWER SURFACE
Level Surface defined by Z = 0

VOLUMES
Approximated Volume by
Trapezoidal Rule: 284.744
Simpson's Rule: 284.925
Simpson's 3/8 Rule: 284.788

CUT & FILL VOLUMES
Positive Volume [Cut]: 391.907
Negative Volume [Fill]: 107.142
Cut minus Fill: 284.765

AREAS
Positive Planar Area
(Upper above Lower): 3291.19
Negative Planar Area
(Lower above Upper): 6708.81
Blanked Planar Area: 0
Total Planar Area: 10000

Positive Surface Area
(Upper above Lower): 3292.02
Negative Surface Area
(Lower above Upper): 6708.82

GRIDDING METHOD: KRIGING, DEFAULT SETTINGS
DATASET: RANDOM SAMPLING POINTS (SITE SCALED TO -20 TO +20)
FILENAME: LLRAN2.SRF

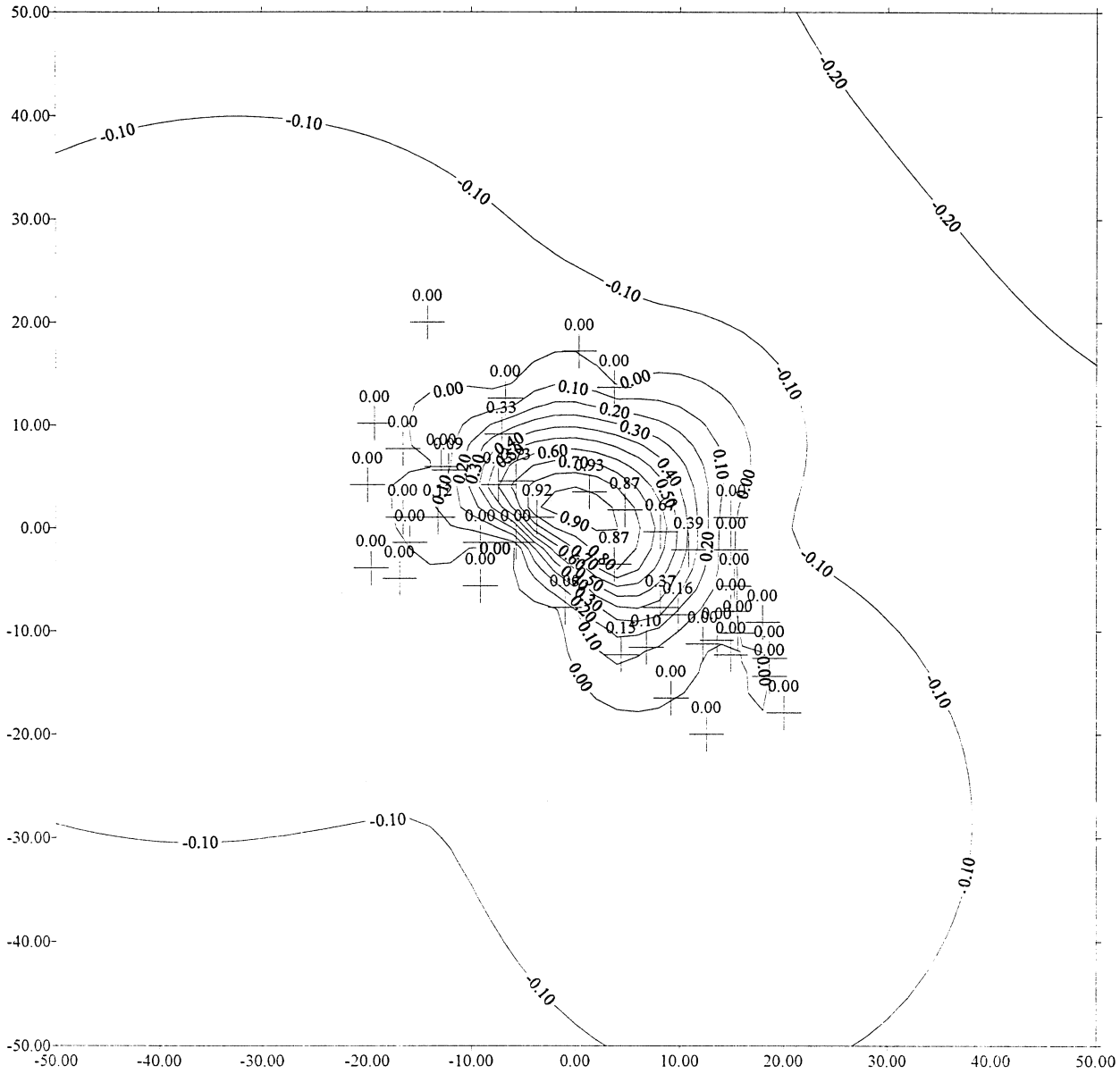

GRIDDING METHOD: KRIGING, DEFAULT SETTINGS
DATASET: RANDOM SAMPLING POINTS (SITE SCALED TO -20 TO +20)
==========

VOLUME COMPUTATIONS

UPPER SURFACE
Grid File: H:/PROJECTS/WR/15000/15690/CALCS/X132/LLRAN2.GRD
Grid size as read: 51 cols by 51 rows
Delta X: 2
Delta Y: 2
X-Range: -50 to 50
Y-Range: -50 to 50
Z-Range: -0.22506 to 0.942976

LOWER SURFACE
Level Surface defined by Z = 0

VOLUMES
Approximated Volume by
Trapezoidal Rule: -724.912
Simpson's Rule: -724.108
Simpson's 3/8 Rule: -724.644

CUT & FILL VOLUMES
Positive Volume [Cut]: 228.374
Negative Volume [Fill]: 953.256
Cut minus Fill: -724.882

AREAS
Positive Planar Area
(Upper above Lower): 804.375
Negative Planar Area
(Lower above Upper): 9195.63
Blanked Planar Area: 0
Total Planar Area: 10000

Positive Surface Area
(Upper above Lower): 806.707
Negative Surface Area
(Lower above Upper): 9195.74

GRIDDING METHOD: INFORMED KRIGING,
NESTED GAUSSIAN VARIOGRAM
DATASET: RANDOM SAMPLING POINTS (SITE SCALED TO -20 TO +20)
FILENAME: LLRAN2A.SRF

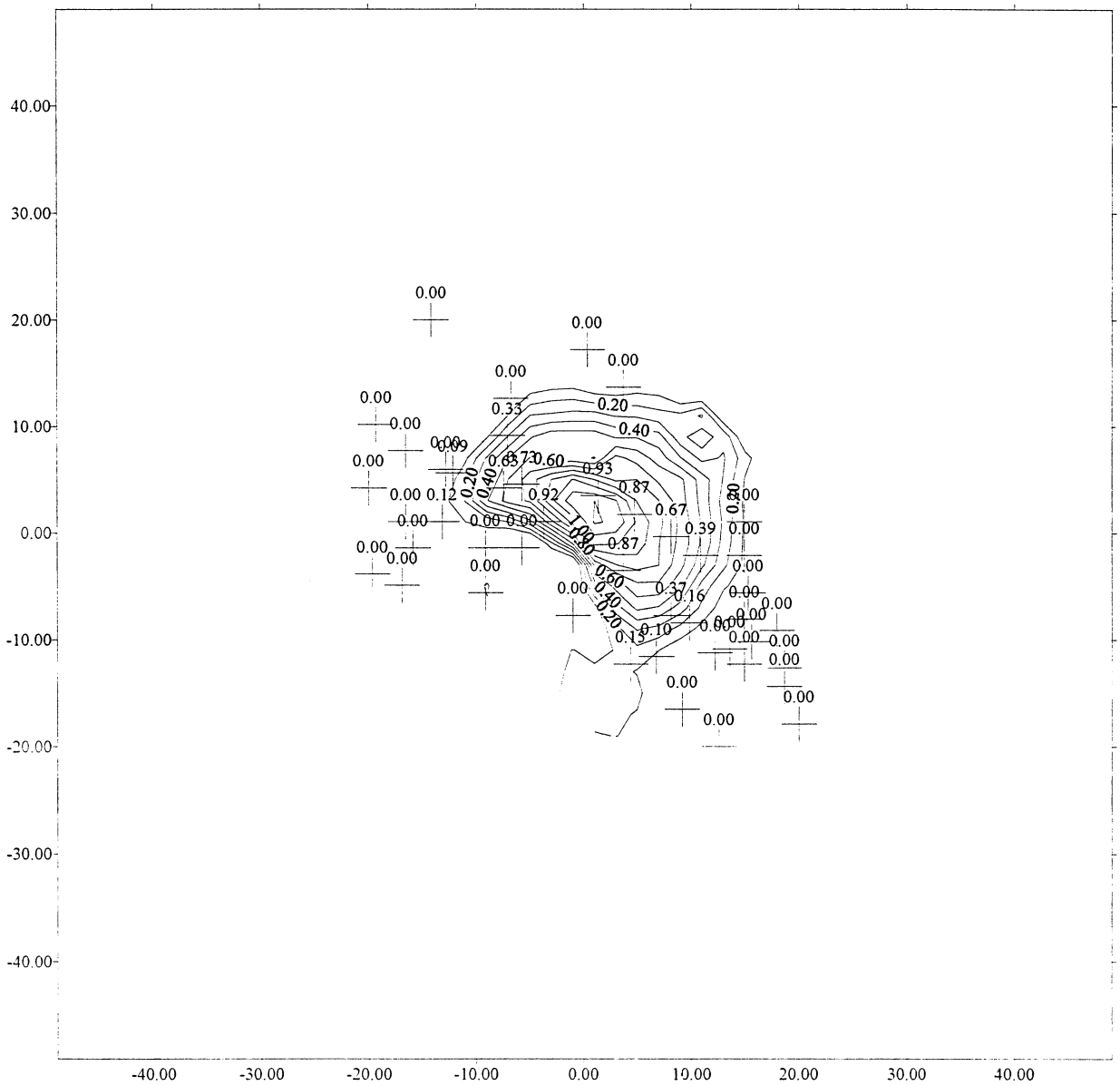

GRIDDING METHOD: MINIMUM CURVATURE (MAX RESIDUAL 0.001)
DATASET: NESTED HERRINGBONE
FILENAME: MHERNST.SRF

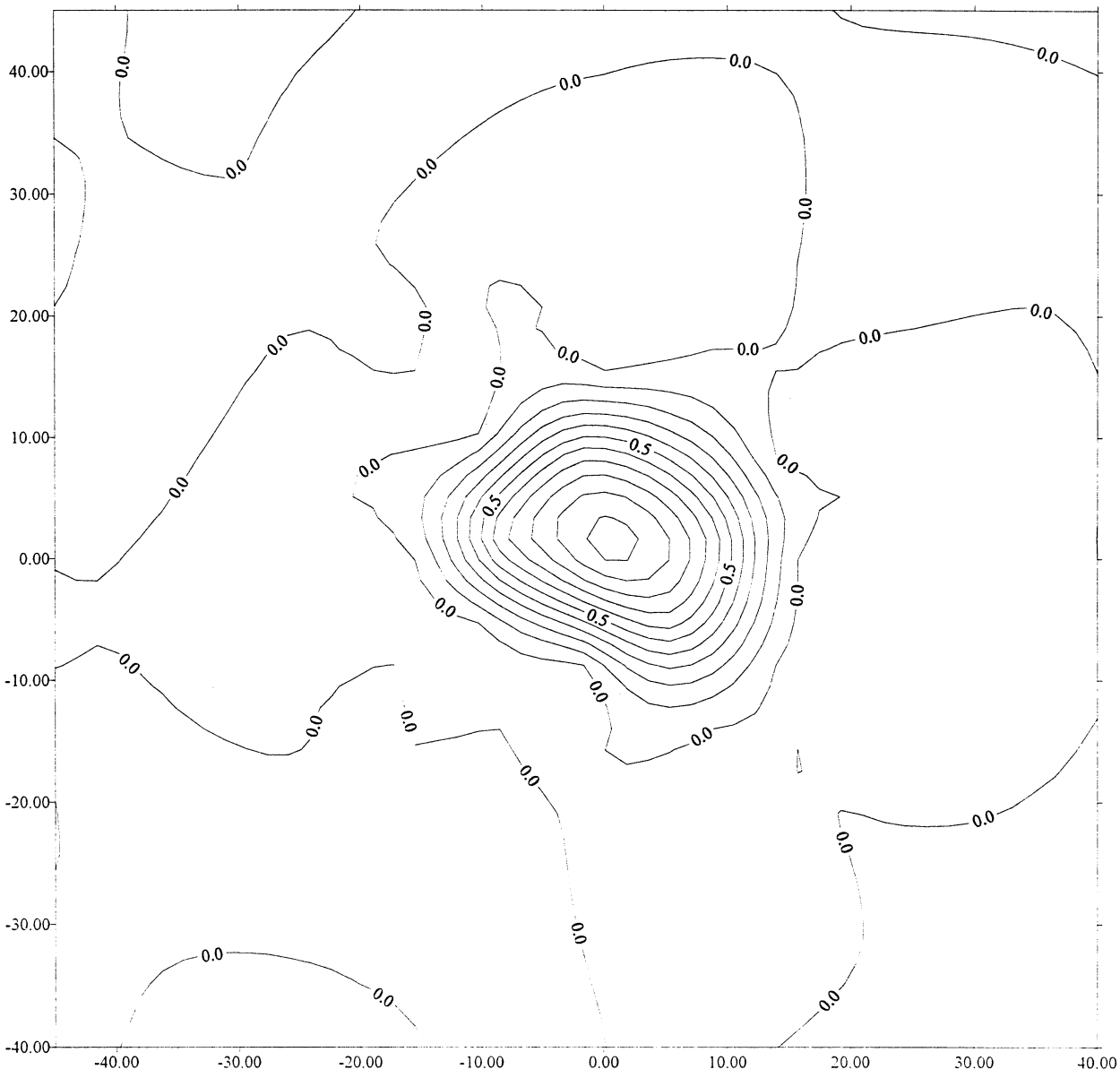

GRIDDING METHOD: NEAREST NEIGHBOUR (THEISSEN POLYGONS)
DATASET: NESTED HERRINGBONE
FILENAME: NHER5NST.SRF

GRIDDING METHOD: NEAREST NEIGHBOUR (THEISSEN POLYGONS)
DATASET: NESTED HERRINGBONE
==========

VOLUME COMPUTATIONS

UPPER SURFACE
Grid File: H:/PROJECTS/WR/15000/15690/CALCS/X132/NHER5NST.GRD
Grid size as read: 50 cols by 50 rows
Delta X: 1.73469
Delta Y: 1.73469
X-Range: -45 to 40
Y-Range: -40 to 45
Z-Range: 0 to 1

LOWER SURFACE
Level Surface defined by Z = 0

VOLUMES
Approximated Volume by
Trapezoidal Rule: 252.773
Simpson's Rule: 250.57
Simpson's 3/8 Rule: 254.261

CUT & FILL VOLUMES
Positive Volume [Cut]: 252.773
Negative Volume [Fill]: 0
Cut minus Fill: 252.773

AREAS
Positive Planar Area
(Upper above Lower): 464.916
Negative Planar Area
(Lower above Upper): 6760.08
Blanked Planar Area: 0
Total Planar Area: 7225

Positive Surface Area
(Upper above Lower): 478.203
Negative Surface Area
(Lower above Upper): 6760.08

GRIDDING METHOD: POLYNOMIAL OF ORDER 4
FOR X & Y WITH MAX TOTAL ORDER 4
DATASET: NESTED HERRINGBONE (65m BY 65m GRID)
FILENAME: PCHRNST.SRF

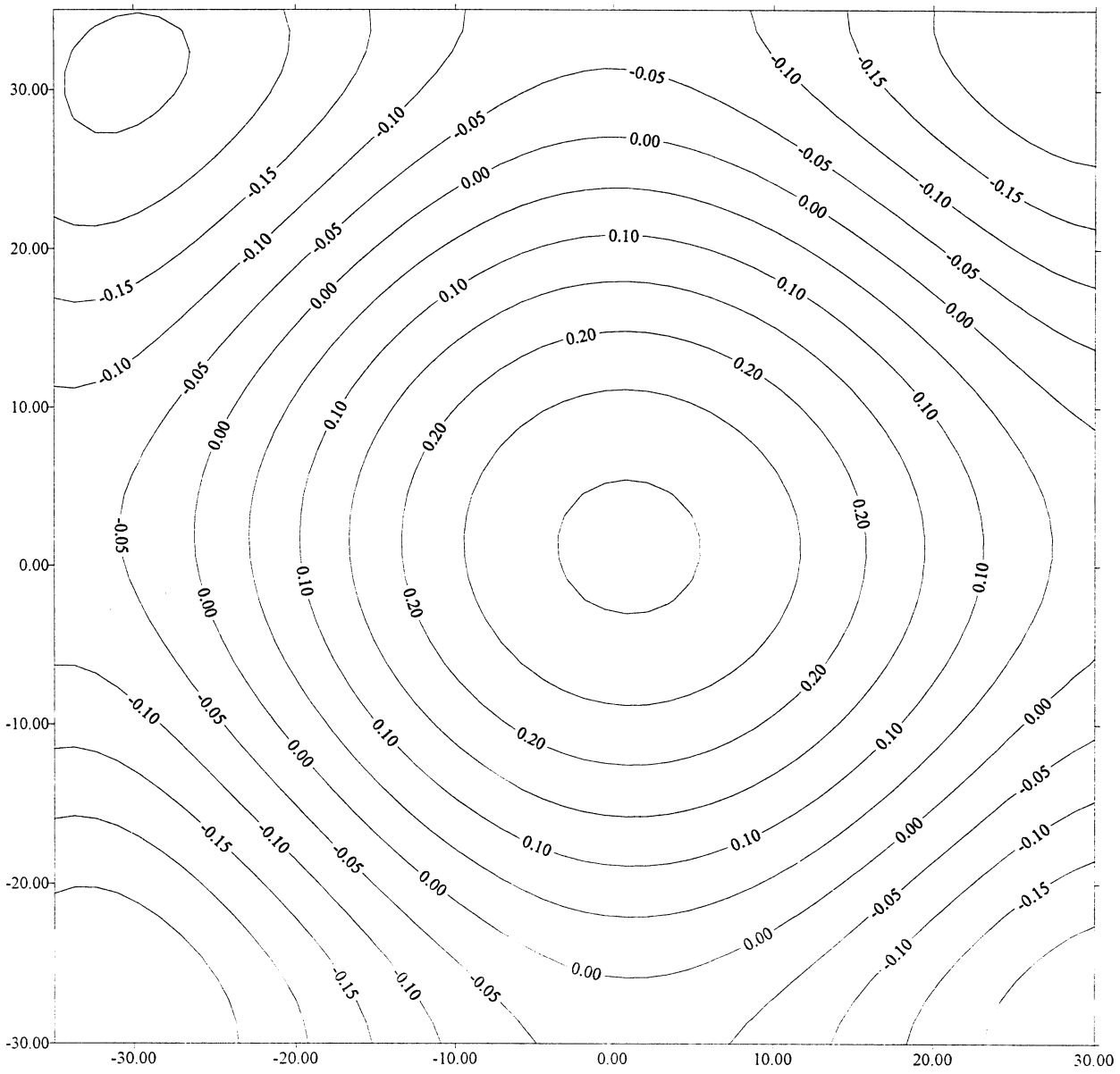

GRIDDING METHOD: POLYNOMIAL OF ORDER 4
FOR X & Y WITH MAX TOTAL ORDER 4
DATASET: NESTED HERRINGBONE (65m BY 65m GRID)
==========

VOLUME COMPUTATIONS

UPPER SURFACE
Grid File: H:/PROJECTS/WR/15000/15690/CALCS/X132/PCHR5NST.GRD
Grid size as read: 50 cols by 50 rows
Delta X: 1.32653
Delta Y: 1.32653
X-Range: -35 to 30
Y-Range: -30 to 35
Z-Range: -0.299681 to 0.311522

LOWER SURFACE
Level Surface defined by Z = 0

VOLUMES
Approximated Volume by
Trapezoidal Rule: 45.7465
Simpson's Rule: 45.7842
Simpson's 3/8 Rule: 45.7854

CUT & FILL VOLUMES
Positive Volume [Cut]: 294.219
Negative Volume [Fill]: 248.464
Cut minus Fill: 45.7553

AREAS
Positive Planar Area
(Upper above Lower): 2120.27
Negative Planar Area
(Lower above Upper): 2104.73
Blanked Planar Area: 0
Total Planar Area: 4225

Positive Surface Area
(Upper above Lower): 2120.52
Negative Surface Area
(Lower above Upper): 2104.94

GRIDDING METHOD: TRIANGULATION
DATASET: SIMPLE HERRINGBONE, PLUME CENTRE KNOWN
FILENAME: THER5.SRF

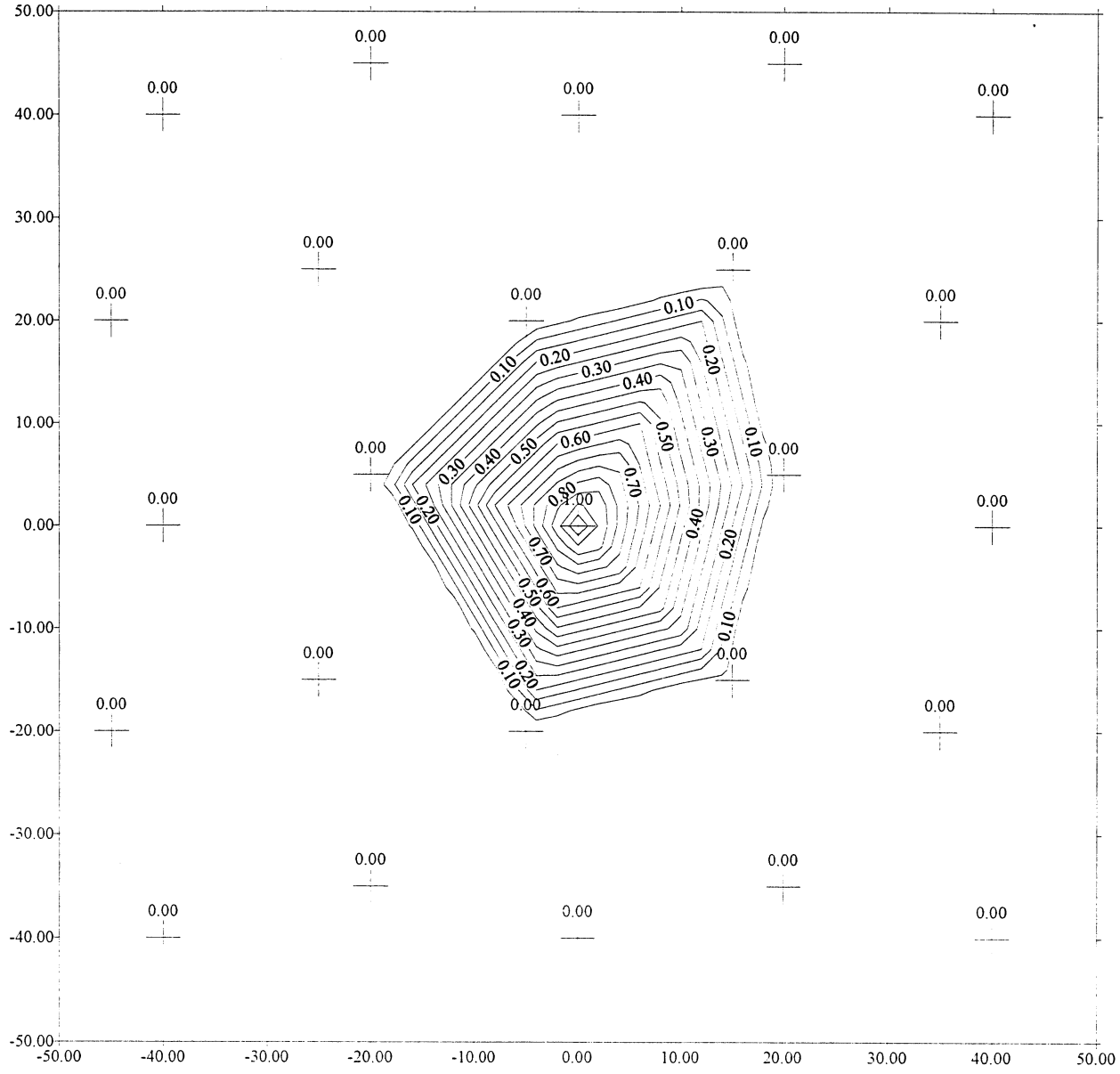

```
GRIDDING METHOD:  TRIANGULATION
DATASET:   SIMPLE HERRINGBONE, PLUME CENTRE KNOWN
================================================


VOLUME COMPUTATIONS

UPPER SURFACE
        Grid File:      H:/PROJECTS/WR/15000/15690/CALCS/
X132/THER5.GRD
        Grid size as read:      51 cols by 51 rows
        Delta X:        2
        Delta Y:        2
        X-Range:        -50 to 50
        Y-Range:        -50 to 50
        Z-Range:        0 to 1

LOWER SURFACE
        Level Surface defined by Z = 0

VOLUMES
        Approximated Volume by
        Trapezoidal Rule:       400.455
        Simpson's Rule: 400.611
        Simpson's 3/8 Rule:     400.37

CUT & FILL VOLUMES
        Positive Volume [Cut]:  400.455
        Negative Volume [Fill]: 0
        Cut minus Fill: 400.455

AREAS
        Positive Planar Area
        (Upper above Lower):    1344
        Negative Planar Area
        (Lower above Upper):    5512
        Blanked Planar Area:    3144
        Total Planar Area:      10000

        Positive Surface Area
        (Upper above Lower):    1345.76
        Negative Surface Area
        (Lower above Upper):    5512
```

GRIDDING METHOD: TRIANGULATION
DATASET: NESTED HERRINGBONE, PLUME CENTRE KNOWN
FILENAME: THER5NST.SRF

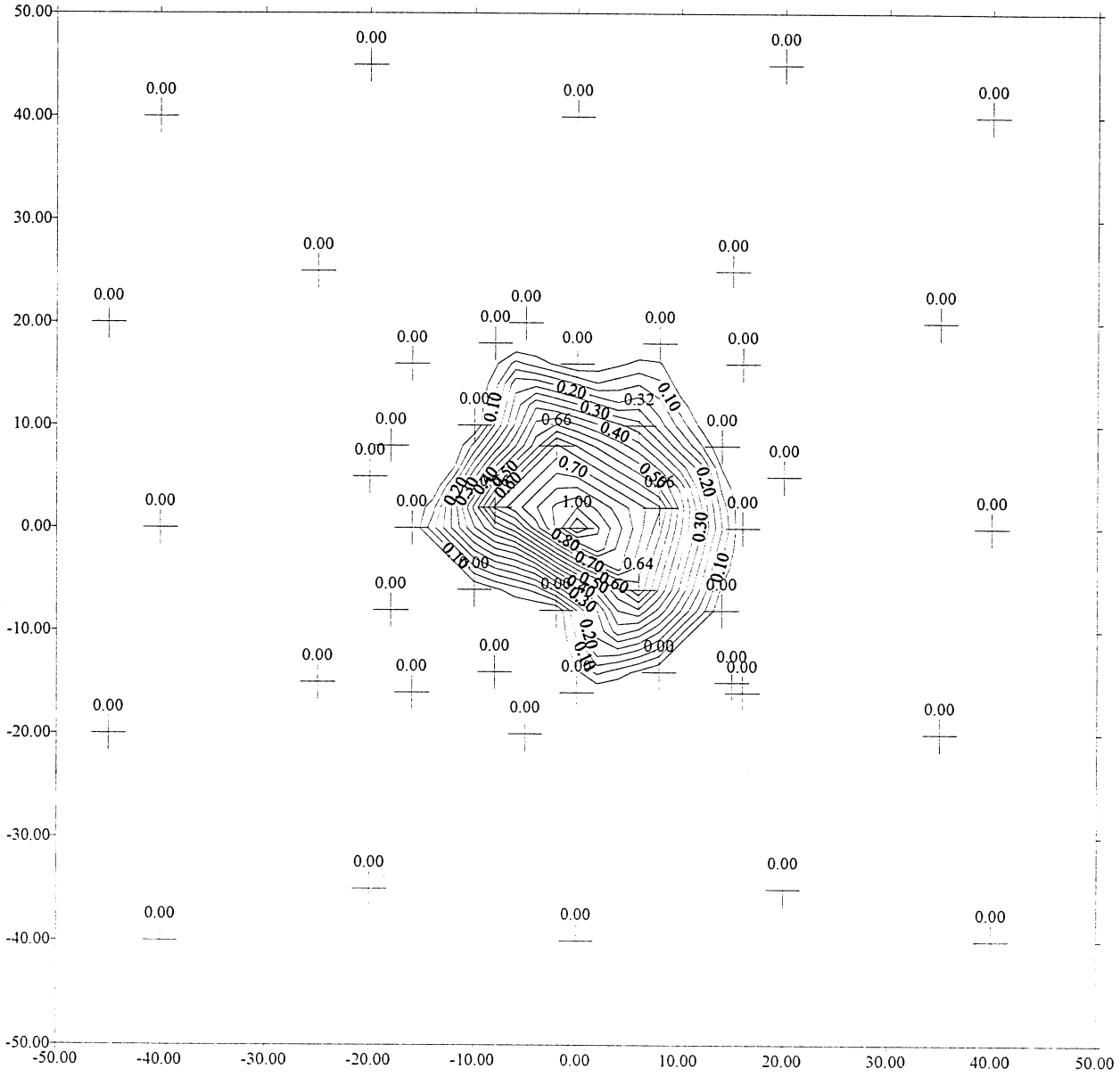

GRIDDING METHOD: TRIANGULATION
DATASET: NESTED HERRINGBONE, PLUME CENTRE KNOWN
==========

VOLUME COMPUTATIONS

UPPER SURFACE
Grid File: H:/PROJECTS/WR/15000/15690/CALCS/X132/THER5NST.GRD
Grid size as read: 51 cols by 51 rows
Delta X: 2
Delta Y: 2
X-Range: -50 to 50
Y-Range: -50 to 50
Z-Range: 0 to 1

LOWER SURFACE
Level Surface defined by Z = 0

VOLUMES
Approximated Volume by
Trapezoidal Rule: 251.853
Simpson's Rule: 251.857
Simpson's 3/8 Rule: 252.914

CUT & FILL VOLUMES
Positive Volume [Cut]: 251.853
Negative Volume [Fill]: 0
Cut minus Fill: 251.853

AREAS
Positive Planar Area
(Upper above Lower): 798
Negative Planar Area
(Lower above Upper): 6058
Blanked Planar Area: 3144
Total Planar Area: 10000

Positive Surface Area
(Upper above Lower): 800.215
Negative Surface Area
(Lower above Upper): 6058

GRIDDING METHOD: TRIANGULATION
DATASET: NESTED HERRINGBONE, PLUME CENTRE UNKNOWN
SAMPLING POINTS OFFSET TO NE
FILENAME: THER5NT3.SRF

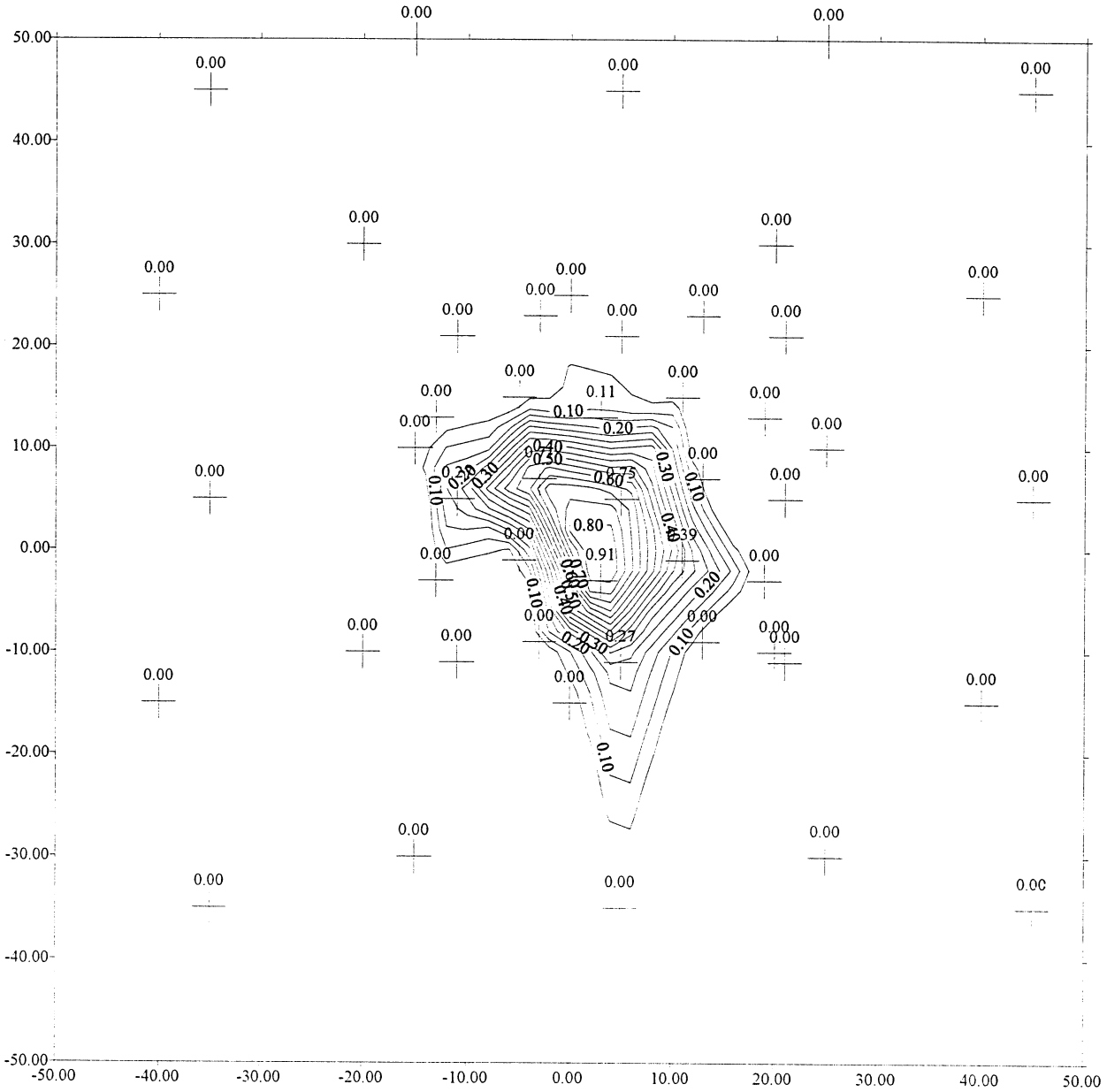

GRIDDING METHOD: TRIANGULATION
DATASET: NESTED HERRINGBONE, PLUME CENTRE UNKNOWN
==========

VOLUME COMPUTATIONS

UPPER SURFACE
Grid File: H:/PROJECTS/WR/15000/15690/CALCS/X132/THER5NT3.GRD
Grid size as read: 51 cols by 51 rows
Delta X: 2
Delta Y: 2
X-Range: -50 to 50
Y-Range: -50 to 50
Z-Range: 0 to 0.849882

LOWER SURFACE
Level Surface defined by Z = 0

VOLUMES
Approximated Volume by
Trapezoidal Rule: 221.723
Simpson's Rule: 221.86
Simpson's 3/8 Rule: 221.264

CUT & FILL VOLUMES
Positive Volume [Cut]: 221.723
Negative Volume [Fill]: 0
Cut minus Fill: 221.723

AREAS
Positive Planar Area
(Upper above Lower): 1020
Negative Planar Area
(Lower above Upper): 5724
Blanked Planar Area: 3256
Total Planar Area: 10000

Positive Surface Area
(Upper above Lower): 1022.04
Negative Surface Area
(Lower above Upper): 5724

GRIDDING METHOD: TRIANGULATION
DATASET: NESTED HERRINGBONE, PLUME CENTRE UNKNOWN
SAMPLING POINTS OFFSET TO NW
FILENAME: THER5NT4.SRF

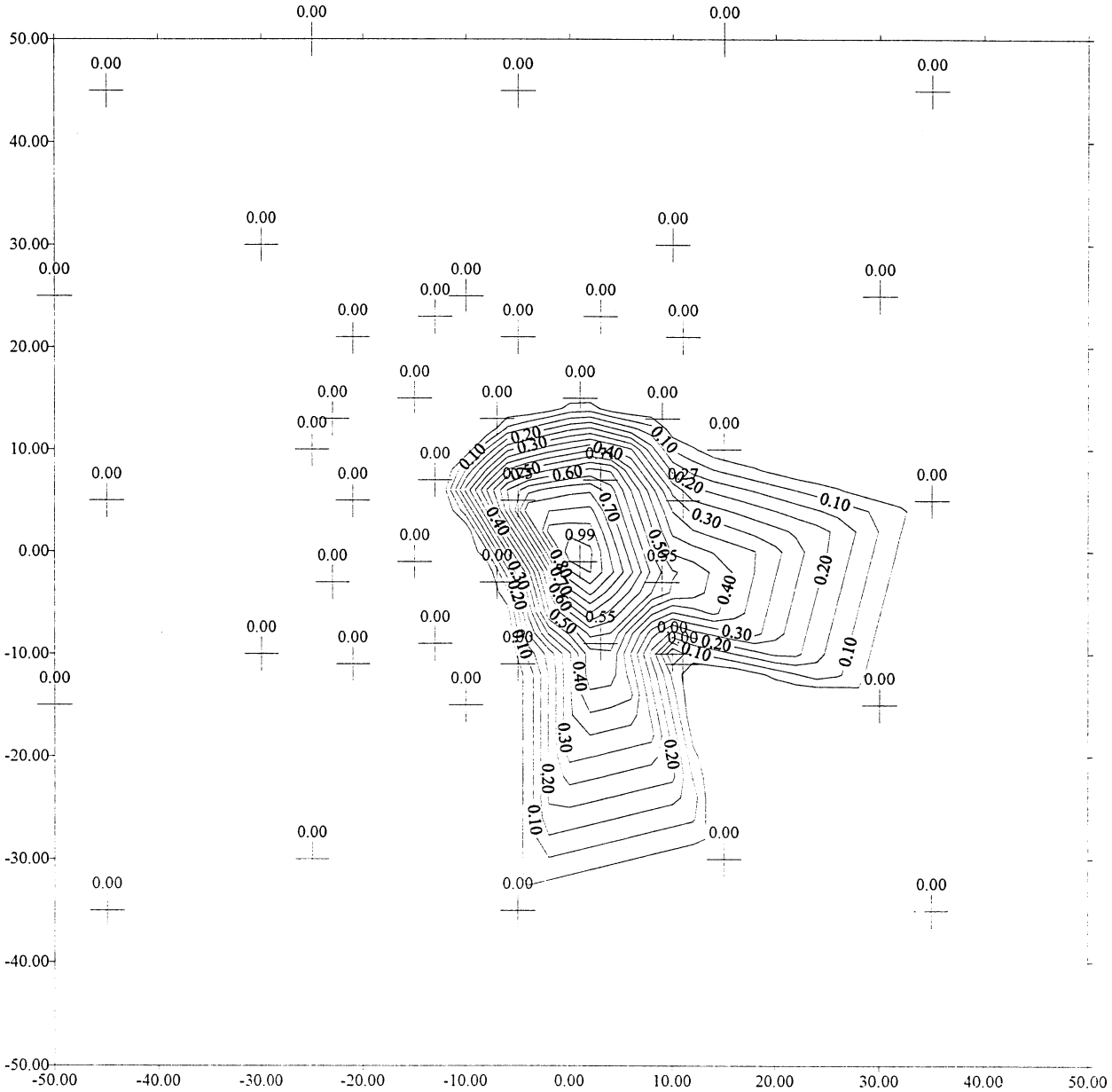

```
GRIDDING METHOD:  TRIANGULATION
DATASET:   NESTED HERRINGBONE, PLUME CENTRE UNKNOWN
           SAMPLING POINTS OFFSET TO NW
================================================


VOLUME COMPUTATIONS

UPPER SURFACE
        Grid File:      H:/PROJECTS/WR/15000/15690/CALCS/
X132/THER5NT4.GRD
        Grid size as read:      51 cols by 51 rows
        Delta X:        2
        Delta Y:        2
        X-Range:        -50 to 50
        Y-Range:        -50 to 50
        Z-Range:        0 to 0.94995

LOWER SURFACE
        Level Surface defined by Z = 0

VOLUMES
        Approximated Volume by
        Trapezoidal Rule:       367.424
        Simpson's Rule: 367.848
        Simpson's 3/8 Rule:     367.395

CUT & FILL VOLUMES
        Positive Volume [Cut]:  367.424
        Negative Volume [Fill]: 0
        Cut minus Fill: 367.424

AREAS
        Positive Planar Area
        (Upper above Lower):    1510
        Negative Planar Area
        (Lower above Upper):    5234
        Blanked Planar Area:    3256
        Total Planar Area:      10000

        Positive Surface Area
        (Upper above Lower):    1512.52
        Negative Surface Area
        (Lower above Upper):    5234
```

GRIDDING METHOD: TRIANGULATION
DATASET: RANDOM SAMPLING (SITE SCALED TO -45 TO + 45m)
FILENAME: TLLRAN1.SRF

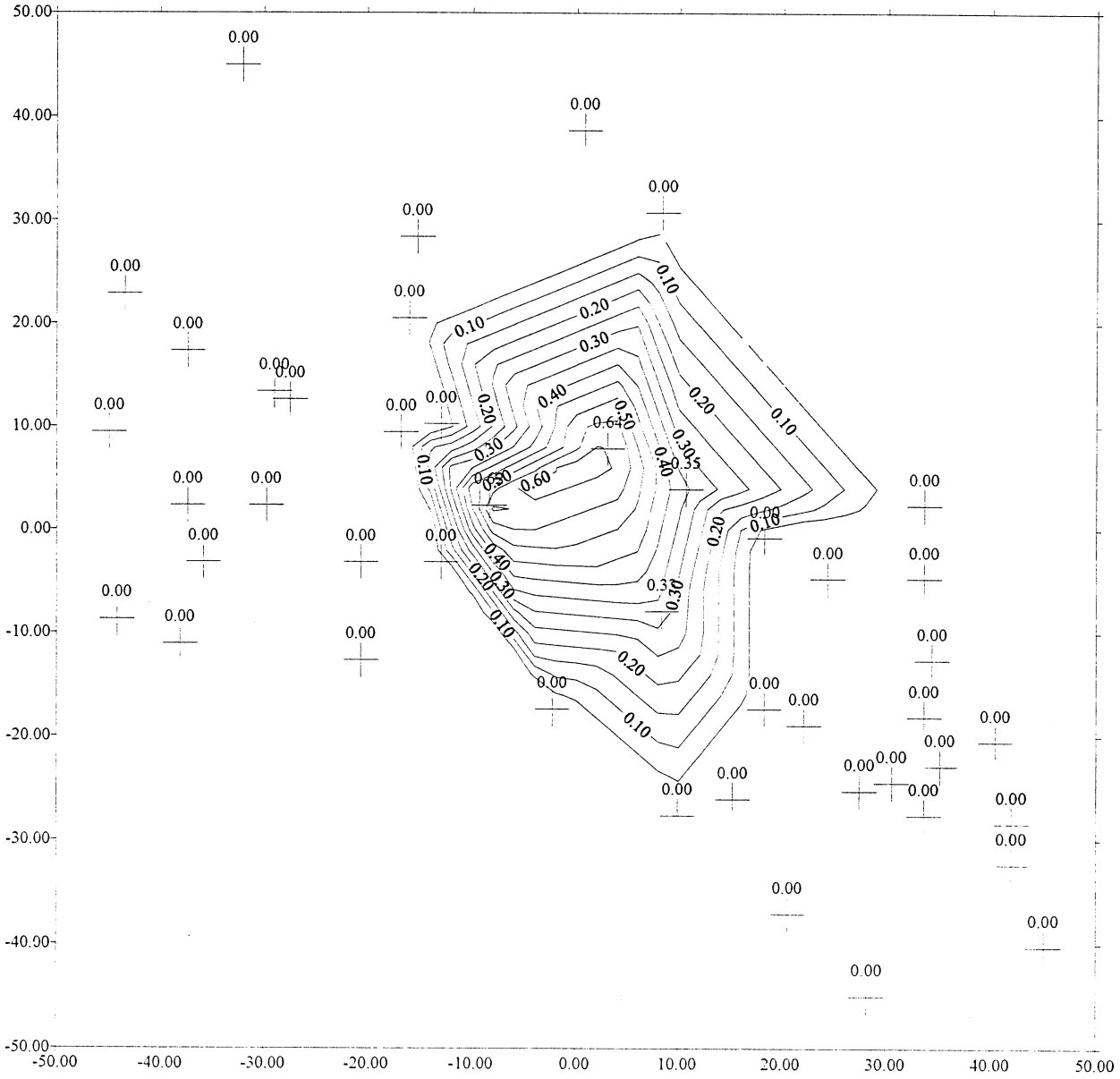

GRIDDING METHOD: TRIANGULATION
DATASET: RANDOM SAMPLING (SITE SCALED TO -45 TO + 45m)
==========

VOLUME COMPUTATIONS

UPPER SURFACE
Grid File: H:/PROJECTS/WR/15000/15690/CALCS/X132/TLLRAN1.GRD
Grid size as read: 51 cols by 51 rows
Delta X: 2
Delta Y: 2
X-Range: -50 to 50
Y-Range: -50 to 50
Z-Range: 0 to 0.628088

LOWER SURFACE
Level Surface defined by Z = 0

VOLUMES
Approximated Volume by
Trapezoidal Rule: 356.379
Simpson's Rule: 356.888
Simpson's 3/8 Rule: 356.302

CUT & FILL VOLUMES
Positive Volume [Cut]: 356.379
Negative Volume [Fill]: 0
Cut minus Fill: 356.379

AREAS
Positive Planar Area
(Upper above Lower): 1710
Negative Planar Area
(Lower above Upper): 2928
Blanked Planar Area: 5362
Total Planar Area: 10000

Positive Surface Area
(Upper above Lower): 1711.2
Negative Surface Area
(Lower above Upper): 2928

GRIDDING METHOD: TRIANGULATION
DATASET: RANDOM SAMPLING (SITE SCALED TO -20 TO +20m)
FILENAME: TLLRAN2.SRF

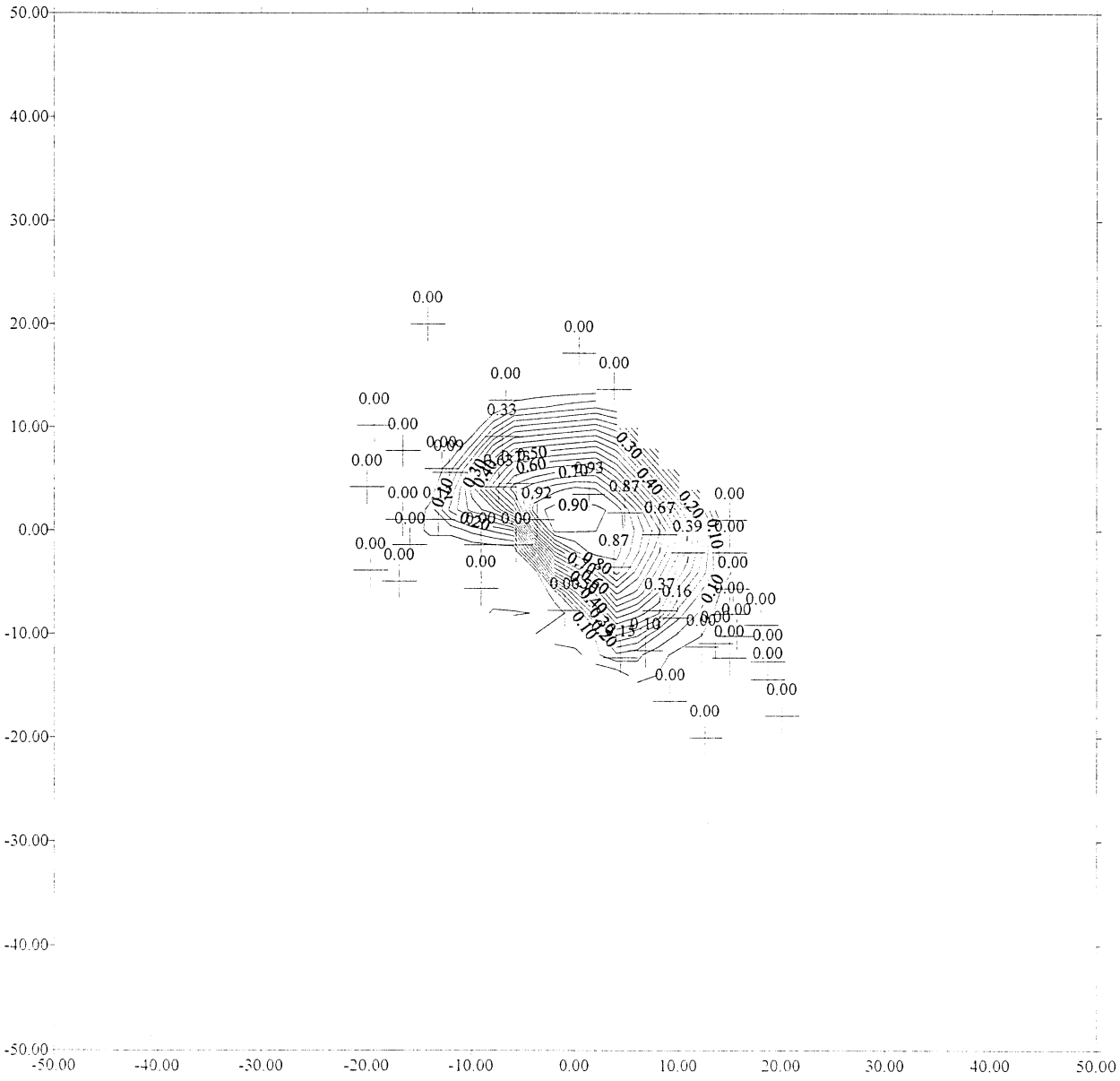

GRIDDING METHOD: TRIANGULATION
DATASET: RANDOM SAMPLING (SITE SCALED TO -20 TO +20m)
==========

VOLUME COMPUTATIONS

UPPER SURFACE
Grid File: H:/PROJECTS/WR/15000/15690/CALCS/X132/TLLRAN2.GRD
Grid size as read: 51 cols by 51 rows
Delta X: 2
Delta Y: 2
X-Range: -50 to 50
Y-Range: -50 to 50
Z-Range: 0 to 0.921538

LOWER SURFACE
Level Surface defined by Z = 0

VOLUMES
Approximated Volume by
Trapezoidal Rule: 203.76
Simpson's Rule: 204.305
Simpson's 3/8 Rule: 202.875

CUT & FILL VOLUMES
Positive Volume [Cut]: 203.76
Negative Volume [Fill]: 0
Cut minus Fill: 203.76

AREAS
Positive Planar Area
(Upper above Lower): 640
Negative Planar Area
(Lower above Upper): 202
Blanked Planar Area: 9158
Total Planar Area: 10000

Positive Surface Area
(Upper above Lower): 642.762
Negative Surface Area
(Lower above Upper): 202

GRIDDING METHOD: DEFAULT KRIGING
DATASET: SAMPLING OVER 2m GRID
FILENAME: TRUE2M.SRF

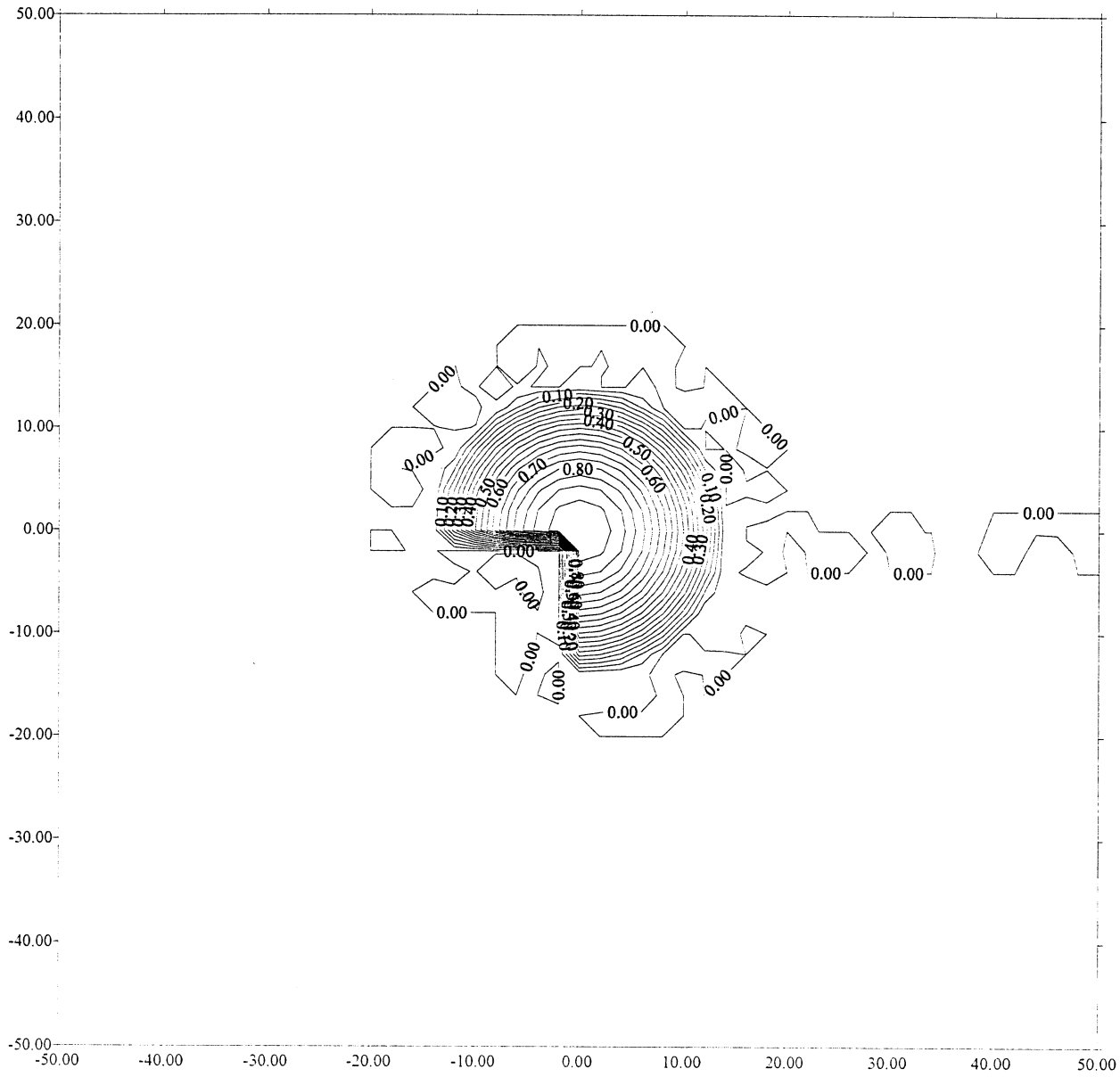

GRIDDING METHOD: DEFAULT KRIGING
DATASET: SAMPLING OVER 2m GRID
==========

VOLUME COMPUTATIONS

UPPER SURFACE
Grid File: H:/PROJECTS/WR/15000/15690/CALCS/X132/TRUE2M.GRD
Grid size as read: 51 cols by 51 rows
Delta X: 2
Delta Y: 2
X-Range: -50 to 50
Y-Range: -50 to 50
Z-Range: -3.2481E-007 to 1

LOWER SURFACE
Level Surface defined by Z = 0

VOLUMES
Approximated Volume by
Trapezoidal Rule: 251.922
Simpson's Rule: 258.383
Simpson's 3/8 Rule: 256.021

CUT & FILL VOLUMES
Positive Volume [Cut]: 251.922
Negative Volume [Fill]: 1.17251E-005
Cut minus Fill: 251.922

AREAS
Positive Planar Area
(Upper above Lower): 897.73
Negative Planar Area
(Lower above Upper): 9102.27
Blanked Planar Area: 0
Total Planar Area: 10000

Positive Surface Area
(Upper above Lower): 903.142
Negative Surface Area
(Lower above Upper): 9102.27

GRIDDING METHOD: TRIANGULATION
DATASET: SAMPLING OVER 2m GRID
FILENAME: TTRUE2M.SRF

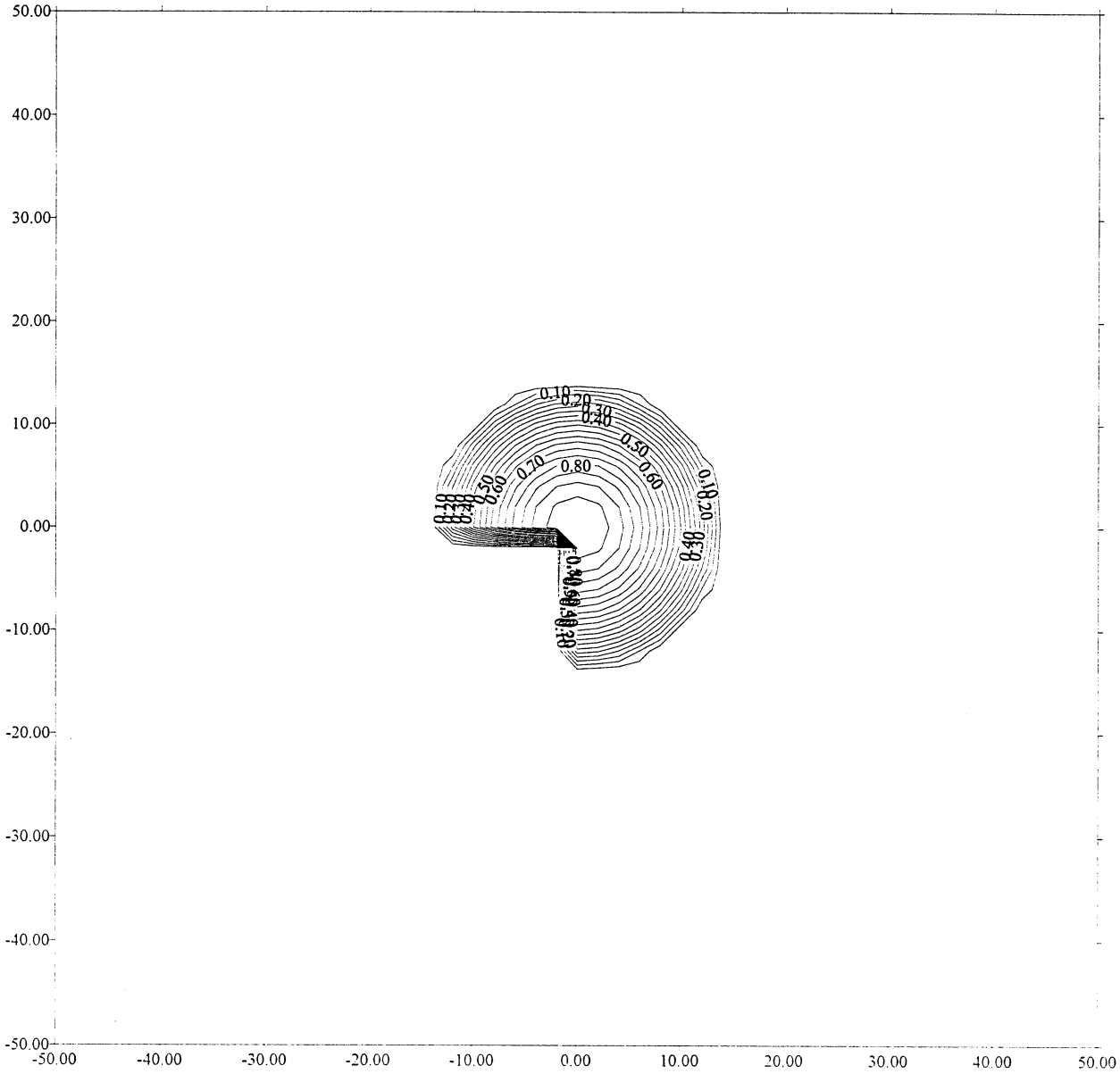

```
GRIDDING METHOD:  TRIANGULATION
DATASET:   SAMPLING OVER 2m GRID
================================


VOLUME COMPUTATIONS

UPPER SURFACE
        Grid File:      H:/PROJECTS/WR/15000/15690/CALCS/
X132/TTRUE2M.GRD
        Grid size as read:      51 cols by 51 rows
        Delta X:        2
        Delta Y:        2
        X-Range:        -50 to 50
        Y-Range:        -50 to 50
        Z-Range:        0 to 1

LOWER SURFACE
        Level Surface defined by Z = 0

VOLUMES
        Approximated Volume by
        Trapezoidal Rule:       251.922
        Simpson's Rule: 258.383
        Simpson's 3/8 Rule:     256.021

CUT & FILL VOLUMES
        Positive Volume [Cut]:  251.922
        Negative Volume [Fill]: 0
        Cut minus Fill: 251.922

AREAS
        Positive Planar Area
        (Upper above Lower):    584
        Negative Planar Area
        (Lower above Upper):    9416
        Blanked Planar Area:    0
        Total Planar Area:      10000

        Positive Surface Area
        (Upper above Lower):    589.413
        Negative Surface Area
        (Lower above Upper):    9416
```

LNAPL plume problem

Nested herringbone sampling pattern